Functional Characterization of *parla* and *parlb* Paralogs in Zebrafish

Rawan Merhi

A thesis submitted in partial fulfillment of the requirements for the
Doctorate in Philosophy degree in Biology

Department of Biology
Faculty of Science
University of Ottawa

ABSTRACT

Parkinson's disease (PD) is the second most prevalent neurodegenerative disease, featuring motor signs such as tremors, bradykinesia, and impaired gait that are often preceded by nonmotor symptoms such as anxiety/depression and olfactory dysfunction. Interestingly, significant olfactory loss was found to be manifested in the majority of PD patients and may precede motor symptoms by years, and thus can be used for the risk assessment of developing PD in asymptomatic individuals. The main pathological feature of PD is the progressive and irreversible loss of dopaminergic (DA) neurons in the substantia nigra pars compacta of the midbrain. Although the detailed etiology of PD remains unclear, most PD cases were found to be sporadic and can be associated with environmental factors. Only 5–10% of patients result from familial PD. With considerable effort in the past two decades, a number of genes associated with familial PD have been identified and interestingly, many of these genes are involved in regulating and maintaining mitochondrial function. The presenilin-associated rhomboid-like (*PARL*) gene was found to contribute to mitochondrial morphology and function and was linked to familial Parkinson's disease (PD). The *PARL* gene product is a mitochondrial intramembrane cleaving protease that acts on a number of mitochondrial proteins involved in mitochondrial morphology, apoptosis, and mitophagy. To date, functional and genetic studies of *PARL* have been mainly performed in mammals. However, little is known about *PARL* function and its role in dopaminergic (DA) neuron development in vertebrates. The zebrafish genome comprises two *PARL* paralogs: *parla* and *parlb*. Here, we show novel information concerning the role of *PARL* in zebrafish by establishing a loss-of-function mutation in *parla* and *parlb* via CRISPR/Cas9-mediated mutagenesis. We examined DA neuron numbers in the adult brain and expression of genes associated with DA neuron function in larvae and adults. We show that loss of *parla*

function, as well as loss of both *parla* and *parlb* function result in loss of DA neurons in the olfactory bulb and telencephalon of adult zebrafish brain. Changes in the levels of *tyrosine hydroxylase* transcripts supported this neuronal loss. Expression of *fis1*, a gene involved in mitochondrial fission, was increased in *parla* mutants and in fish with loss of *parla* and *parlb* function. Furthermore, we showed that loss of *parla* and/or *parlb* function translates into altered locomotion parameters and that loss of *parla* but not *parlb* function results in impaired olfaction. Finally, increased susceptibility to neurotoxin exposure was identified in mutants with loss of both *parla* and *parlb* function but not with loss of *parla* or *parlb* function. These results suggest an evident role for *parla* in the development and/or maintenance of DA neuron function in zebrafish and confirm the existence of redundant and non-redundant functions for the two paralogs, *parla* and *parlb*.

RESUMÉ

La maladie de Parkinson est la deuxième maladie neurodégénérative la plus fréquente et présentant des signes moteurs tels que des tremblements, bradykinésie, et une instabilité posturale qui sont fréquemment précédés par des signes non-moteurs tel que l'anxiété/la dépression et la dysfonction olfactive. Intéressement, une perte olfactive importante se manifeste dans la majorité des cas de la maladie de Parkinson et peut précéder les signes moteurs, éventuellement peut être utilisée comme signe précoce pour le développement de la maladie. La caractéristique pathologique principale de cette maladie est la perte progressive et irréversible des neurones dopaminergiques de la substance noire du mésencéphale. Bien que l'étiologie spécifique de la maladie de Parkinson n'est pas bien claire, la vaste majorité des cas de Parkinson sont sporadiques associés à des facteurs environnementaux. Environ 5-10% des personnes atteintes ont une histoire familiale de la maladie de Parkinson. Des efforts considérables ont été déployés durant les deux dernières décennies pour identifier les gènes associés à la maladie de Parkinson. Intéressement, la plupart des gènes impliqués sont responsables de la régulation et le maintien de la fonction de la mitochondrie. La protéase mitochondriale (PARL) est codée par un gène qui contribue à la régulation de la morphologie et fonction mitochondriales. Il a été établi que le gène *PARL* est associé à la forme familiale de la maladie de Parkinson. Ce gène code pour une protéase qui agit sur des protéines mitochondriales diverses impliquées dans la régulation de la morphologie de la mitochondrie, l'apoptose et la mitophagie. Jusqu'au présent, les études de la fonction de *PARL* ont été notamment effectuées sur les mammifères. Cependant, on connaît peu sur la fonction de *PARL* et son rôle dans le développement des neurones dopaminergiques des vertèbres. Le génome du poisson zèbre (*Danio rerio*) est compris de deux gènes paralogues : *parla* et *parlb*. Dans cette étude, on démontre

des informations nouvelles sur le rôle de PARL dans le poisson zèbre par l'établissement des mutations entraînant une perte de fonction de *parla* et *parlb* au moyen du système de mutagenèse du CRISPR/Cas9. On a examiné le nombre des neurones dopaminergiques dans le cerveau adulte ainsi que l'expression des gènes associés à la fonction de ces neurones dans les poissons larves et adultes. On a demontré que la perte de la fonction de *parla* seul, ainsi que de *parla* et *parlb* simultanément, entraîne une diminution du nombre des neurones dopaminergiques du bulbe olfactif et du télencéphale dans le cerveau adulte des poissons. Les changements au niveau des transcrits de la *tyrosine hydroxylase* supportent la perte neuronale observée. L'expression de *fis1*, un gène impliqué dans la fission mitochondriale, s'est augmentée dans les mutants ayant une perte de fonction de *parla* seul, ainsi que de *parla* et *parlb* simultanément. De plus, on a montré que la perte de fonction de *parla* et/ou *parlb* se traduit par une locomotion altérée. On a aussi montré que la perte de fonction de *parla* mais pas celle de *parlb* entraîne une olfaction compromise. Finalement, on a identifié une augmentation de la susceptibilité à l'exposition aux neurotoxines des mutants ayant une perte de fonction des deux paralogues. Cela n'était pas identifié dans les mutants ayant une perte de fonction uniquement dans l'un de ces paralogues. Ces résultats suggèrent un rôle évident du gène *parla* dans le développement et/ou maintien de la fonction des neurones dopaminergiques dans le poisson zèbre et confirment la présence des fonctions redondantes et non-redondantes des deux paralogues, *parla* et *parlb*.

ACKNOWLEDGEMENTS

First and foremost, I would like to express my great gratitude for having Dr. Marc Ekker as my supervisor. The Ph.D. journey by itself is a tough one and being an expat away from home makes it even tougher. However, having an understanding, caring, and supporting supervisor like you Marc, made this journey not only highly bearable, but enjoyable as well. I am thankful for your genuine guidance, advise and trust, professional mentoring, constructive critics, and suggestions… And much more. Thank you for always encouraging my endeavors and supporting me throughout this enriching experience. Thank you for giving me the so many opportunities to display my work nationally, and internationally, providing me with great reference letters and recommending me to valuable future academic and career positions that would pave my way for a bright future as a scientist.

I also want to thank the members of my advisory committee, Marie-Andrée Akimenko, Tuan Bui, and Bill Willmore for their dedicated time and valuable input, suggestions, and support. I would like to express my sincere gratitude and appreciation for the amazing members of the Ekker and the Akimenko lab. The atmosphere of the workplace was friendly and enjoyable because of you. Among them, I am especially thankful to Michael Kalyn and Hellen Weinschutz Mendes for their great help and support, and their valuable, caring, and friendly work and life advises throughout my Ph.D. journey. I am grateful to have made great friends and colleagues like you, and I wish all of you the best in your future endeavors.

I am also thankful to Vishal Saxena, a great technician and human, who provided me with endless patience and support, and valuable advice and suggestions that helped me get through the struggles I faced in my experiments. Thanks to Gary Hatch for the substantial technical support. I

would also like to express my gratitude to all the undergraduate students whom I mentored and trained throughout those four years. Not only you learned from my expertise, but I, myself, learned a lot from you guys as well. Thank you Amanda Zhu-Pawlowsky for your serious commitment and your precious contributions to this work.

A big thank you to all my close friends in Canada and in Lebanon. You believed in me and supported me immensely, and I cannot be more grateful. A special thank you to a friend whom I met in the lab, that not only became a close friend but a dear sister to me. Thank you Dana ElSaid for always being there for me through the good and the bad, and for always lending me a listening ear. To many more spontaneous Taco nights! I am also deeply grateful for the big support and care provided from overseas from a dear childhood friend. Thank you Grace Jouni for believing in me. It is finally happening!!

I would like to conclude with the biggest thank you and the deepest gratitude to my loving parents. You believed in me since day one, supported my dreams, guided me every step of the way, and taught me how to value education. And yes, mom and dad, you were always right! Education is power, indeed. Thank you for having great faith in me, even during my failures. Thank you for all the sacrifices you made. Thank you for making me become the person I am today. Thank you for the wings you gave me, you truly made me fly. Thank you for my sister and my brother for all the support and love. And thank you God for giving me the strength to keep going and never give up. {My success is only by You}.

Mom, and dad, I dedicate my success and achievements to you.

"The hardest thing to do is leaving your comfort zone. But you have to let go of the life you're familiar with and take the risk to live the life you dream about".

T. Arigo

List of Abbreviations

ATP	- adenine triphosphate
BBB	- blood-brain barrier
bp	- base pair
cDNA	- complementary DNA
CNS	- central nervous system
CRISPR	- clustered regularly interspaced palindromic repeat
DA	- dopaminergic
DAT	- dopamine transporter
DCAA	- amino acid decarboxylase
dpf	- days post-fertilization
DRP-1	- dynamin-related protein 1
DSB	- double-strand break
DYN2	- dynamin-like protein 2
F	- forward
FIS1	- fission protein 1
hpf	- hours post-fertilization
HTRA2	- high temperature requirement A2
IAP	- Inhibitor of apoptosis
IHC	- immunohistochemistry
IMP	- intramembrane protease
kb	- kilobase
KO	- knock-out
MAMP	- mature mitochondrial PARL protein
MFN1	- mitofusin 1
MFN2	- mitofusin 2

MO	- morpholino
mpf	- months post-fertilization
MPTP	- 1-methyl-4-phenyl-1,2,3,6-tetrahydropyridine
mRNA	- messenger RNA
mtDNA	- mitochondrial DNA
NHEJ	- non-homologous end-joining
NTC	- no template control
OB	- olfactory bulb
OPA1	- optic atrophy protein 1
PACT	- PARL C-terminal protein
PAGE	- polyacrylamide gel electrophoresis
PAM	- protospacer adjacent motif
PARL	- presenilin-associated rhomboid-like protease
PCR	- polymerase chain reaction
PD	- Parkinson’s disease
PGAM5	- phosphoglyceromutase 5
PINK1	- PTEN-induced putative kinase 1
qRT-PCR	- real-time quantitative reverse transcription PCR
Rm	- reverse mutant
ROS	- reactive oxygen species
Rwt	- reverse wild-type
sgRNA	- single guide RNA
siRNA	- small interfering RNA
TALENs	- transcription activator-like-effector endonucleases
TH	- tyrosine hydroxylase
UTR	- untranslated region
vDC	- ventral diencephalon
WT	- wild-type

Table of Contents

List of Figures

List of Tables

Statement of Contributions

The experiments presented in this thesis were performed by myself. However, some contributions should be noted. Amanda Zhu-Pawlowsky, an undergraduate student who has worked during several terms under my supervision, has contributed to the results presented in Chapter 3, sections 3.1, 3.4, and 3.5 where she has conducted several experiments. Megan Jung, a former Master's student in our laboratory, has generated the *parlb* ^{d9k} CRISPR mutants I used in my experiments, and has contributed to the initial attempt of generating the mutation in the *parla* gene (results presented in Chapter 3, section 3.1.1). Finally, Michael Kalyn, a current Ph.D. candidate in our laboratory, has contributed to the results presented in Chapter 3, section 3.4.

CHAPTER 1. General Introduction

1.1 Rhomboid proteases

Rhomboid proteases are a type of enzymes that are found in all domains of life. They are intramembrane serine proteases that have their catalytic residues anchored in the lipid bilayer, thus these proteases can cleave membrane proteins within their transmembrane helices. Intriguingly, some eukaryotic rhomboid homologues lack catalytic residues (Lemberg and Freeman, 2007). Thus, it is now noted that a broader superfamily of rhomboid-like proteins exists, consisting of rhomboid proteases and of catalytically inactive pseudoproteases (Freeman, 2014). Rhomboid proteases are one of the most characterized classes of intramembrane proteases (IMPs) which also comprise metallo IMPs, aspartyl IMPs, and glutamyl IMPs (Langosch et al., 2015; Urban and Dickey, 2011).

The first rhomboid gene was characterized in *Drosophila melanogaster* mutant screen, in which it was found that loss of *rhomboid-1* resulted in embryos having a pointed head skeleton phenotype (Jurgens et al., 1984). Subsequently, genetic analyses have shown that *Drosophila* Rhomboid-1 regulates epidermal growth factor receptor signaling in *Drosophila*. Rhomboid-1 was then identified by biochemical studies as an intramembrane serine protease (Lee et al., 2001; Urban et al., 2001). Bioinformatics analyses revealed that rhomboid proteases are found in all eukaryotes and most prokaryotes. Interestingly, all rhomboid-like proteins are characterized by the conserved core of six transmembrane helices known as the rhomboid fold, which is often extended by a seventh transmembrane helix connected to the N- or C-terminus (Figure 1.1A). In addition, the catalytic serine and histidine residues that constitute the rhomboid proteases active center are found in transmembrane helices 4 and 6 of the rhomboid fold, respectively. The rhomboid-like superfamily encompasses five rhomboid proteases, RHBDL 1-4 and PARL, as well as nine pseudoproteases in mammals (Figure 1.1B) (Adrain et al., 2011; Dusterhoft et al., 2017). In

mammals, five rhomboid proteases, RHBDL 1-4, are expressed in the secretory pathway and PARL in mitochondria (Lastun et al., 2016).

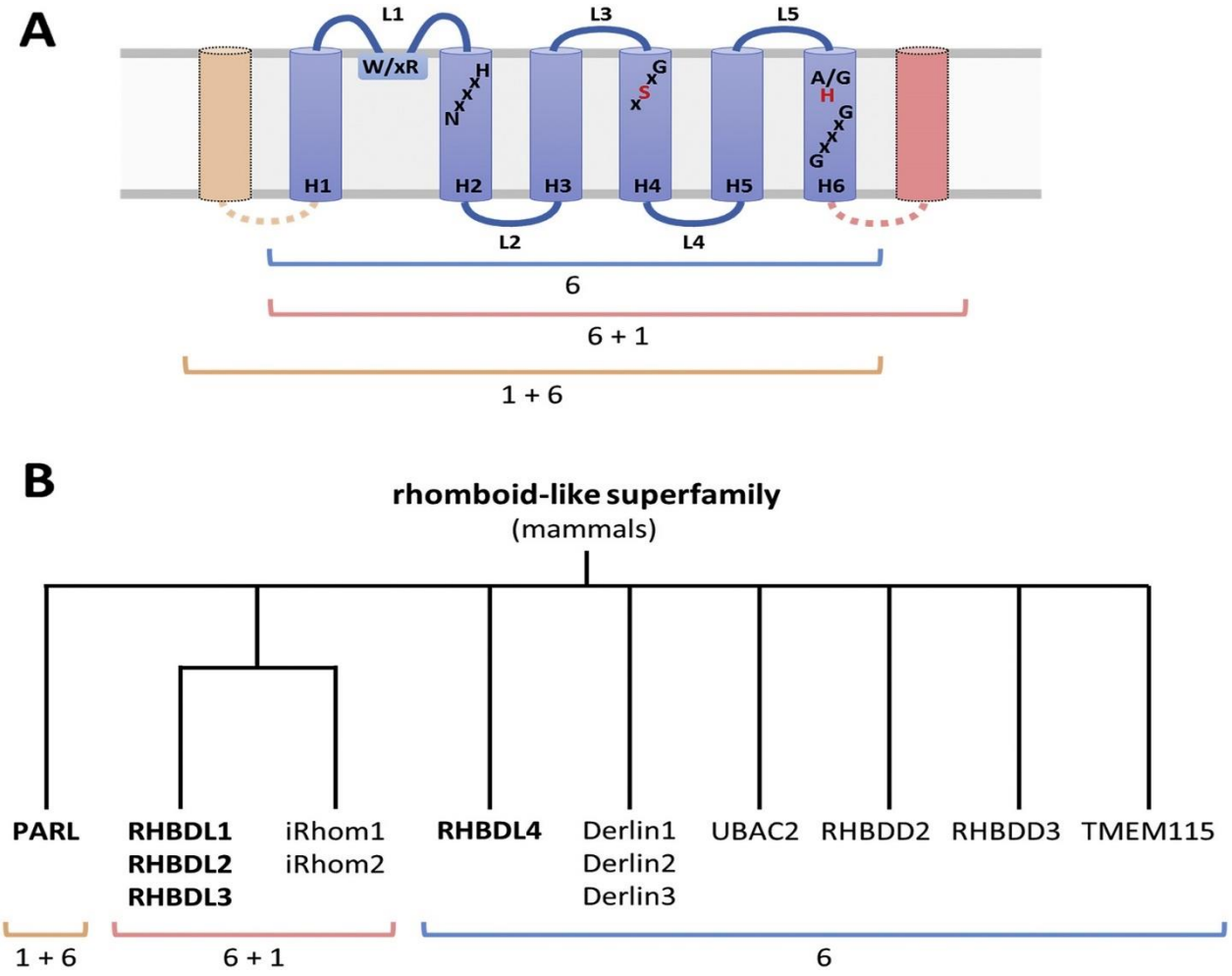

Figure 1.1. Topology of rhomboids in mammals. (A) Schematic representation of the three rhomboid topology classes as well as of the relative positions of the following evolutionary conserved motifs. The GxSx, A/GH, HxxxN, GxxxG and W/xR represent the conserved motifs. **(B)** Schematic representation of the different branches of the rhomboid superfamily in mammals with the corresponding rhomboid topology classes. Figure from Dusterhoft et al., 2017.

1.2 Presenilin-Associated Rhomboid-Like Protease (PARL)

PARL refers to the mammalian nomenclature for the mitochondrial rhomboid protease that is found in the inner mitochondrial membrane, and it is conserved in all eukaryotes. The mitochondrial rhomboids were initially studied in yeast. It was found that the PARL homologue Rhomboid-1 cleaves the membrane tethered GTPase Mgm1p, the yeast homologue of mammalian optic atrophy protein 1 (OPA1), leading to regulation of membrane fission and mitochondrial morphology. Eventually, PARL was studied in mammals intensively and was found to be involved in cleaving several mitochondrial membrane proteins, thus linking it to mitochondrial homeostasis and diseases involving mitochondrial dysfunction (McQuibban et al., 2003; Spinazzi and De Strooper, 2016). However, before identifying PARL as a mitochondrial rhomboid, it was thought that this protein was associated with Presenilin 2 involved in apoptosis, hence PARL's name (Pellegrini et al., 2001). Afterwards, it was shown that the link to presenilin was an artifact and that PARL is a mitochondrial resident protein (McQuibban et al., 2003) but its name was not changed.

PARL is a member of the rhomboid family of intramembrane serine proteases, and it is formed of a core of six transmembrane helices linked to an additional transmembrane helix at the N-terminus (Figure 1.2). This protein is found exclusively in the inner mitochondrial membrane, and like Rhomboid-1, has its C-terminus exposed to the inner membrane space, and N-terminus facing the matrix with a single-pass transmembrane domain joining the two as illustrated in Figure 1.2 (Jeyaraju et al., 2006). The basis for PARL intramembrane proteolytic activity is provided by conserved histidine, serine and asparagine catalytic residues that are contributed by different transmembrane helices (Jeyaraju et al., 2011).

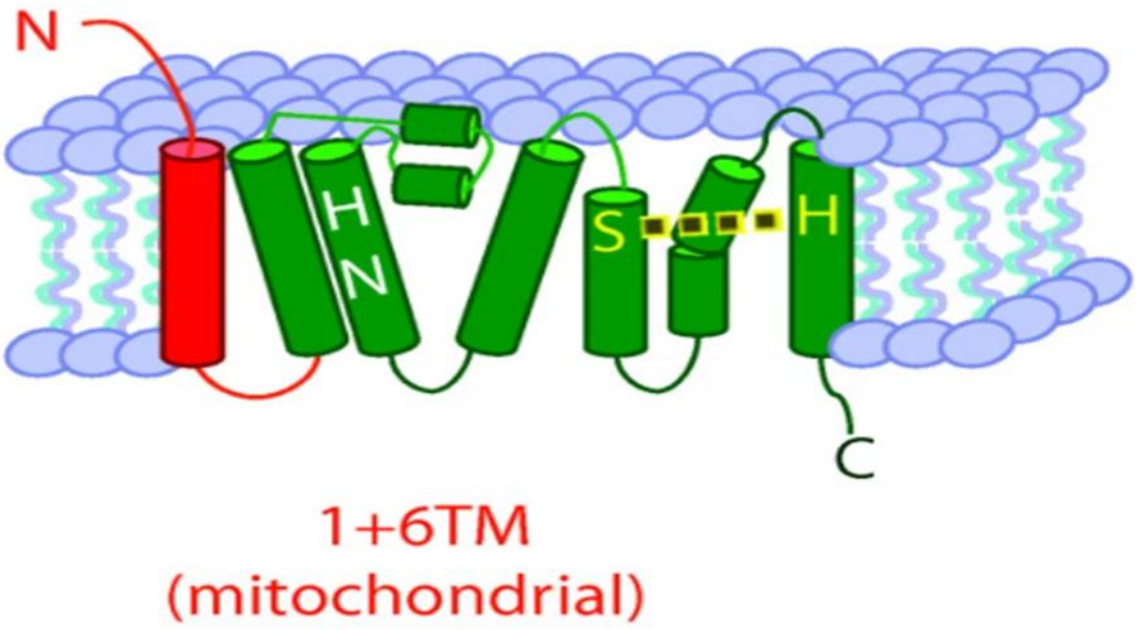

Figure 1.2. Topological form of PARL. Mitochondrial rhomboid protease structure showing an extra TM (1+6 transmembrane) segment added at the amino terminal (red) to the 6 TM core. Catalytic residues are in yellow for nucleophilic chemistry (hydrolysis) and white for electrophilic residues (oxyanion transition state stabilization). Cytoplasm is at the bottom side of the diagram. Figure from Urban and Dickey, 2011.

In mammals, PARL is characterized by a vertebrate-specific N-terminus, referred to as the Pβ domain (spanning amino acids 40-100) whose physiological function has not been identified yet but its biological importance is predicted because of strong sequence conservation in mammals. It was found that the vertebrate-specific N-terminus (Pβ) undergoes two consecutive cleavage events at amino acid positions 52-53 (α-site) and 77-78 (β-site). The α-cleavage is constitutive leading to the removal of the mitochondrial targeting sequence of PARL to generate the mature mitochondrial PARL protein (MAMP) and is thus associated with PARL's import into the mitochondria. The β-cleavage appears to be developmentally controlled and produces the PARL C-terminal protein (PACT), which results in fragmentation of the mitochondrial reticulum and

thus liberates the Pβ peptide (25 amino acid long) that gets exported to the nucleus to activate responses linked to mitochondrial biogenesis (Jeyaraju et al., 2011; Sík et al., 2004). Moreover, two *parl* paralogs were identified in zebrafish: *parla* and *parlb*. Interestingly, the Parla protein showed a 67% amino acid identity to human PARL, higher than for Parlb (55%). Despite that Parl proteins in zebrafish showed high sequence similarities to the mammalian PARL, the Pβ domain was not found to be conserved in zebrafish. Thus, it was hypothesized that the processing of the zebrafish Parl might not be similar to mammals and may not produce a Pβ peptide that is translocated to the nucleus (Noble et al., 2012). This study also suggested that proper dopaminergic (DA) neuron development depends on *parla* rather than *parlb* function.

1.3 PARL substrates

It is important to identify PARLs' substrates for the better understanding of the molecular functions of PARL. It should be taken into consideration that several substrates might be cleaved in different cells and tissues under different physiological conditions. This might explain some of the controversy seen in the field.

1.3.1 Optic Atrophy Protein 1 (OPA1)

By analogy with the yeast system, OPA1 is identified as a substrate for mammalian PARL (McQuibban et al., 2003). Several studies have shown that OPA1 interacts with PARL to inhibit unnecessary apoptosis. For instance, one study has found that overexpression of the soluble form of OPA1 rescues apoptosis seen in *Parl* knockout fibroblasts by counteracting the fast release of cytochrome c. This interaction between OPA1 and PARL was also identified in *Drosophila* and yeast, which indicates a conserved pathway. However, other studies have shown that PARL is not

crucial for OPA1 processing and that there are other proteases involved in OPA1 maturation. More recent studies identified the metalloendopeptidase OMA1 and the ATP-dependent zinc metalloprotease YME1L as the proteases cleaving OPA1 (Anand et al., 2014; Ishihara et al., 2006; Cipolat et al., 2006). Moreover, a recent study performed in 2019 by Spinazzi and colleagues could not confirm differences in OPA1 processing in *Parl*$^{-/-}$ mouse embryonic fibroblasts, suggesting that OPA1 is not a PARL substrate, in contrast to previous reports (Spinazzi et al., 2019). Taken together, these findings lead to the question whether OPA1 is indeed a substrate for PARL.

1.3.2 High Temperature Requirement A2 (HTRA2)

High temperature requirement A2, which is also known as Omiis the only known HtrA family member that is expressed in mammalian mitochondria. It has an important function in mitochondrial homeostasis, and it protects from neurodegeneration. During apoptosis, HTRA2 is released from the mitochondrial intermembrane space to the cytosol where it promotes cleavage of inhibitor of apoptosis proteins (IAPs). Several studies have shown that *HtrA2*$^{-/-}$ mice are characterized by severe subcortical neurodegeneration and increased apoptosis leading to lethality before the age of six weeks (Rathke-Hartlieb et al., 2002; Yang et al., 2003). These phenotypes seen in *HtrA2*$^{-/-}$ mice are similar to the ones identified in *Parl*$^{-/-}$ mice and the first evidence claiming that HtrA2 could be Rhomboid-7 substrate was shown in studies done in *Drosophila* (Whitworth et al., 2008). However, there is controversy in mammals as to whether HTRA2 is a PARL substrate. One paper has proposed that HtrA2 interacts with Parl via another protein which is Hax1. Another more recent paper claimed that HTRA2 is not a PARL substrate as differences in HTRA2 processing were absent in *Parl*$^{-/-}$ MEFs (Chao et al., 2008; Spinazzi et al., 2019). Therefore, whether HTRA2 is a PARL substrate remains an open question.

1.3.3 PTEN-Induced Putative Kinase 1 (PINK1)

PINK1 is a mitochondrial kinase expressed at the inner membrane and is known to regulate mitophagy and has a crucial role in the regulation of complex I activity. Previous studies have shown that when there's disruption of the electrochemical mitochondrial potential, PINK1 accumulates at the outer mitochondrial membrane. PINK1 then phosphorylates PARKIN and UBIQUITIN leading to autophagic engulfment of defective organelles (Morais et al., 2014; Shiba-Fukushima et al., 2012; Vives-Bauza et al., 2010). It is considered that defective mitophagy leads to the pathogenesis of PINK1-associated Parkinson's disease. Whitworth and colleagues claimed that PINK1 was a mitochondrial rhomboid substrate because *rhomboid-7* deficient flies have impaired Pink1 processing (Whitworth et al., 2008). Subsequently, several studies were done in mammals in which it was found that large PINK1 accumulation in mitochondria was seen after down regulation or deletion of PARL (Greene et al., 2012; Jin et a., 2010; Meissner et al., 2011).

1.3.4 Phosphoglyceromutase 5 (PGAM5)

PGAM5 is a phosphoglyceromutase enzymes member involved in the conversion of 3-phosphoglycerate to 2-phosphoglycerate in glycolysis. However, PGAM5 has lost its mutase activity during evolution and has a mitochondrial localization signal. It was shown that PGAM5 has developed Serine/Threonine (Ser/Thr) phosphatase activity (Takeda et al., 2009; Wang et al., 2012).

Sekine and colleagues provided the first evidence claiming that PGAM5 is a PARL substrate (Sekine et al., 2012). PGAM5 was shown to be resident of the inner mitochondrial membrane and in contrast to PINK1, an increase in PGAM5 proteolytic processing was detected during mitochondrial potential collapse (Sekine et al., 2012). Previous studies have found that after PARL

down regulation, PGAM5 processing is blocked which led to the accumulation of its unprocessed form. In contrast, overexpression of PARL resulted in an increase in processed PGAM5 levels (Urban and Wolfe, 2005).

1.4 Mitochondrial dynamics

Mitochondria are highly dynamic organelles present in most eukaryotes and undergo continual fusion and fission events to generate every cell's energetic requirements and execute a broad range of functions such as the synthesis of essential metabolites, the generation of adenosine triphosphate (ATP) in cells, Ca^{2+} homeostasis, the production of endogenous reactive oxygen species (ROS) and programmed and unprogrammed cell death (Mishra and Chan, 2016; Suen et al., 2008; Westermann, 2012). Bioenergetically impaired mitochondria are rescued by fusion with the healthy mitochondrial network, whereas severely damaged mitochondria are segregated through fission and then degraded by mitophagy (Twig et al., 2008). Several key proteins such as PINK1 and PARKIN have been found to play a major role in mitophagy (Narendra et al., 2010) and dysregulation of the PINK1/PARKIN pathway has emerged as a disease mechanism for neurodegenerative disorders, most notably Parkinson's disease (PD) (Pickrell and Youle, 2015).

Neurons are known to be extensively active, metabolically, and they have limited glycolytic capacity. Thus, neurons in the brain are energetically demanding cells that require mitochondrial function maintenance (Kann and Kovacs, 2007). Several studies claimed that mitochondrial dysfunction characterized by abnormal fusion, fission, and trafficking events, is one of the most documented abnormalities in all major neurodegenerative diseases (Lin and Beal, 2006). Due to their involvement in intermediate metabolism and the production of ROS,

mitochondria can rapidly turn on a death promoting cascade characterized by excessive ROS production, and resulting in the release of pro-death proteins, disrupted ATP synthesis, mitochondrial membrane depolarization and the activation of cell death pathways. Thus, cells have developed a defense mechanism against dysfunctional mitochondria through the selective sequestration and subsequent degradation of the aberrant mitochondrion before activation of apoptosis. This process of selective clearance of damaged mitochondria in cells is termed mitochondrial autophagy, or mitophagy (Kubli and Gustafsson, 2012).

In case of severe damage, mitochondria can also promote apoptosis. Apoptosis is a naturally occurring process by which a cell is directed to undergo programmed cell death and is crucial to the normal development and function of an organism. Apoptosis initiation signals can be intrinsic or extrinsic. The best known intrinsic pathway is through mitochondria dysfunction. The steps involved in this process start with an alteration in the mitochondrial membrane potential, production of ROS, opening of the permeability transition pore, and the release of the intermembrane space protein, cytochrome c which in turn activates the apoptotic peptidase activating factor 1 (Apaf-1), promoting a downstream caspase death program (Kubli and Gustafsson, 2012).

1.4.1 Mitochondrial fission

In mitochondrial fission, the key regulator is dynamin-related protein 1 (Drp1) which is a large GTPase mainly found in the cytosol. Several receptor proteins such as the mitochondrial fission 1 protein (Fis1), the mitochondrial fission factor receptor (Mff) and the mitochondrial dynamics protein (MiD48/51) promote the recruitment of Drp1 to the mitochondrial outer

membrane which will then oligomerize into a ring-like structure (Loson et al., 2013; Smirnova et al., 2001). Dyn2 which is another dynamin-like protein, was also found to regulate the last step of membrane division after Drp1 is recruited and polymerized (Gao et al., 2017; Lee et al., 2016) (Figure 1.3A). Fission events are important for the sequestration of severely damaged mitochondria by mitophagy (Kubli and Gustafsson, 2012).

1.4.2 Mitochondrial fusion

In mitochondrial fusion, both the outer and inner membranes are involved, and fusion regulation occurs via at least three large GTPase proteins: Mitofusin 1 (Mfn1) and Mitofusin 2 (Mfn2) that promote outer membrane fusion and OPA1 promoting inner membrane fusion (Santel and Fuller, 2001). Mitochondrial fusion is also dependent on these proteins self-assembly and GTPase activity. It has been suggested that outer membrane fusion is promoted through Mfn1 and Mfn2 coiled-coil domains interaction to form homo-oligomeric or hetero-oligomeric complexes to link the membranes together (Figure 1.3B). Fusion events are crucial for the rescue of bioenergetically impaired mitochondria by rejoining them with a healthy mitochondria network (Ishihara et al., 2004; Kubli and Gustafsson, 2012).

1.4.3 Mitochondrial trafficking

Pathological and physiological states can lead to mitochondrial transport to sites with bioenergetics requirements. There are two types of mitochondrial movements: one is along microtubules and is fast, and the other is along actin filaments and is slow. These types of movements are bidirectional (anterograde and retrograde) and are mediated by different motor-

adaptor complexes. Kinesin-1, dynein, Miro1 and 2 and Milton1 and 2 form the core of the motor-adaptor complex (Figure 1.3C,D). The anterograde motor kinesin-1 and the retrograde motor dynein/dynactin complex interact directly with mitochondrial Milton and Miro to drive their movement along the microtubules (Frederick and Shaw, 2007; Glater et al., 2006; Guo et al., 2005). In addition to movement along microtubules, actin filaments are also included in mitochondrial movement by the involvement of actin motors such as Myo2 and Myo19 (Altmann et al., 2008) (Figure 1.3E).

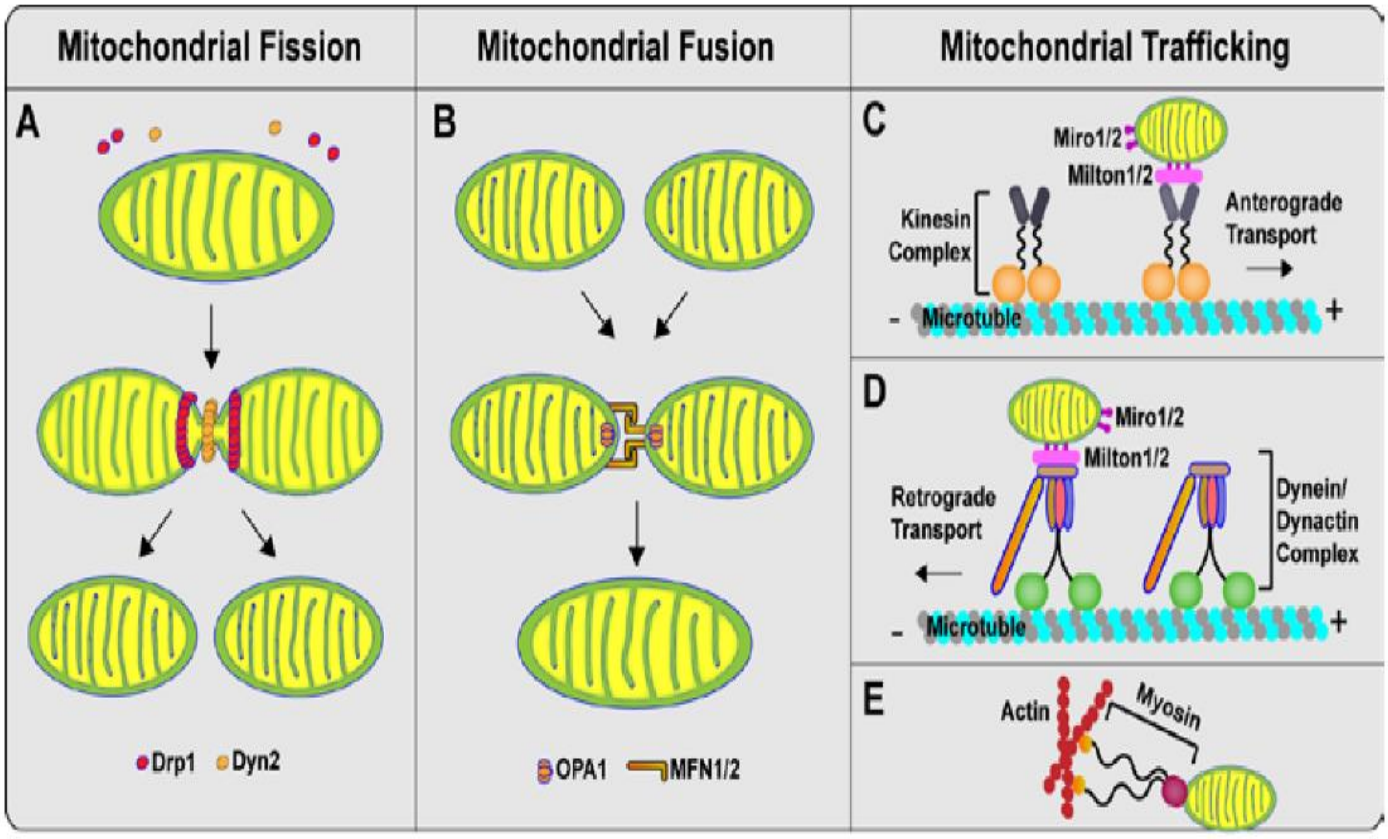

Figure 1.3. Graphical representation of mitochondrial dynamics in mammals. (A) Mitochondrial fission, (B) Mitochondrial fusion, (C-E) Mitochondrial trafficking. Figure from Gao et al., 2017.

1.5 Putative PARL functions

Mitochondrial rhomboid function was studied thoroughly in yeast but not in mammals. Thus, the knowledge of PARL functions in mammals remains limited and sometimes the present data are contradictory or deduced indirectly from the understanding of their substrates (Spinazzi and De Strooper, 2016).

1.5.1 Function of PARL in apoptosis

Several studies were previously done and have shown that *Parl*$^{-/-}$ mice are characterized by increased apoptosis rates. This increase was explained by a higher cytochrome c release that was noticed in cell cultures after treatment with pro-apoptotic stimuli. Another study has found that there was an increase in apoptotic markers in the striatum of mice treated with siRNA against Parl accompanied with ischemia (Cipolat et al., 2006; Yoshioka et al., 2013). OPA1, a dynamin-like mitochondrial GTPase, functions cooperatively in an intrinsic apoptotic mechanism, inhibiting cell death through stabilizing mitochondrial morphology. OPA1 is an anti-apoptotic protein, slowing the release of cytochrome c by controlling the shape of mitochondrial cristae, keeping the junctions between the intra-cristae tight. During apoptosis, the OPA1 heterooligomer is disrupted, leading to unraveling of the cristae and cytochrome c diffusion to the inner membrane space (Figure 1.4). As discussed above in section 1.3.1 and 1.3.2, soluble OPA1 and HTRA2 are prominent candidates that link PARL to apoptosis although it was not confirmed that they are direct substrates for PARL. PGAM5 has also been shown to be involved in apoptosis (Cipolat et al., 2006; Takeda et al., 2009) but it is still unclear whether abnormal PGAM5 processing is essential and sufficient to promote apoptosis in mice. It is hypothesized that other mechanisms

lead to the phenotypes seen in *Parl*$^{-/-}$ mice, however, the cause for the reduced life span and the chronic illness phenotypes seen in *Parl*$^{-/-}$ mice needs further investigation. Surprisingly, a recent study done by Spinazzi and colleagues suggested that the neurodegeneration observed in *Parl*$^{-/-}$ mice was associated with massive necrosis and not altered apoptosis (Spinazzi and De Strooper, 2016; Spinazzi et al., 2019).

1.5.2 Function of PARL in mitophagy

It was shown that PINK1 and PGAM5, which are mammalian PARL substrates, are involved in mitophagy, at least *in vitro* (Meissner et al., 2011; Wang et al., 2012). When mitochondria are depolarized, PINK1 processing by PARL is prevented as PINK1 remains at the outer membrane. This leads to the recruitment of PARKIN, an E3 ubiquitin ligase, promoting ubiquitination of its substrate which induces mitophagy (Figure 1.4). Several studies have claimed that PARL is a potential regulator of this canonical import pathway, suppressing mitophagy when inappropriate by proteolytically processing PINK1 in a mitochondrial membrane potential-dependent manner mitophagy pathway. However, this involvement is limited to *in vitro* studies (Greene et al., 2012).

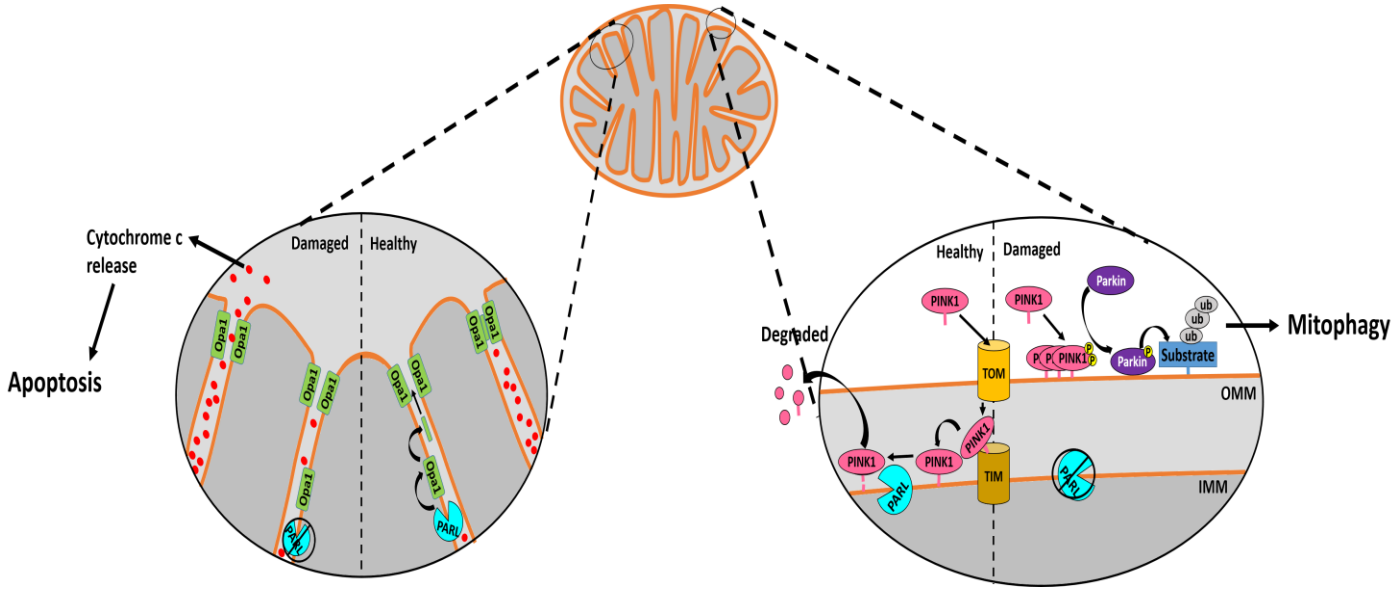

Figure 1.4. Schematic representation of PARL function in mammalian mitochondria. In a healthy mitochondrion, the cleavage of OPA1 by PARL prevents apoptosis. A damaged mitochondrion undergoes apoptosis following cytochrome c release to the inner membrane space. On the other hand, in a healthy mitochondrion, PINK1 cleavage by PARL prevents mitophagy. In a damaged mitochondrion, PINK1 accumulates at the outer leading to mitophagy. Figure from Cipolat et al., 2006.

1.6 PARL in Parkinson's disease

Parkinson's disease (PD) was first described by James Parkinson (Parkinson, 1817). It is considered now the second most common neurodegenerative disease, after Alzheimer's disease. PD is characterized by the progressive loss (degeneration) of dopaminergic (DA) neurons in the substantia nigra pars compacta and by the existence of intracytoplasmic inclusions (Lewy bodies) formed of α-synuclein in DA neurons. In general, PD is considered an idiopathic disease, with most of the cases being sporadic in nature and less than 10% of PD cases are due to well-defined environmental or genetic factors (Alexander, 2004). Interestingly, motor phenotypes of the few familial PD cases are somehow similar to the phenotypes of the sporadic cases, suggesting a commonality in their underlying mechanisms. Thus, we can imply that analysis of the rare genetic

forms of PD may promote better understanding of the pathogenesis of both sporadic and familial forms of PD.

Several genes were found to be involved in non-heritable PD including *α-synuclein*, *Parkin*, *DJ-1*, *Pink1* and *Lrrk2* (Cookson, 2005; Farrer, 2006; Klein and Schlossmacher, 2006; Whitworth et al., 2008). The first link between PARL and PD was established when Pink1 was found to be Rhomboid-7 substrate in *Drosophila* (Whitworth et al., 2008). Interestingly, it was found that a missense mutation, c.230G > A, existed in the *PARL* gene of two PD patients (Shi et al., 2011). This mutation promoted the substitution of a serine to an asparagine at codon 77 (p.Ser77Asn) and was found to be positioned in a phosphorylation site which is highly conserved in the PARL N-terminus and which plays a crucial role in regulation of PARL β cleavage (Jeyaraju, 2006; Shi et al., 2011). Intriguingly, two subsequent studies done on a high number of PD patients, failed to detect a c.230G > A mutation or other mutations in *PARL* gene, indicating that *PARL* mutations are a very rare genetic cause of PD (Heinitz and Klein, 2011; Wüst et al., 2015).

Since PARL plays a role in several pathways in response to mitochondrial dysfunction (as discussed earlier), including the PINK1/PARKIN mitophagy pathway, and the intrinsic apoptotic pathway, it has been proposed that PARL may lead to mitochondrial dysfunction in PD. However, the detailed etiology of PD with respect to PARL's role in DA neuron degeneration is still not well understood. Cipolat and colleagues have shown that *Parl* knockout mice present mild neurodegeneration in the thalamus and striatum (Cipolat et al., 2006). Interestingly, PARL deficiency only affects mice in early adulthood and since PARL is an anti-apoptotic protein that functions in OPA1 processing in mammals, it is suggested that PARL could be used for designing drug target for the control of apoptosis in adults with neurodegenerative disorders, such as PD.

Another link between PD and PARL was shown by the phenotypes seen in *Pgam5*$^{-/-}$ mice. These mice were characterized by neurodegeneration of DA neurons in the substantia nigra pars compacta at one year of age, and by a decreased level of dopamine and dopamine metabolites, in addition to locomotor impairment which was almost enhanced by L-DOPA therapy (Lu et al., 2014). In zebrafish, two *parl* paralogs have been identified: *parla* and *parlb* (Noble et al., 2012). Both *parl* transcripts were found to be expressed during embryonic development and in adult tissues. Morpholino-mediated knockdown of *parla* and/or *parlb* results in mild neurodegeneration supported by a decrease in DA cell numbers. In addition, the patterning of DA neurons is disrupted in the ventral diencephalon. Interestingly, overexpression of zebrafish *pink1* leads to the rescue of larval mortality and DA neurons abnormalities, suggesting that similarly to mammals and *Drosophila*, *parl* is genetically upstream of *pink1* (Noble et al., 2012).

1.7 Zebrafish model for mitochondrial-related diseases

The zebrafish, *Danio rerio*, is considered a good vertebrate model organism for studying human disease. This could be attributed to the high conservation of physiological functions and genetic information between zebrafish and humans, to the inexpensive and easy maintenance of zebrafish and to their short generation time (almost three months). Furthermore, zebrafish are characterized by high fecundity and by the optical clarity of their embryos which makes imaging and observation easier. Genetic manipulation in zebrafish is easy and efficient, especially for loss of gene function studies that can be attained by gene silencing techniques, including morpholino (MO) knockdown and transcription activator-like-effector endonucleases (TALENs).

Furthermore, many behavioral assays have been developed to investigate alterations in motor activity and sensory responses, particularly at the larval stages (Steele et al., 2014).

For mitochondrial-related diseases, zebrafish mitochondrial DNA (mtDNA) is 70% identical to human mtDNA and has the same complement of 37 genes (Broughton et al., 2001). In addition, strand-specific nucleotide and codon usage are conserved among the vertebrate mitochondrial genomes. Thus, modeling human mitochondria-related diseases in zebrafish, particularly PD, is considered a valid approach that can lead to further understanding the etiology behind these diseases.

1.8 Zebrafish DA system homology to humans

Zebrafish (*Danio rerio*) has emerged as a model for the study of movement disorders and neurodegenerative diseases. The neuronal circuitries involved in movement in zebrafish are well characterized, with essential molecular mechanisms being highly conserved and analogous to humans. It has been established that loss of DA neurons in zebrafish is associated with movement disorders, and it has been shown that DA neurons in the olfactory bulb (OB) carry sensory response to odor (Friedrich and Korsching, 1997; Metzger, 2019; Sebastian et al., 2012). Moreover, despite the remarkable anatomical differences between fish and mammals, it has been shown that more than 70% of all human disease genes have functional homologs in zebrafish (Robea et al., 2020). Zebrafish models of PD have and continue to contribute to our better understanding of familial PD.

There is conservation of several structural and functional characteristics of the zebrafish central nervous system (CNS) as compared to humans at the cellular, molecular and tissue level. Zebrafish are characterized for having a well-developed network of cerebral DA neurons. In the adult zebrafish brain, DA neurons have been described in the telencephalon, diencephalon, olfactory bulb, pretectum, and preoptic area. Despite notable differences, the zebrafish brain organization shows similarities to the human brain. In zebrafish, DA neurons are first detected at 18 h post-fertilization (hpf) in the ventral diencephalon (vDC) (Kimmel et al., 1995). At 3 days post-fertilization (dpf), the central nervous system is well developed. It has been previously suggested that clusters of DA neurons in the posterior tuberculum of the zebrafish brain vDC have ascending projections to the basal telencephalon of the subpallium and that these neurons are equivalent to the DA system found in the substantia nigra of the midbrain of mammals that have projections to the striatum (Rink and Wullimann, 2002). However, Tay and colleagues (Tay et al., 2011) have recently identified an endogenous DA system in the subpallium that provides most of the local DA projections and that also connects to the vDC. It has been suggested that the observed DA neurons in the subpallium indicate that a predominant telencephalic dopamine source in zebrafish may be derived locally (Tay et al., 2011).

Tyrosine hydroxylase (TH) is the rate-limiting enzyme in dopamine biosynthesis and an important marker of catecholaminergic neurons (Daubner et al., 2011). TH hydroxylates tyrosine to L-DOPA which in turn is converted to dopamine by aromatic amino acid decarboxylase (DCAA) (Figure 1.5). TH is commonly used in studies to label DA neurons. Two genes, *th1* and *th2*, encode the TH enzyme in zebrafish, and both Th1 and Th2 proteins are highly similar to the mammalian TH. Immunohistochemical analysis of Th1 was performed as it is widely expressed

in all brain regions, whereas Th2 is localized to hypothalamic, posterior tubercular, and preoptic regions of the zebrafish brain (Barrios et al., 2020; Candy and Collet, 2004; Vaz et al., 2018).

Intriguingly, the progression of the neural phenotype of PD symptoms cannot be followed *in vivo* in mammals, but it can be effectively studied in the zebrafish system, with familial PD being one of the most commonly modeled neurodegenerative mitochondrial diseases in zebrafish (Steele et al., 2014). Accordingly, zebrafish can represent a crucial model for improving our understanding of the pathogenesis of human mitochondrial diseases beyond the current state of knowledge and can contribute to the development of novel therapeutic approaches to treat these conditions.

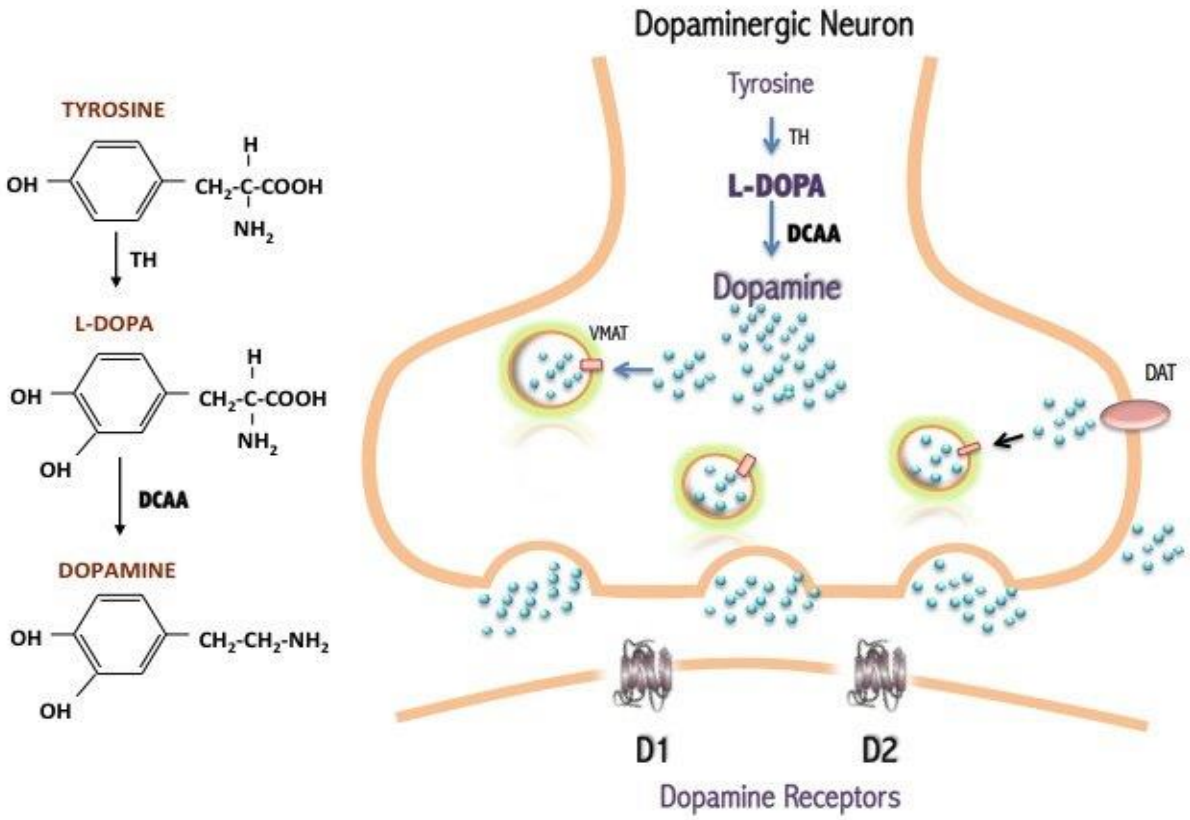

Figure 1.5. Graphical representation of the synthesis of dopamine from tyrosine in the dopaminergic nerve terminals. DCAA: aromatic acid decarboxylase; DAT: dopamine transporter; TH: Tyrosine Hydroxylase; D1: D1-like dopamine receptor; D2: D2-like dopamine receptor. Figure from Bravo et al., 2014.

1.9 The MPTP neurotoxin and its mode of action

The environmental neurotoxin 1-methyl-4-phenyl-1,2,3,6-tetrahydropyridine (MPTP) was first discovered by Langston and colleagues (1983) for its ability to induce parkinsonism in drug abusers that injected a drug containing MPTP intravenously. Since then, MPTP is one of the most widely used neurotoxins in PD animal models (Chia et al., 2020; Langston et al., 1983). Neurotoxin-based animal models induce the rapid neurodegeneration of nigrostriatal DA neurons which mimic the sporadic PD. MPTP is capable of crossing the blood-brain barrier (BBB) and is metabolized by monoamine oxidase B (MAO-B) in glial cells to the toxic form MPP^+ which in turn gets transported into DA neurons by the dopamine transporter (DAT) as it is structurally analogous to dopamine (Ramsay et al., 1991) (Figure 1.6). Following transportation of MPP^+ to DA neurons, it gets concentrated in the mitochondria, binds to NADH dehydrogenase, and leads to electron transport inhibition from NADH to CoA. MPP^+ results in the selective damage of DA neurons due to its inhibition effect on complex I which leads to the accumulation of ROS and the reduction of ATP synthesis (Yan et al., 2013).

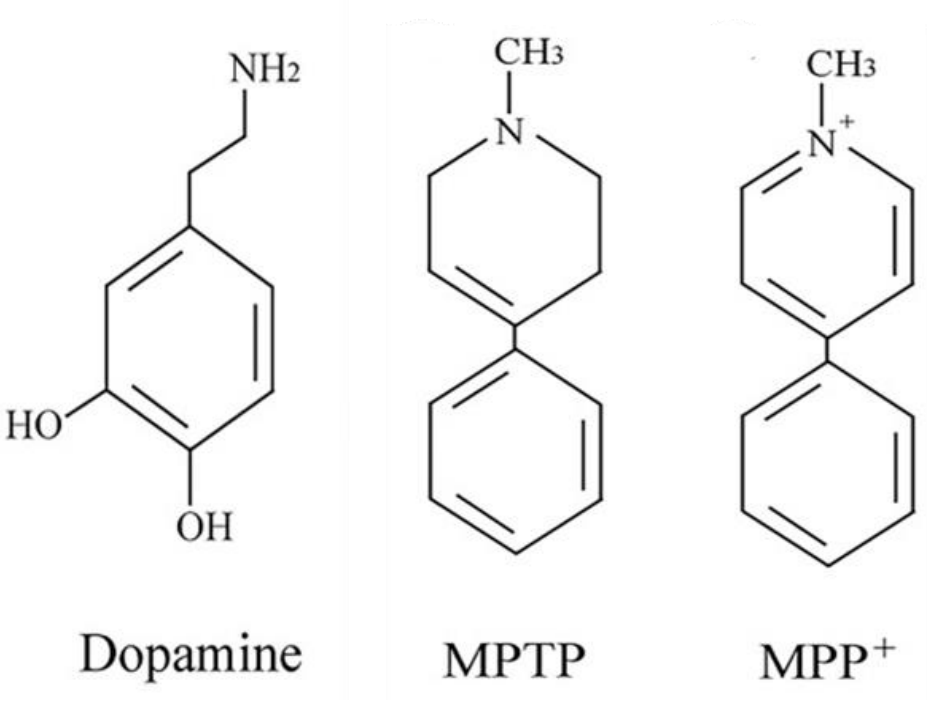

Figure 1.6. Structures of dopamine and some of the main neurotoxins used to reproduce features of PD in animal models. MPTP: 1-methyl-4-phenyl-1,2,3,6-tetrahydropyridine; MPP^+: 1-methyl-4-phenylpyridinium ion. Figure from Zeng et al., 2018.

1.10 MPTP zebrafish model of Parkinson's disease

The neurotoxin MPTP could replicate parkinsonism in a variety of species such as mice, primates, and humans, thus, MPTP administration to animal models is considered as a classical model of PD (Burns et al., 1985). Previous studies have shown that adult zebrafish displayed behavioral impairments following exposure to MPTP. Moreover, zebrafish larvae showed behavioral, developmental, and dopaminergic sensitivity to MPTP (Bretaud et al., 2004; Kalyn et al., 2019; Sarath Babu et al., 2016). Taken together, these findings suggest that zebrafish is a valuable model for the study of mitochondrial dysfunction in PD and the molecular mechanisms that underly neurotoxicity of PD-inducing agents.

1.11 CRISPR/Cas9 genomic editing

The clustered regularly interspaced palindromic repeat (CRISPR)-Cas9 nuclease system is an approach to genetic engineering, which promotes the ability to induce site-specific changes of endogenous genomic loci (Charpentier and Doudna, 2013; Zhang et al., 2014). This approach is different from the protein-guided DNA cleavage of the earlier strategies of genomic editing such as the zinc-finger nucleases (ZFNs) and the transcription activator-like effector nucleases (TALENs). CRISPR/Cas9 system mainly relies on small RNA for sequence specific cleavage of DNA, making it an easy approach for application and has already been found to successfully knockout a variety of genes in zebrafish and in other species (Zhang et al., 2014).

CRISPR-Cas9 genomic editing originates from the type II CRISPR-Cas system in bacteria and archaea as a form of adaptive immunity against viruses and plasmids (Jinek et al., 2012). Type II system uses a single CRISPR-associated protein (Cas)-9 containing a HNH nuclease domain and a RuvC-like nuclease domain. Following invasion, the foreign DNA is fragmented and inserted into CRISPR loci, then transcribed and processed into short CRISPR RNAs (crRNA). These crRNA anneal to trans-activating RNA (tracrRNA) and direct sequence specific silencing of foreign nucleic acids by Cas9 through the addition of site-specific double-stranded breaks in the target DNA (Jinek et al., 2012). These DNA breaks promote the activation of cellular DNA repair processes, including non-homologous end-joining (NHEJ)-mediated DNA repair which may generate desired insertions, deletions, or substitutions at the loci of interest. These mutations can lead to the alteration, or they can even abolish the function of target genes (Charpentier and Doudna, 2013; Zhang et al., 2014) (Figure 1.7).

Constraints on the range of targetable sequences are due to sequence requirements imposed by the T7 promoter used to make single guide RNAs (sgRNAs) (GG at the 5′ end of the transcript)

and by the requirement for a protospacer adjacent motif (PAM) sequence (NGG) in genomic DNA just at 3′ of the target site.

Several studies have successfully used the CRISPR/Cas9 system on zebrafish including a study performed by Hwang and colleagues (Hwang and Al, 2013). Their findings show that frequencies of mutagenesis do not appear to depend upon which DNA strand (sense or antisense) was targeted by the sgRNA, and as compared to ZFNs and TALENs, germline transmission of gRNA:Cas9-induced mutations is expected to be as efficient and the frequency of deformed or dead embryos similar but with an increased risk of off-target mutations. In addition, using Cas9 and several gRNAs with different target sites, CRISPR/Cas9 can simultaneously induce genomic alterations at several independent sites (Hwang and Al, 2013).

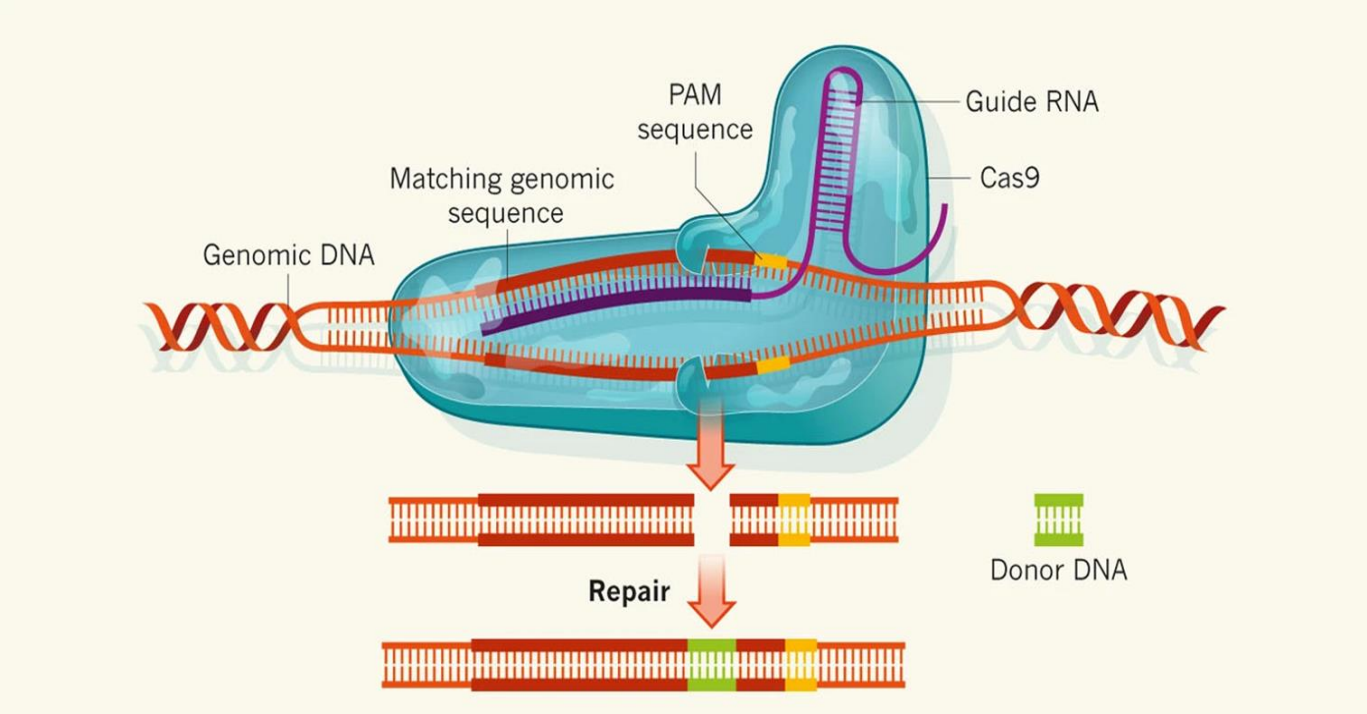

Figure 1.7. Graphical representation of the CRISPR/Cas9 mechanism. The guide RNA binds to the matching genomic sequence leading to Cas9 recruitment which induces double-strand breaks promoting the activation of the two types of repair mechanisms: Non-homologous end joining (NHEJ), and Homology-directed repair (HDR). Figure from Charpentier and Doudna, 2013.

1.12 CRISPR/Cas9 protocol for genome editing in zebrafish

The CRISPR/Cas9 type II system of *Streptococcus pyogenes* has been optimized and successfully used in vertebrate cells to edit genomes (Jinek et al., 2012; Zhang et al., 2014). The dual tracrRNA:crRNA complex has been engineered as a single guide RNA (sgRNA) containing all crucial crRNA and tracrRNA components permitting it to lead Cas9 cleavage of target DNA.

For zebrafish genome editing, the CRISPR/Cas9 system is the fastest and most convenient approach to induce deletions or insertions since laborious and time-consuming cloning steps can be avoided. Following the selection of one or multiple target sequences, oligonucleotides are designed through online software, followed by potential off-target site check (Figure 1.8A). The annealed and cloned sgRNA oligonucleotides are then transcribed and purified to be microinjected in zebrafish embryos at the one-cell stage (Figure 1.8B). To validate whether CRISPR/Cas9 mutagenesis was successful before proceeding to the subsequent steps, the mutation can then be detected through genotyping which involves PCR amplification of the DNA extracted from the injected embryos, followed by visualization of the predicted mutant and the wild-type (WT) bands on gel (Figure 1.8C). Once the mutation is detected and validated by sequencing, the injected embryos are raised to sexual maturity followed by F0 germline transmission detection which is performed by breeding the fish that might be carrying the expected mutation with a WT fish, followed by genotyping of the resulting offspring (Figure 1.8B,C). This can be performed at an early stage, for instance, 24 hours post-fertilization (dpf). Further selection and crossing are achieved until fish from the second generation (F2) are obtained. Phenotypic and functional analyses could then be conducted on the F2 mutant fish. The timing for the complete process described above can be accomplished within about 7 months in an ideal situation where the different steps were smoothly achieved (Gagnon et al., 2014; Hruscha and Schmid, 2015).

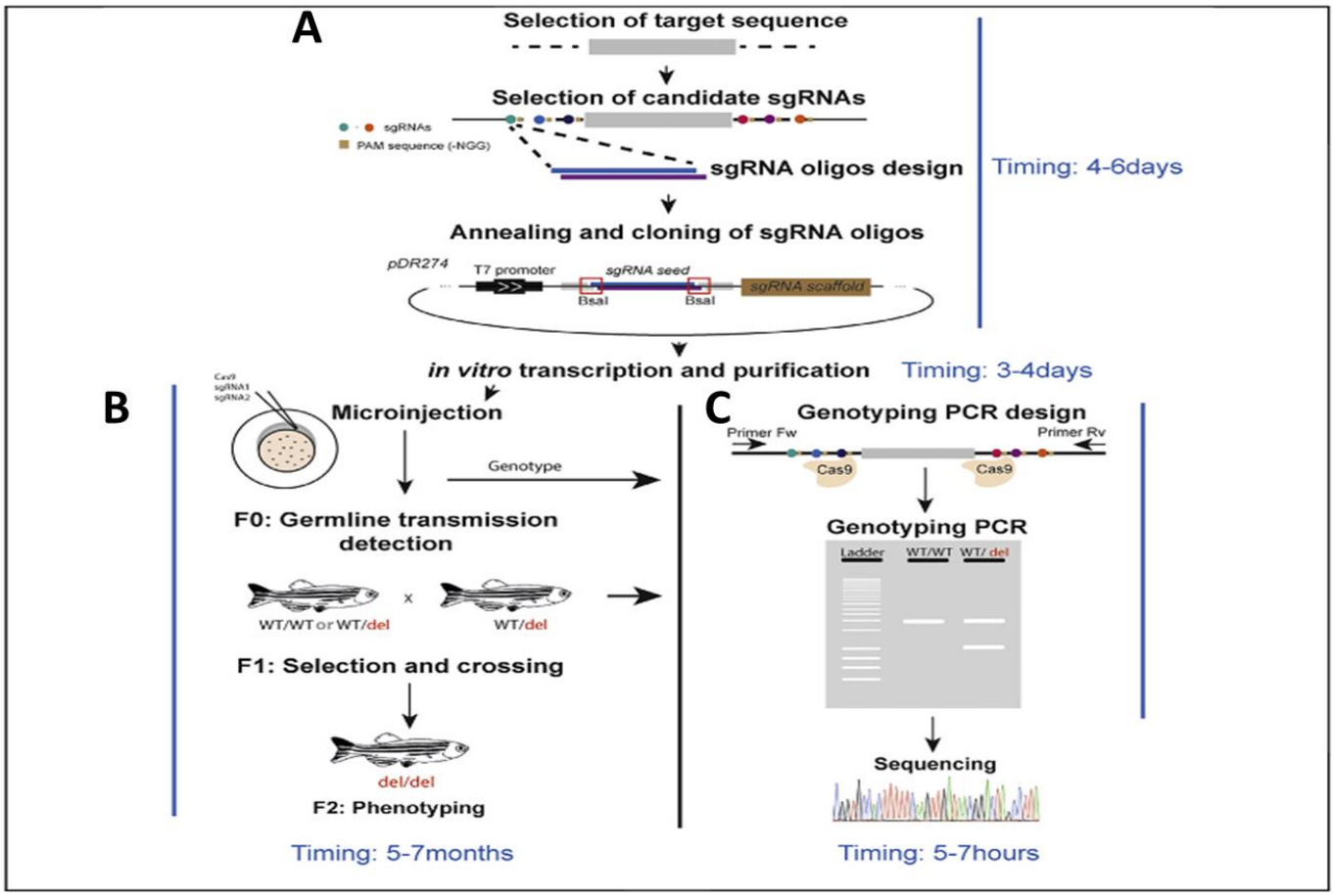

Figure 1.8. Graphical representation for the generation of zebrafish mutants by CRISPR/Cas9-mutagenesis. (A) Selection, design, and synthesis of sgRNA oligonucleotides. (B) Microinjection of the sgRNAs, genotyping and phenotyping. (C) Genotyping PCR design followed by sequencing. Figure from Hruscha and Schmid, 2015.

1.13 Statement of inquiry

Mitochondrial dysfunction has been implicated in the etiology of most PD pathologies. Defective mitochondrial form and function in the DA neurons of sporadic and familial PD is well known although the underlying mechanisms are still not clear. Zebrafish has emerged as a model for the study of movement disorders and neurodegenerative diseases as they possess high genetic similarities with humans as well as common neural circuitry and brain organization. Zebrafish models of PD have and continue to contribute to our better understanding of familial and sporadic PD.

PARL is a mitochondrial protein that is conserved across the different species and plays a crucial role in the regulation of mitochondrial dynamics and function. Mutation in the *PARL* gene was found to be a rare cause of the early onset of PD. The function of PARL is well studied and characterized in *yeast, Drosophila*, and mammals; however, it is poorly understood in vertebrates. A previous morpholino study performed by Noble and colleagues (2012) has identified two *parl* paralogs in zebrafish: *parla* and *parlb*. Morpholino-mediated knockdown of *parla* and/or *parlb* results in mild DA neurodegeneration and mis-patterning.

As the effects of the morpholino knockdown are transient and lasts for few days at the larval stages, and as *PARL* function remains to be fully characterized in zebrafish, particularly in the adult brain, we were interested in studying the effects of the heritable loss of *PARL* function. Thus, the overall goal of the research presented in this thesis is to establish *parla* and *parlb* knockout (KO) lines via CRISPR/Cas9 mediated mutagenesis to perform a functional analysis and characterization in zebrafish.

We hypothesize that if the zebrafish paralogs, *parla* and *parlb*, are implicated in the same processes and mitochondrial mechanisms as their mammalian homolog, *PARL*, then the loss of *parla* and/or *parlb* function may result in a decrease in DA neuron cell number in the adult brain, that this neuronal loss may translate to locomotor and behavioral impairing phenotypes, and that the loss of *parla* and/or *parlb* function may affect mRNA levels of functionally-related mitochondrial genes. We also predict that the loss-of-function of the paralogs will increase susceptibility of the mutants to environmental neurotoxin exposure.

In addressing the hypotheses postulated above and by better understanding the function of the two paralogs, *parla* and *parlb*, in adult zebrafish and larvae, we hope to contribute to the general knowledge of the molecular pathways and better understand the implication of *PARL* in the pathogenesis of PD.

CHAPTER 2. Material and Methods

2.1 Animal Care and Husbandry

All experiments were conducted using protocols approved by the University of Ottawa Animal Care Committee, and procedures were performed under the Animal Care and Veterinary Service guidance according to the Canadian Council for Animal Care ethical code BL-2081. Adult zebrafish were housed in circulating water systems at 28.5 °C under a 14 h light/10 h dark cycle. Embryos were obtained from the natural spawning of adult zebrafish. The embryonic stages were expressed in days post-fertilization (dpf) and adult stages in months post-fertilization (mpf).

2.2 CRISPR Design, sgRNAs Synthesis and Microinjections

A current zebrafish genome annotation (GRCZ11) in Ensembl was used for zebrafish gene coding and transcript information. For sgRNA design, CHOPCHOP software was employed (Montague et al., 2014). A published protocol from Gagnon et al. (2014) was followed to generate templates for sgRNA transcription by annealing gene specific oligonucleotides containing the T7 promoter sequence, the 20 base pairs (bp) target site (Tables 2.1,2.2,2.3) followed by the PAM sequence, and a complementary region of 80 bp constant oligonucleotide. For the 1.4 kb deletion in the *parla* gene (*parla* ^{ot510}), we synthesized three sgRNAs to be injected simultaneously to achieve multi-exon deletion. For the 15 kb deletion in the *parla* gene (*parla* ^{ot511}), we synthesized four sgRNAs and for the 17 kb deletion in *parlb* gene (*parlb* ^{ot512}), we synthesized four sgRNAs. All sgRNAs were transcribed using the MAXIscript T7 kit (Life Technologies), and the resulting RNA was purified using 5M ammonium acetate and ethanol precipitation. RNA bands were detected by electrophoresis on a 1% agarose gel and RNA purity and concentrations were measured using NanoDrop 1000 spectrophotometer (ThermoFisher, Waltham, MA, USA). Zebrafish embryos were microinjected at the 1-cell stage. An injection solution was prepared as follows: 40 ng/µL for each sgRNA, 20 ng/µL Cas9 protein (New England BioLabs), and 0.1% Phenol Red (Sigma).

Dead and deformed fish embryos were removed, and healthy ones were raised to adult fish as F_0 founders.

Table 2.1. List of target sequences of *parla* gene for sgRNAs generation and list of primers designed for amplification of *parla* ^{ot510} mutation.

Region Targeted	Target Sequence	Orientation
5′ UTR	GGCGCGCTGTGAGCCGGAAG	5′-3′
5′ UTR	GGAAAGCGCAGTTTTATGCA	5′-3′
Exon 2	GCCAAATGACTTGGTGGGCC	3′-5′
Primer	**Sequence (5'-3')**	
F	CTCCAACAGGAGCCGCTATG	
Rm	CTAGGGATTTTGTGCATGCTTAC	
Rwt	ATTCATTATCCTGACAGGCC	

Table 2.2. List of target sequences of *parla* gene for sgRNAs generation and list of primers designed for amplification of *parla* ^{ot511} mutation.

Region Targeted	Target Sequence	Orientation
5′ UTR	GGCGCGCTGTGAGCCGGAAG	5′-3′
5′ UTR	GGAAAGCGCAGTTTTATGCA	5′-3′
Exon 9	GGACCAGGAGGTGGCAGCAA	5′-3′
Exon 9	GGTGACTGGAGGAGATAAAA	5′-3′
Primer	**Sequence (5'-3')**	
F	CTCCAACAGGAGCCGCTATG	
Rm	ACATTTAAACTCGGGGGCAG	
Rwt	ATTCATTATCCTGACAGGCC	

Table 2.3. List of target sequences of *parlb* gene for sgRNAs generation and list of primers designed for amplification of *parlb* ^{ot512} mutation.

Region Targeted	Target Sequence	Orientation
Exon 1	GGAGGAGCTGCTTCATGAAA	5′-3′
Exon 9	GGATATTGCCGGTCTACTTT	3′-5′
Exon 10	GGCAGACCTGGACCAGGTGG	3′-5′
3'UTR	GGGGAACGTTACACACACAA	3′-5′
Primer	**Sequence (5'-3')**	
F	AAAACACTGTCCCGAGTTGC	
Rm	AAAGCAGGACCGTTTTAAACAA	
Rwt	ACCCTTGGTAGCGTTTACCC	

2.3 Description of parla and *parlb Mutations*

Two of the three simultaneously injected sgRNAs resulted in the deletion of 1.4 kilobases (kb) corresponding to the region that spans exon 1 to exon 2 (EX1_2del according to the Nomenclature for the description of sequence variations (den Dunnen and Antonarakis, 2001)) in the genomic DNA sequence of the *parla* gene (Results section Figure 3.1). Based on the Zebrafish Information Network (ZFIN) nomenclature conventions, we named the resulting mutant line *parla* ^{ot510}. Four simultaneously injected sgRNAs resulted in the deletion of 15 kb corresponding to the region that spans exon 1 to exon 9 (EX1_9del) in the genomic DNA sequence of the *parla* gene (Results section Figure 3.10). We named the resulting mutant line *parla* ^{ot511}. Four simultaneously injected sgRNAs resulted in the deletion of 16.6 kb corresponding to the region that spans exon 1 to exon 10 (EX1_10del) in the genomic DNA sequence of the *parlb* gene (Results section Figure 3.13). We named the resulting mutant line *parlb* ^{ot512}.

For genotyping, genomic DNA was extracted from fins followed by PCR amplification using forward (F) and reverse (Rm) primers that flank the target sites to amplify the mutant band and another reverse primer (Rwt) that binds to the region between the target sites to amplify the WT band (primer sequences are listed in Table 2.1,2.2,2.3). PCR products for the mutant and WT were separated by gel electrophoresis on a 1% agarose gel and sizes of the resulting bands for the *parla* ^{ot510} line were 500 bp for wild type and 350 bp for the mutant. For the *parla* ^{ot511} line, sizes of the resulting bands were 500 bp for wild type and 250 bp for the mutant. For the *parlb* ^{ot512} line, sizes of the resulting bands were 300 bp for wild type and 275 bp for the mutant. Deletion was further confirmed by Sanger sequencing and sequencing data showed that deletion junctions resulted from the precise ligation of the blunt-ended double-strand breaks (DSBs) created by Cas9; each DSB occurred exactly 3 bp upstream of the PAM sequence.

2.4 PAGE Assay for parlb ^{d9k} Mutant Line

A 5-nucleotide deletion in exon 1 of the *parlb* gene was previously achieved by CRISPR/Cas9 mutagenesis (Jung, 2017). One sgRNA was injected in 1-cell stage embryos that resulted in a premature termination codon in the amino acid sequence (at codon 39). The first amino acid affected by the mutation was located at residue 9, converting a Lysine (K) to an Aspartic acid (D) and thus, the mutant line was termed *parlb* ^{d9k} (Jung, 2017). To detect the 5-nucleotide deletion, genomic DNA was extracted from zebrafish caudal fins or embryos and PCR amplified using primer pairs as listed in Table 2.4. After being denatured for 5 min and left for 5 min at 25°C to re-anneal, PCR products were subjected to 10% polyacrylamide gel electrophoresis (PAGE) at 150 V for 60 min. PAGE gels were stained for 30 minutes in solution containing Tris/borate/EDTA (TBE) and 0.15% RedSafe (Fischer Scientific). Gels were washed 2x15 min in TBE buffer and visualized.

Table 2.4. List of primers designed for amplification of *parlb* ^{d9k} mutation.

Primer	Sequence (5'-3')
F	AAAACACTGTCCCGAGTTGC
R	AAAGCAGGACCGTTTTAAACAA

2.5 Collection of Zebrafish Brain Tissue

Zebrafish brain tissue was collected from both male and female fish and results were pooled together as no gross morphological differences were observed between brains of the two sexes. Adult fish were euthanized on ice in system water followed by immediate decapitation. The whole head was fixed in 4% PFA/PBS overnight at 4 °C. After dissection, brains were placed for additional 20 min in PFA for post-fixation. The tissue was washed with PBS and then immersed in 30% sucrose/PBS overnight at 4 °C. Whole brains were incubated in a solution of 1:2 30%

Sucrose: OCT Compound (Tissue-Tek, VWR Canada) for 10 min, placed in cryomolds, and frozen in liquid nitrogen. Cryosections of 18 μm were obtained with a CM3050S cryostat (Leica, Concord, ON) in quadruplicate slides.

2.6 Histology and Immunohistochemistry (IHC)

Sections were first allowed to rest for 30 min at room temperature, and then an antigen retrieval protocol was performed. Sections were treated for 20 min at 85 °C in 0.01M sodium citrate/0.05% Tween-20 solution and cooled down to room temperature (RT) for 15 min prior to blocking. Sections were then rehydrated in PBST (PBS with 0.1% Tween-20) and blocked in 10% fetal bovine serum in PBST for 2 h at RT. The primary antibody that binds to tyrosine hydroxylase (TH) (mouse anti-TH, Temecula, CA; Cat No. AB318) diluted 1:450 was used according to the manufacturers' instructions and protocol optimization. The primary antibody incubation was carried out overnight at 4 °C in 1% fetal bovine serum in PBST. Sections were then washed 3× for 5 min with PBST and incubated in the dark for 2 h at room temperature with the secondary antibody (goat anti-mouse IgG Alexa 488; Thermo Fisher Scientific, Cat No. A-11001) diluted 1:1000. Slides were finally washed in PBST and mounted using Vectashield mounting media (Vector Labs, Burlington, Canada). Images were acquired with either an Olympus FV1000 Confocal microscope or a Zeiss AxioPhot Fluorescence Microscope. Acquired images were processed using Olympus Fluoview Software or ImageJ. Cell counts were obtained from Z-stacking images acquired from several planes to form a composite 3-Dimentional (3D) set of data for each tissue sample. The images combined at different focus distances give a resulting image with a greater depth of field than any of the individual source images. Four to 5 tissue samples of comparable planes and areas were counted throughout the olfactory bulb (OB) and telencephalon and were averaged for each fish. Relative TH+ cell counts were calculated by comparing the

summed average number of TH+ cells with WT. Confocal images show representative single planes.

2.7 RNA Isolation, cDNA Synthesis and qRT-PCR

Total RNA was extracted from the dissected whole brain of each adult fish using homogenization with TriZol (InVitrogen, ThermoFisher, Waltham, MA, USA) according to manufacturer's protocol. The same homogenization technique and protocol were used for total RNA extraction from pooled larvae and total RNA was extracted from three biological replicates which were the result of three different breedings. Concentration and purity of extracted RNA were obtained using NanoDrop 1000 spectrophotometer (ThermoFisher, Waltham, MA, USA). Synthesis of cDNA was accomplished using the iScript™ cDNA Synthesis Kit (Life Science Research, Bio-Rad, St Laurent, QC, Canada) following the manufacturer's protocol. qRT-PCR reactions were constituted of 5 µL SsoFast™ EvaGreen® Supermix (Bio-Rad), 0.4 µL forward primer, 0.4 µL reverse primer, 0.2 µL nuclease-free water, and 4 µL cDNA. Reactions were performed in triplicates using the Bio-Rad CFX96 instrument. Normalized quantification of the number of *parla, parlb, th1, dat, opa1, pink1, mfn1,* and *fis1* transcripts was achieved through the comparative Cq (ΔΔCq) method using three reference genes: *Beta-Actin (β-Act), ribosomal protein l13a (rpl13a),* and *elongation factor 1 alpha (ef1a)*. The difference between the Cq values (ΔCq) of the gene of interest and the reference gene was calculated for each experimental sample. Then, the difference in the ΔCq values between the experimental and control samples (ΔΔCq) was calculated. The fold-change in expression of the gene of interest between the two samples is equal to $2^{\wedge(-\Delta\Delta Cq)}$. A standard curve for each gene of interest was performed and primer efficiency was automatically generated by the Bio-Rad CFX96 software and was found to be between 86 and 110 %. Efficiency values below or above that range were discarded, and conditions such as primer concentrations or annealing

temperature were then optimized to get better efficiency values. Oligonucleotide primers' sequences are listed in Table 2.5.

Table 2.5. List of primers designed for qRT-PCR.

Primer	Forward Sequence (5′-3′)	Reverse Sequence (5′-3′)
parla	GTGTTTTGTTGTTGGCGGGT	ATGTAGACAGCAGCATCGG
parlb	ATCACGCAGCACATCTTCCT	TATTAGTGGCTCGCGCTTCC
th1	GACGGAAGATGATCGGAGACA	AGAAATCGGAACATGGCGG
dat	AGACATCTGGGAAGGTGGTG	ACCTGAGCATCATAGAGGCG
opa1	GCTTGAGCCCTTGGAAAAGGAA	TGGCAGGTGATCTTGAGTGTTGT
pink1	GGCAATGAAGATGATGTGGAAC	GGTCGGCAGGACATCAGGA
mfn1	CTGGGTCCCGTCAACGCCAA	ACTGAACCACCGCTGGGGCT
fis1	CCCTGAACCTTCCAGTGTTT	GTCTCTGGAAACGGGTCCTT
β-Act [1]	CGAGCTGTCTTCCCATCCA	TCACCAACGTAGCTGTCTTTCTG
rpl13a [1]	TCTGGAGGACTGTAAGAGGTATGC	AGACGCACAATCTTGAGAGCAG
ef1a [1]	CTGGAGGCCAGCTCAAACAT	ATCAAGAAGAGTAGTACCGCTAGCATTAC

[1] Reference: Tang et al. (2007).

2.8 Swimming Activity

The effects of DA neuron loss on motor function were addressed in adult zebrafish. Fish were allowed to acclimate by swimming freely for a 2-min period in individual static tanks, followed by a 5-min recording period. The parameters analyzed for behavioral assessment were total distance travelled by the fish, average velocity, and inactivity duration. Swimming activity was recorded using the ZebraLab software and the ZebraCube tracking system (ViewPoint Life Science, Lyon, France). The tracking system consists of LED lights, infrared illumination, and a mounted camera for recording swimming under dark and light conditions.

2.9 Olfactory Function

Olfactory function was tested according to Godoy et al. 2020. Briefly, tanks used for this experiment were customized and contained a mid-tank division which divided the tank into a neutral zone, and left and right arms. Each adult zebrafish was allowed to swim freely in the tank for 2 min prior to the addition of the repulsive stimulus cadaverine (Sigma-Aldrich) (80 µL of 1 mM stock solution) to the arm where the fish was located. The time spent in each area was recorded for another 3 min. This elapsed time was sufficient to allow the stimulus to diffuse throughout one of the tank's arms without reaching a different tank area. The ratio of time spent in the stimulus arm was calculated post-stimulus by dividing the percentage of time spent in stimulus by the total recording time. Cadaverine was delivered with a micropipette into the rearmost portion of the arm. Control animals received the same volume of system water.

2.10 Environmental Toxin Preparation and Exposure

At 3 dpf, larvae were sorted and placed into each well of a 6-well plate in a solution volume of 3 mL (according to Kalyn et al., 2019). De-chorionated larvae were treated at 3 dpf until 7 dpf at room temperature (~23 ºC) . Five different concentrations were chosen to determine an accurate lethal dosage (0.1, 0.25, 0.5, 1 and 2 mM). MPTP solutions were only added at the first day of treatment and the solutions were not changed daily and replaced to avoid error and variation. The timeline for the treatment is illustrated in Figure 2.1. Toxins were discarded in accordance with current safety protocols. 1-methyl-4-phenyl-1,2,3,6-tetrahydropyridine hydrochloride (MPTP; C12H15N - HCl, Product: M0896, CAS: 23007-85-4, Sigma, Oakville, ON, Canada) was reconstituted in distilled water to a stock concentration of 500 mM. MPTP was further diluted to the working concentrations of 0.1 mM, 0.25 mM, 0.5 mM, 1 mM, and 2 mM. All treatments were conducted in the dark to avoid any photosensitivity.

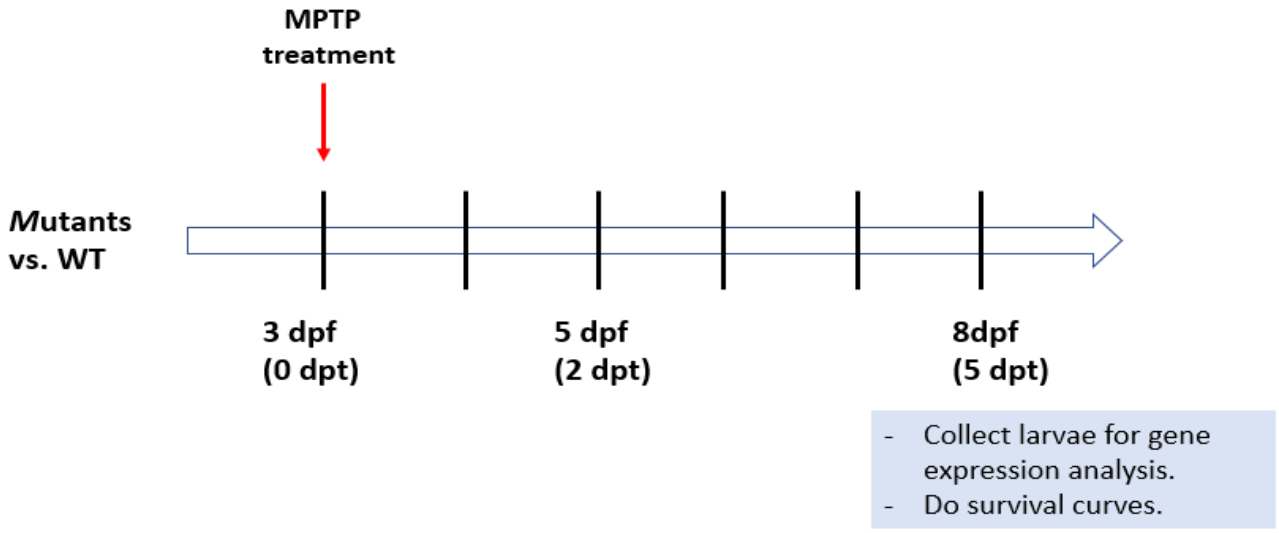

Figure 2.1. MPTP treatment timeline. Larvae at 3 days post-fertilization (dpf) were treated with 0.1, 0.25, 0.5, 1 or 2 mM of MPTP. At 5 days post-treatment (5 dpt), treated larvae were collected for subsequent analyses.

2.11 Acridine Orange Staining

Live embryos were stained with 10 µg/mL of acridine orange (3,6- Bis(dimethylamino)acridine hydrochloride zinc chloride double salt; Sigma-Aldrich, St Louis, MO, USA) in embryo media for 60 min in the dark at room temperature (~23 ºC). Embryos were washed three times with fresh embryo media, anesthetized in 0.2 mL of 0.4% tricainemesylate (ethyl 3-aminobenzoate methanesulfonate; Sigma-Aldrich, Oakville, ON, Canada) and visualized under a Leica fluorescent dissection microscope. At least 10 embryos were examined from each group.

2.12 Statistical Analysis

Statistical analysis was performed using the software GraphPad Prism v.7 (San Diego, CA, USA). DA neuron loss was analyzed using a two-way ANOVA followed by Tukey's multiple comparison

test. Gene expression data were analyzed using a multiple *t*-test comparison followed by Holm-Sidak method to determine significance. The total distance, average velocity, and inactivity duration were analyzed using a one-way ANOVA followed by Dunnett's multiple comparison test. Zebrafish olfactory function statistical power was assessed using multiple comparison *t*-test with Holm–Sidak post-hoc correction. Data are shown as the mean ± standard error of the mean (SEM) or as the median with 95% confidence intervals (CI). When the number of data points (*n*) is lower than 10, only the data and median are shown. When $n > 10$, error bars are included (Goedhart, 2017). Statistical significance was determined when p-value < 0.05 and was indicated as * $p < 0.05$, ** $p < 0.01$, *** $p < 0.001$.

CHAPTER 3. Results

3.1 Generation of mutant lines with loss of *parla* and/or *parlb* function by CRISPR/Cas9 mutagenesis.

Some of the results described in Chapter 3, more specifically in sections 3.1.2, 3.2.1, 3.2.2, 3.3.1, 3.4.1, and 3.4.2 were published in Merhi et al., 2021 (Merhi, R.; Kalyn, M.; Zhu-Pawlowsky, A.; Ekker, M. Loss of *parla* Function Results in Inactivity, Olfactory Impairment, and Dopamine Neuron Loss in Zebrafish. *Biomedicines* **2021**, *9*, 205. https://doi.org/10.3390/biomedicines9020205)

3.1.1 Initial attempt

To study long-term effects of *parla* and *parlb* functional deficiency in a germline-transmitting mutation model, we used CRISPR/Cas9-induced mutagenesis to generate *parla* and/or *parlb* mutants. Mutants with loss of *parlb* function having a 5-nucleotide deletion that resulted in a frameshift mutation were previously generated in the lab.

To generate *parla* mutants, we used ZiFiT software where we identified the highest-scoring target for the *parla* sequence. However, the *parla* gene sequence in the zebrafish population raised at our fish facility showed the presence of a single nucleotide polymorphism (SNP) in the selected *parla* target sequence (GGGGTTTAG^{T}TGTTGTTCAGG). For that, we designed two guide RNAs (sgRNAs) complementary to two adjacent target sequences located in the 5' untranslated region (5'UTR) of the *parla* gene and microinjected them simultaneously along with Cas9 protein in approximately 200 one-cell stage embryos. These primary injected fish were raised to sexual maturity (~3 months old) and bred with WT fish. We then genotyped their embryos to determine whether the mutation was transmitted though the germline. To assess germline transmission efficiency, 10-15 embryos from each founder fish were collected at 24 hours post-fertilization (hpf). We determined germline transmission efficiency from each founder fish to be 0% for the two *parla* sgRNAs used (n=15). In other words, primary injected fish produced 100% WT offspring when bred to WT fish. Thus, we considered that generation of *parla* mutants was not successful.

We then decided to modify our mutagenesis approach by switching from inducing deletions of a few nucleotides to inducing a multi-exon deletion. Using ZiFit and CHOCHOP software, we designed 4 sgRNAs complementary to two target sites in the 5'UTR, one target site

in exon 2 and one target site in exon 3 (Figure 3.1). The list of target sequences without the PAM site is shown in Table 3.1 below.

Table 3.1. List of target sequences in *parla* gene for sgRNAs generation.

Region Targeted	Target Sequence	Orientation
5′ UTR	GGCGCGCTGTGAGCCGGAAG	5′-3′
5′ UTR	GGAAAGCGCAGTTTTATGCA	5′-3′
Exon 2	GCCAAATGACTTGGTGGGCC	3′-5′
Exon 3	GGCTGGACAAAGTTCGCCCC	5′-3′

The deletion of exon 1 to exon 3 would result in the loss of the translation start codon and the mitochondrial localizing signal in Parla protein. The absence of a translation start codon might lead to no protein being synthesized unless an alternative start codon is used. We employed the same genotyping method used with the previously injected sgRNAs. Primary injected fish raised to adulthood were bred with WT fish and their resulting embryos were genotyped at 24 hpf to check whether the predicted mutations would be transmitted to the germline (Ekker et al., 2016). The efficiency was determined to be 40% and was further confirmed by sequencing. Founder fish that were positive for the somatic mutation were then bred to WT fish, then fish with germline transmission of the mutation were identified to generate F1 generation fish which were further fin clipped and genotyped.

3.1.2 Generation of a *parla* mutant line with exon 1 and 2 deletion (*parla* ^{ot510})

Following the simultaneous injection of sgRNAs that bind to the 5'UTR, and sgRNA that binds to exon 2 (Figure 3.1), 30 injected embryos were collected at 24 hpf followed by genotyping to confirm that the sgRNAs injected were successful in inducing the expected mutation in *parla* gene.

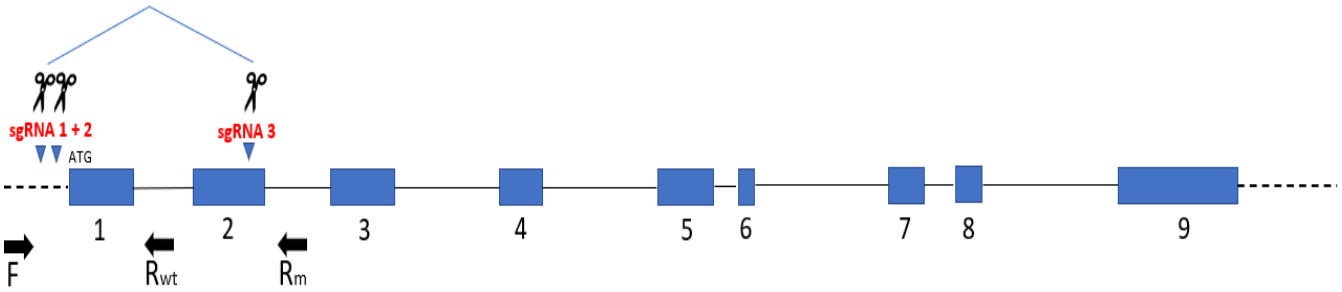

Figure 3.1. Exon 1 and 2 deletion in the *parla* gene by CRISPR/Cas9-mediated mutagenesis. The deleted region is indicated by the blue lines on top of sgRNA 1 and 3. Exons are represented with blue boxes and introns with black lines between the exons. The dashed line represents the 5'UTR and 3'UTR region. Primers used in genotyping are represented by F (forward primer), Rwt (reverse primer for the WT), and Rm (reverse primer for the mutant).

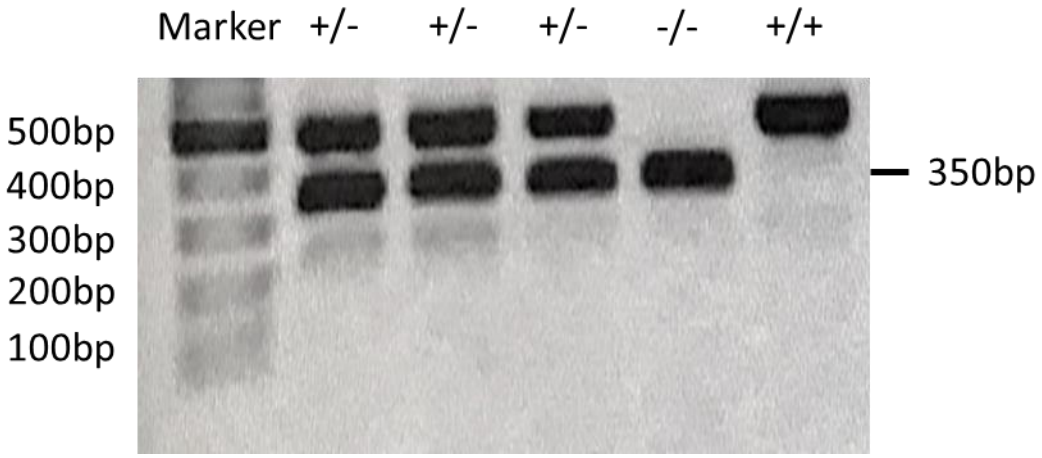

Figure 3.2 Detection of *parla* mutant bands in adult F2 offspring. Agarose gel showing WT band (500 bp) and mutant band (350 bp). The marker used is a 10 kb DNA ladder mix (GeneRuler^{TM}). +/+ refers to WT. +/− and −/− refer to heterozygous and homozygous mutants, respectively.

The mutant bands observed on agarose gel (Figure 3.2) were extracted, purified then sequenced using the reverse mutant primer (Rm) to confirm exon deletion in *parla* genomic sequence. Using NCBI BLAST, we compared the mutant sequence obtained by sequencing to the WT *parla* sequence that is flanked by the forward primer (F) and the reverse mutant primer (Rmut) (Figure 3.3). Therefore, we confirmed the deletion of around 1.4 kb in the *parla* gene. Based on cDNA sequencing data for the *parla* gene previously performed by Noble and colleagues (Noble et al., 2012) and based on Ensembl database, we obtained the cDNA sequence following deletion, then we determined the potential protein sequence using Expasy database (Swiss Bioinformatics Resource Portal). A deletion from the amino acid Methionine 1 to Arginine 71 (M1_R71del) is predicted to have occurred.

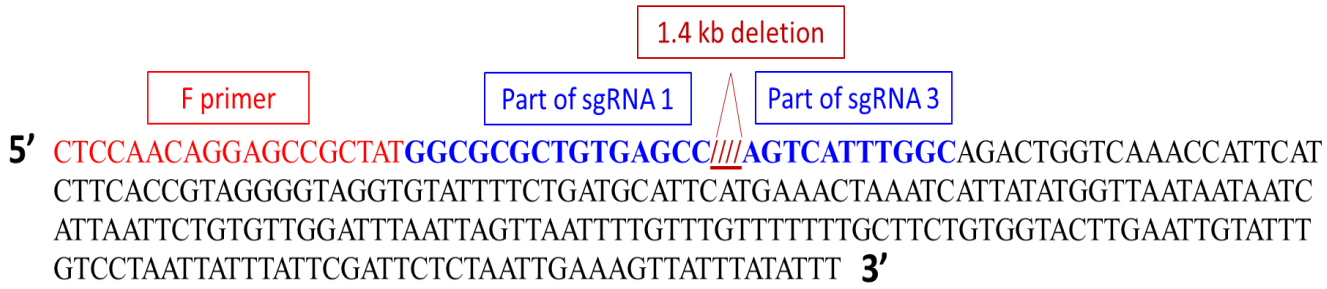

Figure 3.3. Schematic representation of *parla* nucleotides obtained by sequencing the 350 bp mutant band. The forward primer (F) is shown in red. Part of the sgRNA1 and 3 are shown in blue. The 1.4 kb deleted region is indicated by the red lines. The sequence shown is from the 5' to the 3' end relative to the transcribed region.

A slightly smaller deletion of 1.3 kb was also detected on gel and confirmed by sequencing (Figure 3.4). Sequencing results show that, similarly to the 1.4 kb deletion described above, the same nucleotides were deleted for the 1.3 kb deletion. However, we suspect that the DNA repair mechanism might have probably added around 100 nucleotides, thus, leading to a smaller deletion of 1.3 kb in the *parla* gene.

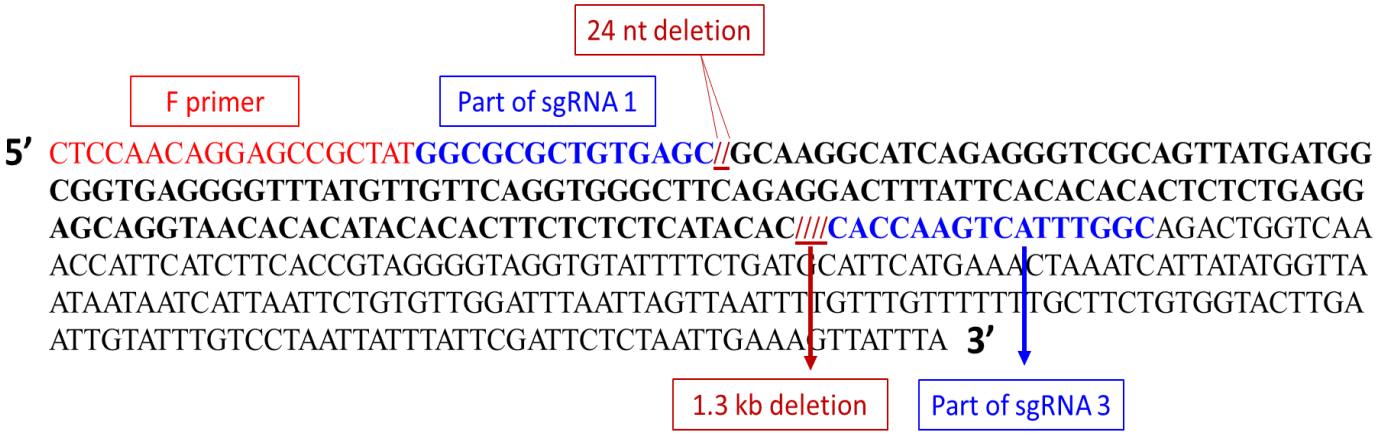

Figure 3.4. **Schematic representation of *parla* nucleotides obtained by sequencing the 400 bp mutant band.** The forward primer (F) is shown in red. Part of the sgRNA1 and 3 are shown in blue. A 24- nucleotide deleted region is indicated by the red lines besides sgRNA1. The 1.3 kb deleted region is indicated by the red arrow. The nucleotides shown in bold represent the unexpected region detected by sequencing. The sequence shown is from the 5’ to the 3’ end relative to the transcribed region.

To assess germline transmission efficiency, we bred founder fish with WT fish and genotyped around 30 of their embryos individually using the forward (F) primer and reverse mutant (Rmut) primers (Appendix Figures A.1,A.2,A.3). Furthermore, we bred one of the *parla* founder fish (founder 1) to *parlb* ^{d9k} homozygous fish to generate the *parlb*; *parla* double homozygous mutant line (Appendix Figure A.4). Germline transmission efficiency was then calculated as the number of mutant embryos over the total number of screened embryos. Germline transmission efficiencies for founder 1, 2, 3 and founder 1 bred to *parlb* ^{d9k} fish were calculated and found to be 15.15%, 23.33%, 16.67% and 15% respectively.

Following assessment of germline transmission efficiency, we raised the F1 fish to sexual maturity, genotyped them to isolate the heterozygous fish and then bred them together to get the F2 generation. We isolated homozygous, heterozygous and WT fish from the F2 generation by fin clipping followed by genotyping. The *parla* mutant line that resulted from founder fish 1 was referred to as *parla* ^{ot510}. We decided to use this mutant line in our future analyses.

Fish from the F1 generation that resulted from breeding founder 1 with *parlb* ^{d9k} homozygous fish were then fin clipped and genotyped (Figure 3.5). Knowing that the *parlb* mutation consisted of a 5-nucleotide deletion, we performed PAGE which could detect small indels (Figure 3.6).

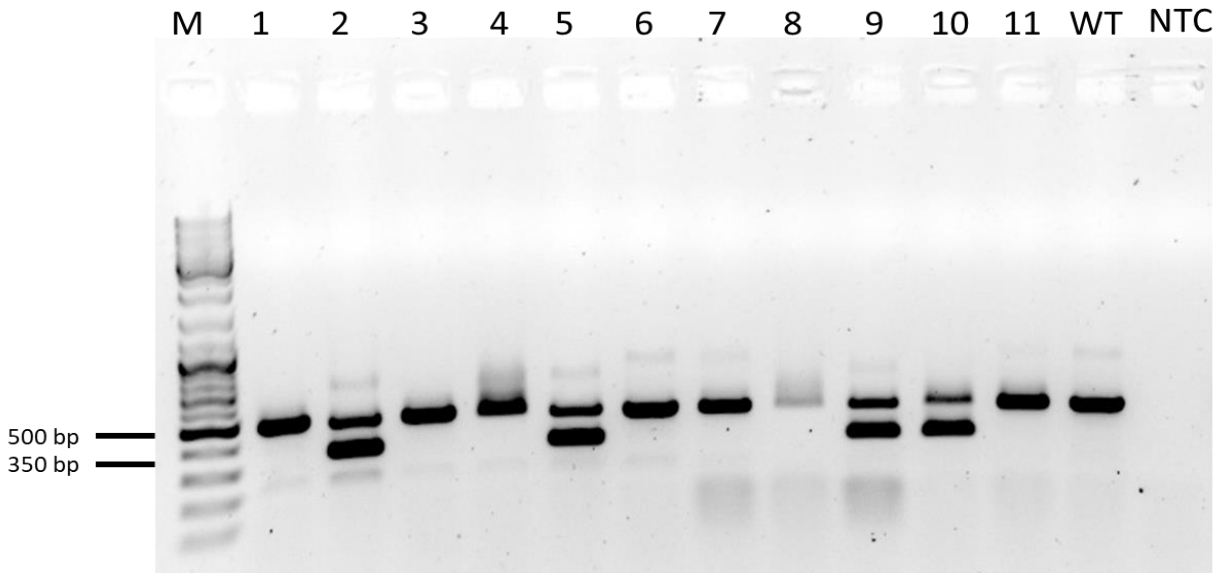

Figure 3.5. Agarose gel result for F1 offspring of founder 1 fish bred to *parlb* ^{d9k} homozygous fish. A total number of 11 fish were fin clipped and genotyped for the detection of *parla* mutant band and the WT band using the forward primer (F), reverse mutant primer (Rmut) and reverse WT primer (Rwt). The size of the mutant band observed is 350 bp observed in fish 2, 5, 9 and 10. The size of the WT band is 500 bp. The marker (M) used is a 10 kb DNA ladder mix (GeneRuler^{TM}). No template control is referred to as NTC. A wild-type sample (WT) was used as a control.

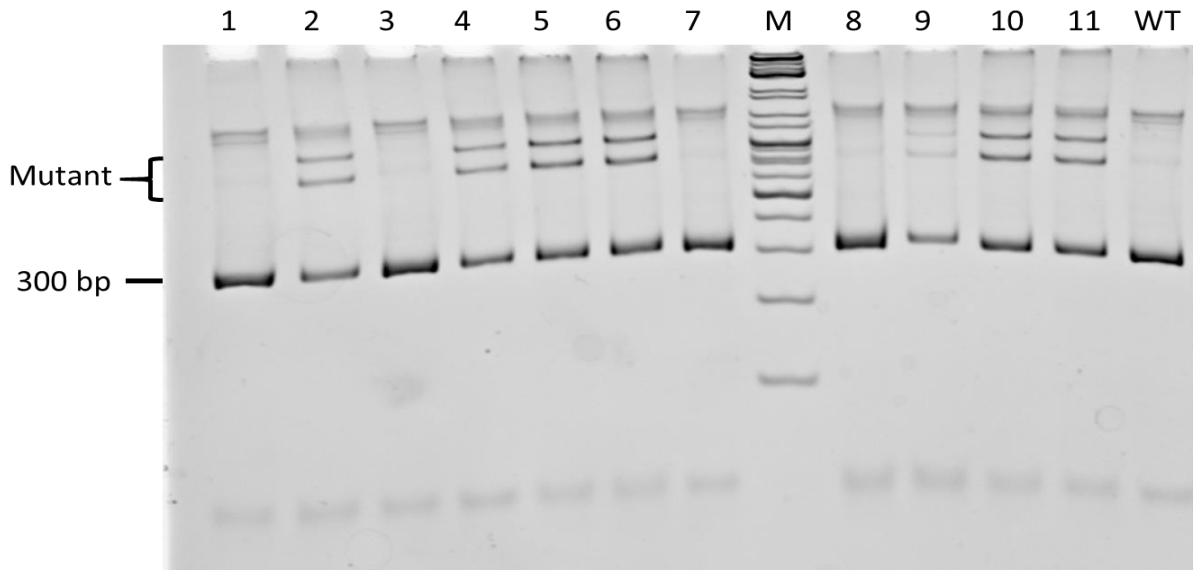

Figure 3.6. PAGE result for F1 offspring of founder 1 fish bred to *parlb* ^{d9k} homozygous fish. A total number of 11 fish were fin clipped and genotyped for the detection of 5-nucleotide *parlb* deletion using the forward primer (F), reverse mutant primer (Rmut) and reverse WT primer (Rwt). The mutant band is a heteroduplex detected in fish 2, 4, 5, 6, 10 and 11. The size of the WT band is 300 bp. The marker (M) used is a 10 kb DNA ladder mix (GeneRuler^{TM}). A wild-type sample (WT) was used as a control.

Fish that were heterozygous for *parla* and *parlb* mutations (*parla* $^{+/ot510}$*; parlb* $^{+/d9k}$) were bred together to generate the F2 generation. Fish from the F2 generation were then fin clipped, genotyped, and isolated in separate tanks based on their genotype for future analyses (Figure 3.7). As the mutant band for homozygous for *parlb* mutation fish looks similar on gel as the WT band, we decided to perform an additional PAGE analysis in which we mixed the sample genomic DNA with the WT genomic DNA. This way, if the sample was homozygous for *parlb*, then a heteroduplex, similar to the one observed for heterozygous fish would be detected on gel. However, if the sample was WT, then a single WT band would be detected on gel (Figure 3.8).

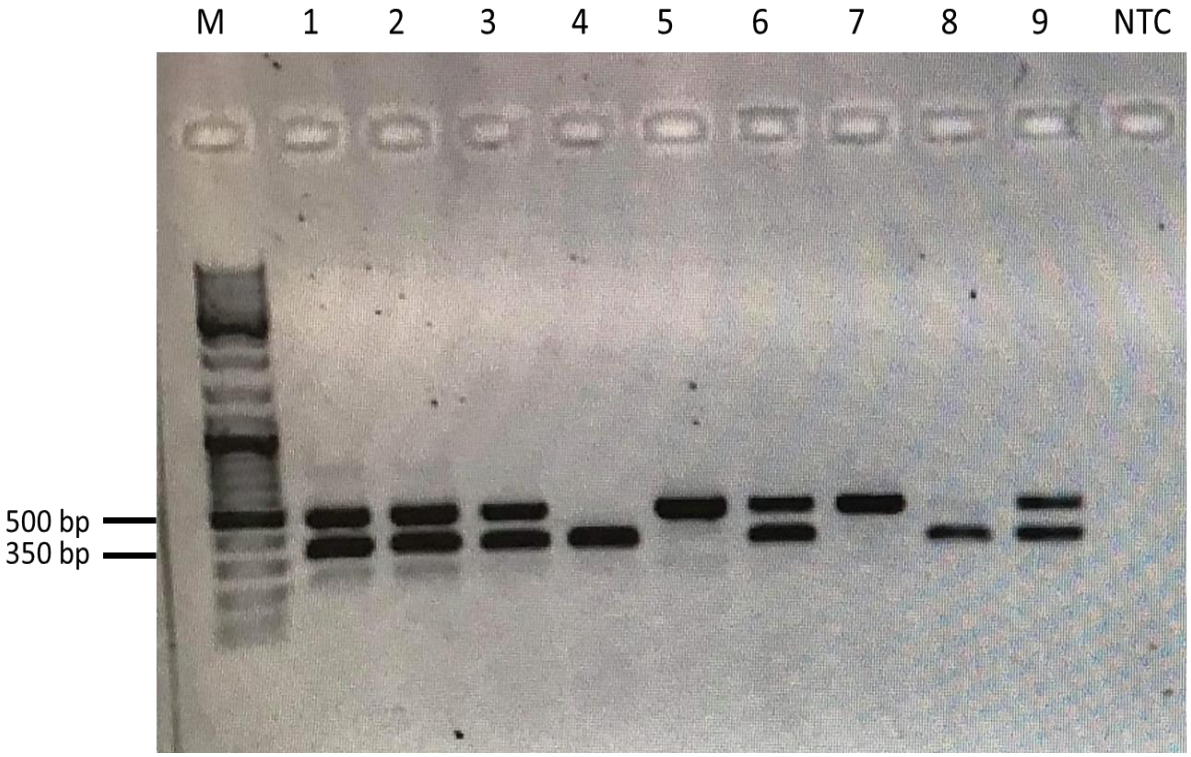

Figure 3.7. Agarose gel result for F2 offspring of founder 1 fish bred to *parlb* ^{d9k} homozygous fish. We show in this gel a total number of 9 fish that were fin clipped and genotyped for the detection of *parla* mutant band and the WT band using the forward primer (F), reverse mutant primer (Rmut) and reverse WT primer (Rwt). The size of the mutant band observed is 350 bp. Fish 1, 2, 3, 6 and 9 were heterozygous for *parla* mutation (*parla* $^{+/ot510}$). Fish 4 and 8 were homozygous for *parla* mutation (*parla* ^{ot510}). Fish 5 and 7 were WT (*parla* $^{+}$). The size of the WT band is 500 bp. The marker (M) used is a 10 kb DNA ladder mix (GeneRuler^{TM}). No template control is referred to as NTC.

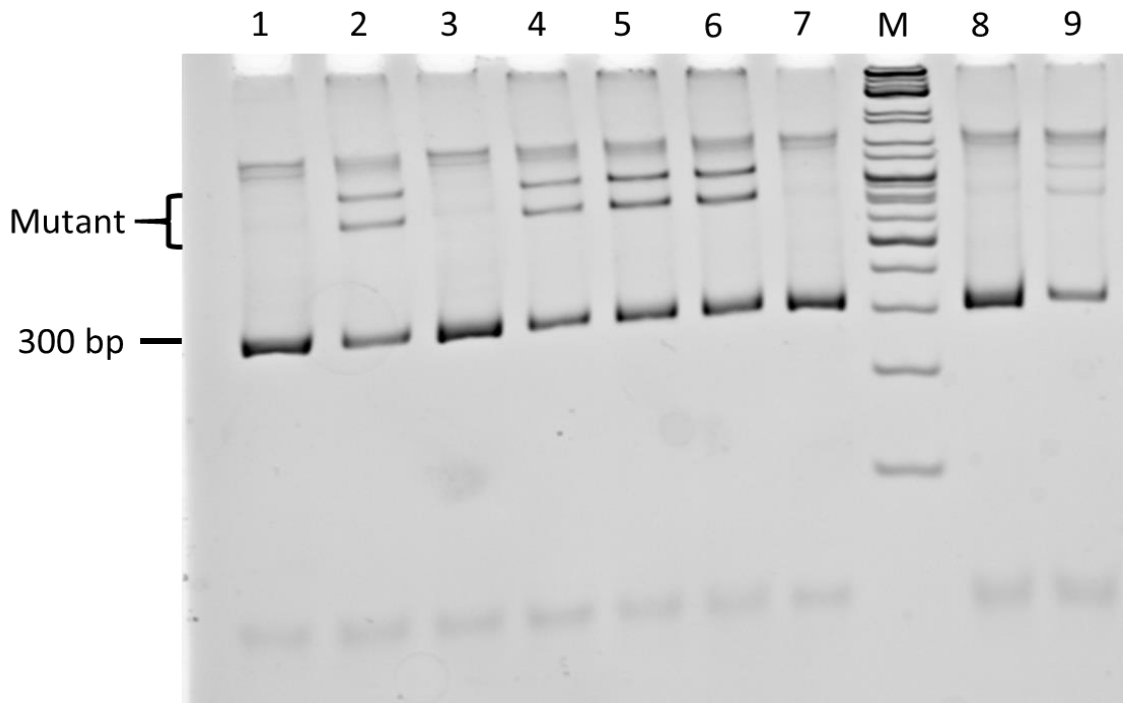

Figure 3.8. PAGE result for F2 offspring of founder 1 fish bred to *parlb* ^{d9k} homozygous fish. We show in this gel the same 9 fish that were fin clipped and genotyped in Figure 3.16 for the detection of 5-nucleotide *parlb* deletion using the forward primer (F), reverse mutant primer (Rmut) and reverse WT primer (Rwt). Genomic DNA for the samples was mixed with WT DNA. The only homozygous fish is fish 2. Fish 1, 3, 7, 8 and 9 are WT fish. As depicted from the gel in Figure 3.16, fish 4, 5 and 6 are indeed heterozygous for *parlb* mutation. The size of the WT band is 300 bp. The marker (M) used is a 10 kb DNA ladder mix (GeneRuler^{TM}).

We monitored the double knockout fish (*parlb* ^{d9k}*; parla* ^{ot510}) throughout development to assess any phenotypic abnormality. In general, no gross morphological change was observed. However, slow development was noticeable by the significantly smaller body size of the double knockout fish (Figure 3.9). Similarly, we noticed that there was slow development of male breeding tubercles in the mutants as compared to WT fish (*parla* $^{+}$*; parlb* $^{+}$) (data not shown). By 3 months post-fertilization (mpf), identifying the gender of the double knockout fish was very challenging.

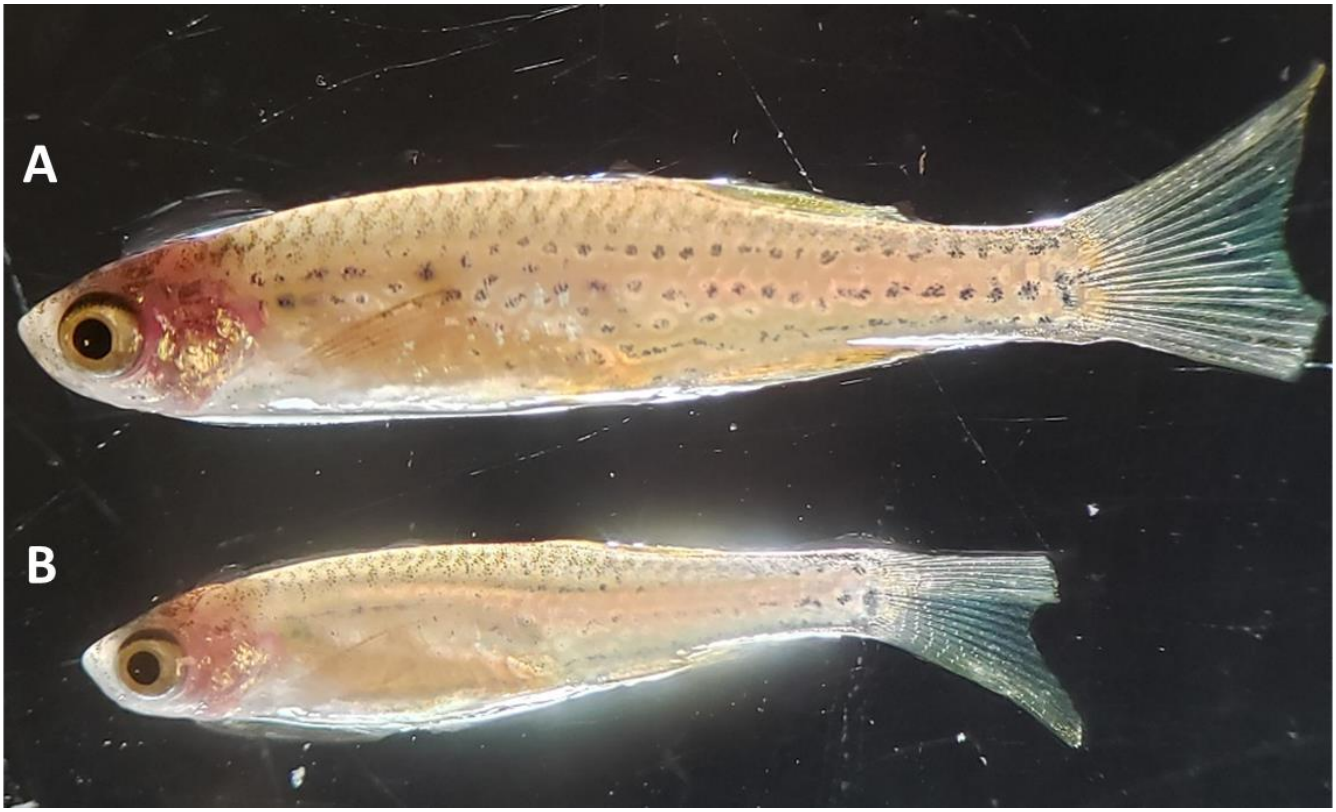

Figure 3.9. Image taken under the dissecting microscope showing size differences of **(B)** double homozygous fish (*parlb* ^{d9k}*; parla* ^{ot510}) and **(A)** WT fish (*parlb* $^{+}$*; parla* $^{+}$) at 60 dpf.

3.1.3 Generation of a *parla* mutant line with a 15 kb deletion (*parla* ^{ot511})

Based on Ensemble genome browser, the total *parla* gene sequence length is around 18 kb. The *parla* ^{ot510} mutation described previously consisted of a 1.4 kb deletion in the *parla* gene. We decided to induce a larger deletion by injecting 4 sgRNAs, two of them bind to two target sites located at the 5' UTR region. The other two bind at target sites found in the last exon 9 of the *parla* gene (Figure 3.10). Target site sequences are found in Material and Methods (Table 2.2).

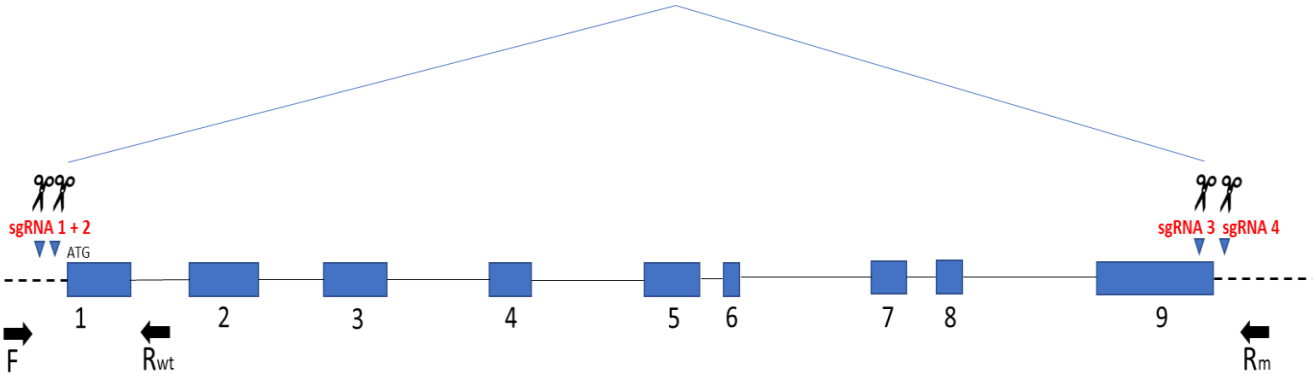

Figure 3.10. Exon 1 to 9 deletion in the *parla* gene by CRISPR/Cas9-mediated mutagenesis. The deleted region is indicated by the blue line that links sgRNA 2 and 3. Exons are represented with blue boxes and introns with black lines between the exons. The dashed line represents the 5'UTR and 3'UTR region. Primers used in genotyping are represented by F (forward primer), Rwt (reverse primer for the WT), and Rm (reverse primer for the mutant).

The four sgRNAs were injected simultaneously in approximately 200 one-cell stage embryos. At 24 hours post-injection, 20 individual embryos were collected for genotyping to confirm the presence of the mutation. A potentially mutant band was only detected in 1 embryo out of the 20 genotyped embryos (Figure 3.11). Thus, mutation efficiency was only 5%. Figure 3.11 shows genotyping results of 16 embryos.

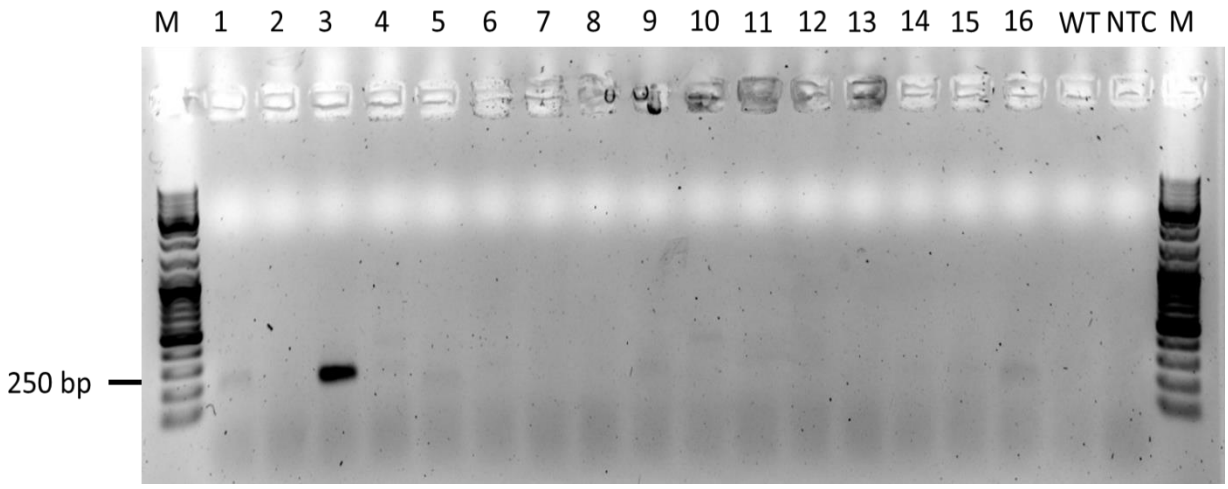

Figure 3.11. Detection of *parla* mutation on agarose gel in embryos 24 hours post-injection of the sgRNAs using forward primer (F) and reverse mutant primer (Rmut). Genotyping result of 16 individual embryos is shown in this figure. Size of the mutant band is 250 bp observed in embryo 3. The marker used is a 10 kb DNA ladder mix (GeneRuler^{TM}). No template control is referred to as NTC. A wild-type sample (WT) was used as a control.

To confirm whether the band detected for embryo 3 is a mutant band, we excised this band from gel followed by DNA extraction, purification and then sequencing using the reverse mutant primer (Rm) to confirm exon deletion in the *parla* genomic sequence. Using NCBI BLAST, we compared the mutant sequence obtained by sequencing to the WT *parla* sequence that is flanked by the forward primer (F) and the reverse mutant primer (Rmut) (Figure 3.12). The predicted length of the WT band was around 15.4 kb, however, the mutant band was predicted at approximately 250 bp. The actual mutant band size observed on agarose gel (250 bp) matches the size of the predicted mutant band (Figure 3.11). Therefore, we confirmed the deletion of around 15 kb in the *parla* gene.

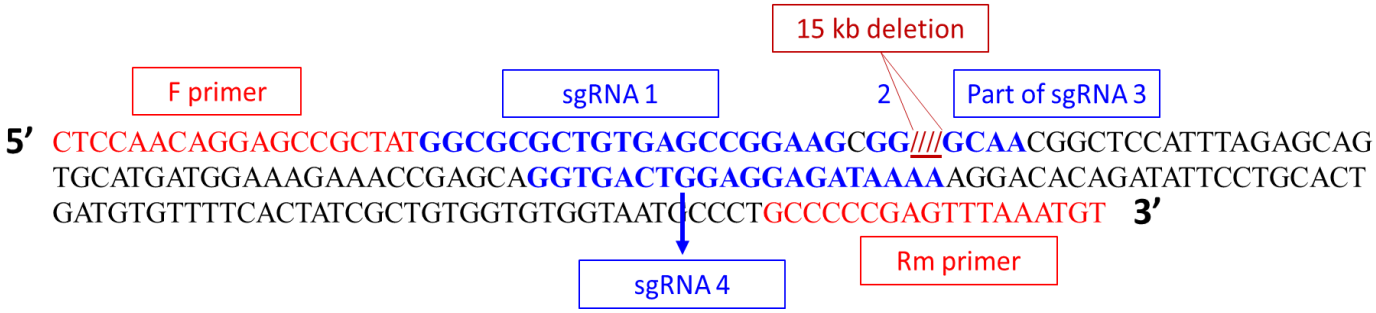

Figure 3.12. Schematic representation of *parla* nucleotides obtained by sequencing the 250 bp mutant band. The forward primer (F) and the reverse mutant primer (Rm) are shown in red. The entire sequence of the sgRNA 1 and sgRNA 4, as well as part of the sgRNA 2 and 3 sequences are shown in blue. The 15 kb deleted region is indicated by the red lines. The sequence shown is from the 5’ to the 3’ end.

Injected embryos were raised to sexual maturity then bred with WT fish to identify founder fish that would successfully transmit the mutation to the offspring. Once identified, offspring were raised then fin clipped and genotyped to identify heterozygous F1 fish that carry the mutation. Heterozygous fish were then bred together to generate F2 generation fish that were again raised and genotyped. Fish homozygous for the *parla* mutation were isolated and raised in separate tanks. The 15 kb deletion mutant line was referred to as *parla* ^{ot511} but was not used in our subsequent experiments and analyses.

3.1.4 Generation of a *parlb* mutant line with a 16.6 kb deletion (*parlb* ^{ot512})

Given the successful deletion of approximately 15 kb in the *parla* gene, we decided to similarly induce a large deletion in the *parlb* gene. To establish a double knockout line carrying *parla* ^{ot510} mutation and a large deletion in the *parlb* gene, we designed, synthesized, and injected four sgRNAs in *parla* ^{ot510} mutant fish. One of these sgRNAs binds to a target site in exon 1, another one binds to a target site in exon 9 and two sgRNAs bind respectively to the last exon 10

and 3'UTR region of the *parlb* gene (Figure 3.13). Target site sequences are found in Material and Methods (Table 2.3).

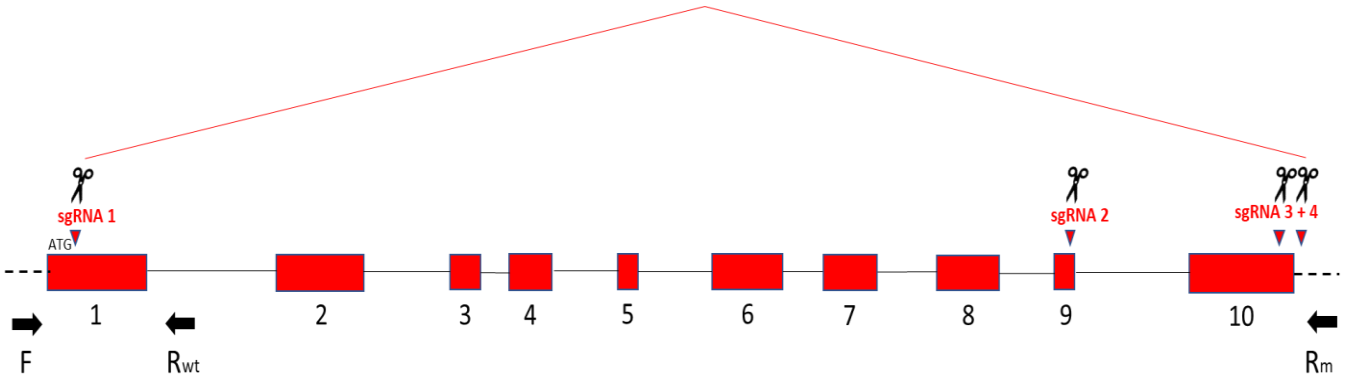

Figure 3.13. Exon 1 to 10 deletion in the *parlb* gene by CRISPR/Cas9-mediated mutagenesis. The deleted region is indicated by the red line that links sgRNA 1 and 4. Exons are represented with red boxes and introns with black lines between the exons. The dashed line represents the 5'UTR and 3'UTR region. Primers used in genotyping are represented by F (forward primer), Rwt (reverse primer for the WT), and Rm (reverse primer for the mutant).

The four sgRNAs were injected simultaneously in around 200 one-cell stage embryos. At 24 hours post-injection, 5 pools of 10 embryos each were collected for genotyping to confirm the presence of the mutation. Figure 3.14 shows the mutant bands observed on agarose gel for the genotyped embryos.

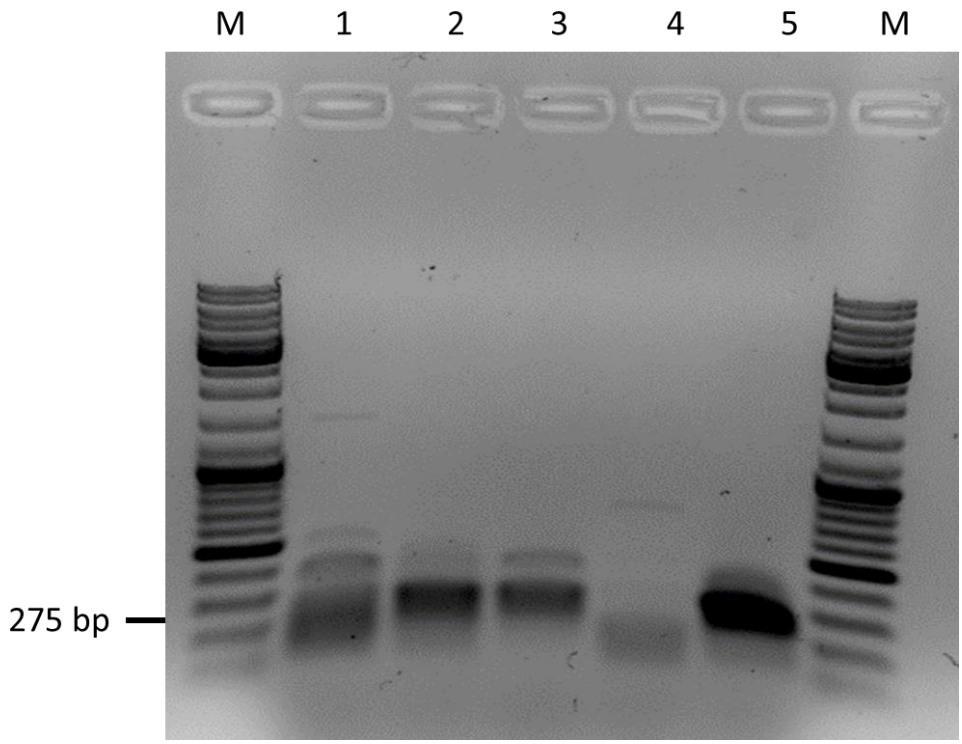

Figure 3.14. **Detection of *parlb* mutation on agarose gel in 24 hours post-fertilization F1 generation embryos.** Five pools (1, 2, 3, 4 and 5) of 10 embryos each were used. Several mutant bands appear but the most obviously detected band is around 275 bp observed in pools 1, 2 and 3. The marker used is a 10 kb DNA ladder mix (GeneRuler^{TM}).

We raised the injected embryos to sexual maturity and then bred them with *parla* ^{ot510} homozygous mutants to identify founder F0 fish that would successfully transmit the mutation to the offspring. Once identified, offspring were raised then fin clipped and genotyped to identify heterozygous F1 fish that carry the mutation (Figure 3.15). Heterozygous fish were then bred together to generate F2 generation fish that were again raised and genotyped. Fish that are homozygous for *parlb* mutation were isolated and raised in separate tanks. The 16.6 kb deletion mutant line was referred to as *parlb* ^{ot512}.

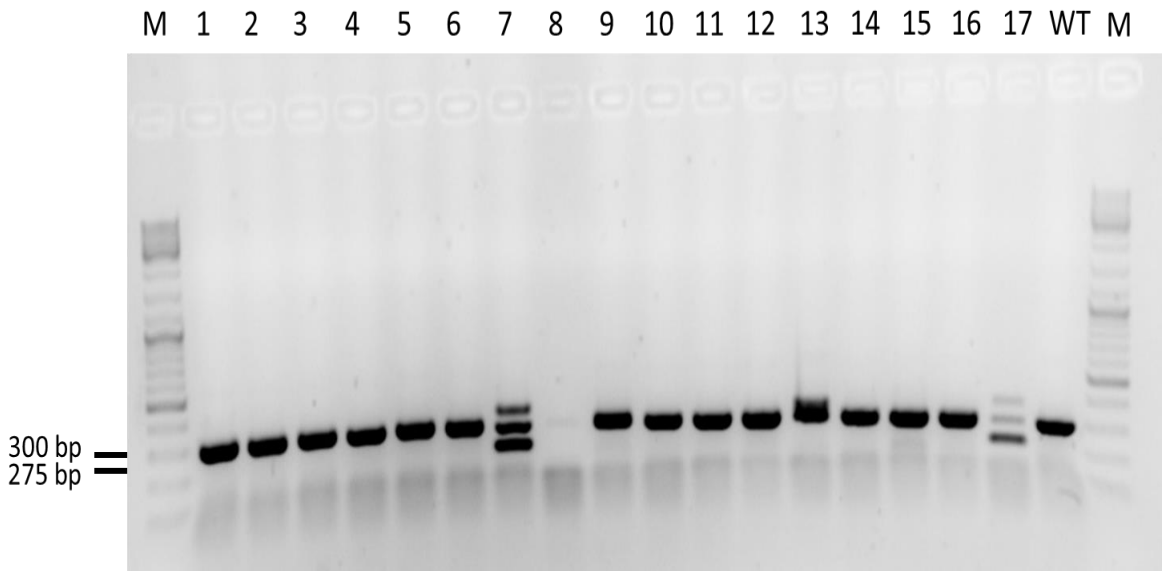

Figure 3.15. Agarose gel result for F1 offspring of founder fish bred to *parla* ^{ot510} homozygous fish. A total number of 17 fish were fin clipped and genotyped for the detection of *parlb* mutant band and the WT band using the forward primer (F), reverse mutant primer (Rmut) and reverse WT primer (Rwt). The size of the mutant band is 275 bp observed in fish 7 and 17. The size of the WT band is 300 bp. The marker (M) used is a 10 kb DNA ladder mix (GeneRuler^{TM}). A wild-type sample (WT) was used as a control.

We excised the 275 bp mutant band from gel followed by DNA extraction, purification and then sequencing to confirm exon deletion in *parlb* genomic sequence. The total length of the predicted WT band was around 16.9 kb, however, the predicted mutant band was around 275 bp long. The actual mutant band size observed on agarose gel (275 bp) matches the predicted size of the mutant band. Therefore, we confirmed the deletion of around 16.6 kb in *parlb* gene and we named this mutation *parlb* ^{ot512}.

3.1.5 Lethality of the double mutants (*parlb* ^{ot512}*; parla* ^{ot510})

Following the confirmation of *parlb* ^{ot512} mutation by sequencing, we bred two heterozygous fish (7 and 17) identified by genotyping (Figure 3.15) with *parla* ^{ot510} mutants. As fish 7 and 17 were of the same gender, they couldn't be bred together. At 1 dpf, 16 out of 40 embryos were dead. The remaining fish (around 24) were raised to adulthood. Surprisingly, we found only 8 fish out of the 24 at around 2 months. Those fish were subsequently genotyped. Five of the 8 fish were found to be heterozygous for *parlb* mutation (*parlb* $^{+/ot512}$) and 3 fish were WT for *parlb* mutation (*parlb* $^{+}$). Fish that are heterozygous for *parlb* mutation (*parlb* $^{+/ot512}$) were raised to sexual maturity and bred together to obtain the double mutant fish (*parlb* ^{ot512}*; parla* ^{ot510}). Interestingly, following breeding of the heterozygous fish, we noticed a mortality rate of more than 50% by 45 dpf. Surprisingly, this percentage (50%) exceeds the predicted percentage of double homozygous mutants (25%) that resulted from this breeding. One explanation could be that some of the mutants that were heterozygous for the loss of the *parlb* gene and homozygous for the loss of *parla* (*parlb* $^{+/ot512}$; *parla* ^{ot510}) might have died.

Therefore, we suspected lethality of the double mutant fish and/or fish that are simultaneously homozygous for *parla* mutation and heterozygous for the *parlb* mutation (*parlb* $^{+/ot512}$*; parla* ^{ot510}). Lethality of the double mutant fish was confirmed by the absence of double mutants following genotyping of approximately 50 fish at 45 dpf.

Next, we decided to investigate the timepoint at which the double mutant fish were dying. Therefore, we decided to euthanize a total number of 30 fish at 5 dpf, followed by whole-larvae DNA extraction and genotyping to check viability of the double mutant fish at 5 dpf (Figure 3.16). Based on the breeding we performed, and based on Mendelian genetic ratios, the probability of getting double mutant fish was 1/4. Interestingly, 7 out of the 30 genotyped fish were double KO

mutants, which corroborates the expected 1/4 ratio. This confirmed that the double mutant fish do not die prior to 5 dpf.

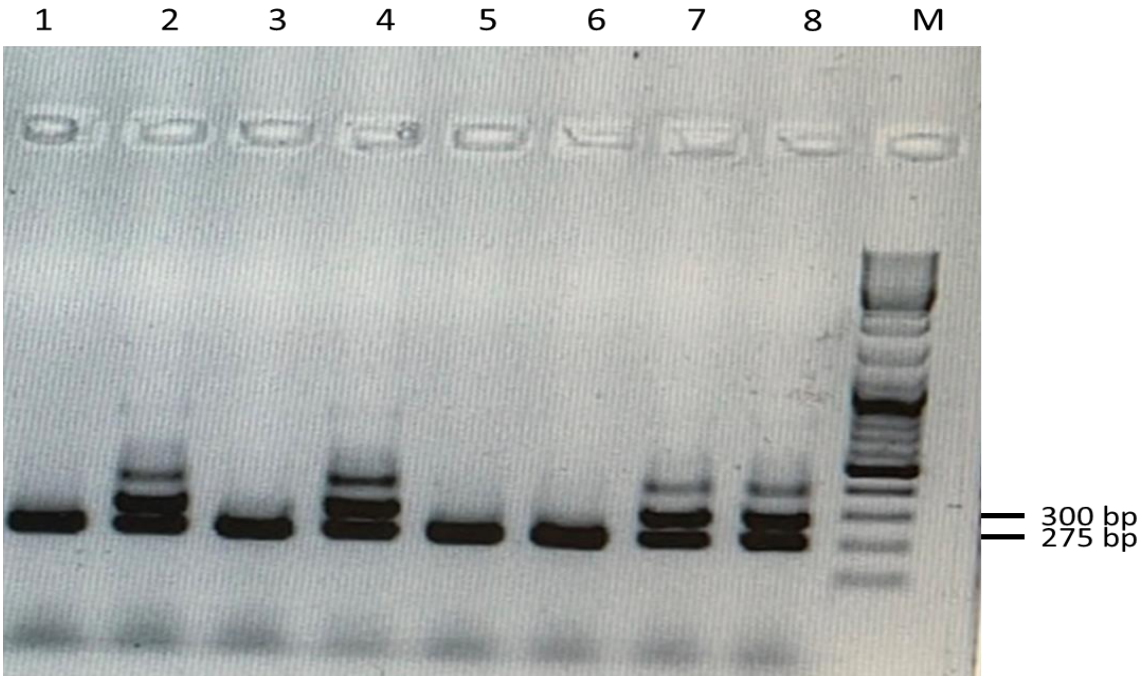

Figure 3.16. Agarose gel result for 5 dpf larvae showing 8 fish that were euthanized and genotyped for the detection of *parlb* ^{ot512} mutant band and the WT band using the forward primer (F), reverse mutant primer (Rmut) and reverse WT primer (Rwt). The size of the mutant band is 275 bp. The size of the WT band is 300 bp. Fish 1, 3, 5 and 6 are homozygous for the *parlb* mutation. The remaining fish are heterozygous for the mutation. The marker (M) used is a 10 kb DNA ladder mix (GeneRuler^{TM}). A wild-type sample (WT) was used as a control.

As double mutants (*parlb* ^{ot512}*; parla* ^{ot510}) were still viable by 5 dpf, we decided to genotype living larvae by fin clipping them at 5 dpf, then isolate the double KO fish and monitor them for any developmental defects and lethality. A total of 32 larvae were genotyped, 6 of them were found to be double KO fish, 19 were homozygous for the *parla* mutation and heterozygous for *parlb* mutation (*parlb* ^{ot512}*; parla* ^{ot510}), and 7 were WT larvae (*parlb* $^{+}$*; parla* $^{+}$) (Figure 3.17).

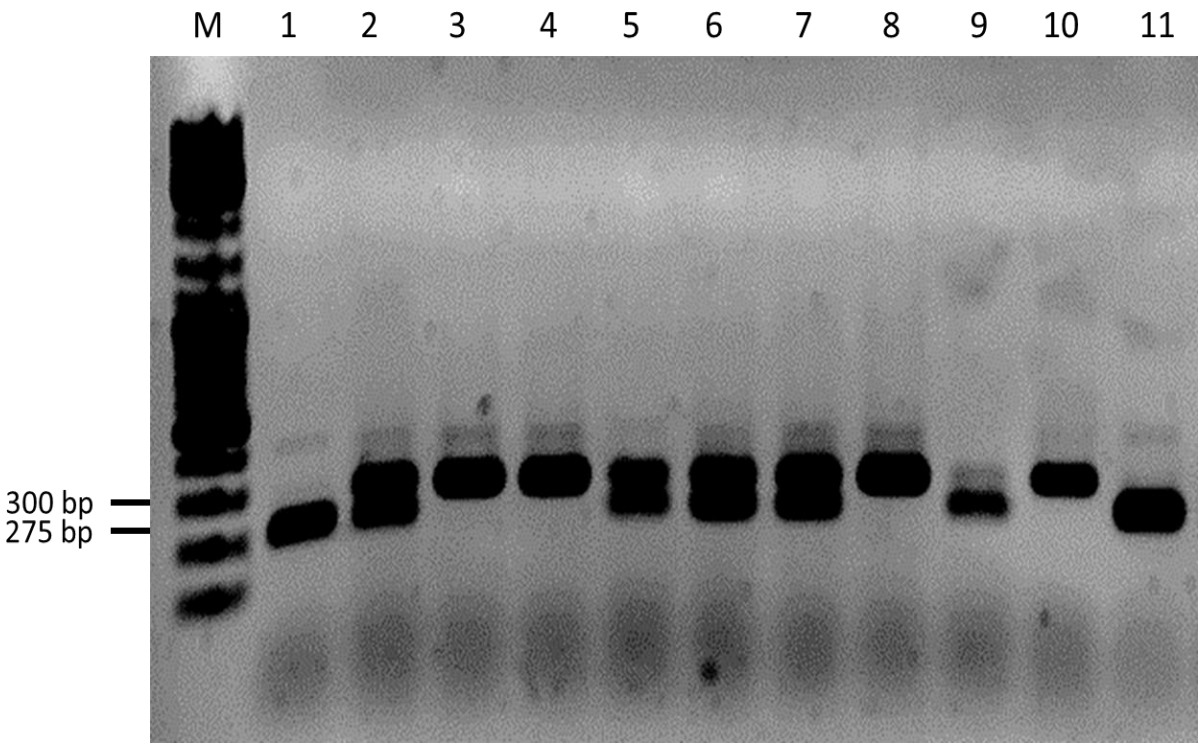

Figure 3.17. Agarose gel result for 5 dpf larvae showing 11 fish that were fin clipped and genotyped for the detection of *parlb* ^{ot512} mutant band and the WT band using the forward primer (F), reverse mutant primer (Rmut) and reverse WT primer (Rwt). The size of the mutant band is 275 bp. The size of the WT band is 300 bp. Fish 1, 9 and 11 are homozygous for the *parlb* mutation. The remaining fish are either heterozygous for the mutation (2, 5, 6 and 7) or WT fish (3, 4, 8 and 10). The marker (M) used is a 10 kb DNA ladder mix (GeneRuler^{TM}).

Keeping the genotyped larvae at optimum conditions with daily feeding and water change rituals, we noticed that double KO larvae were less active and motile as compared to the fish that are homozygous for *parla* mutation and heterozygous for the *parlb* mutation (*parlb* $^{+/ot512}$*; parla* ^{ot510}) and as compared to the WT fish starting at 9 dpf. Surprisingly, throughout development, we noticed some phenotypic and swimming defects in the double mutant fish as well as in some of the fish that were heterozygous for *parlb* and homozygous for *parla* (*parlb* $^{+/ot512}$; *parla* ^{ot510}). We observed these fish under the dissecting microscope and noticed that most of these fish did not have a properly inflated swim bladder as compared to fish that are WT for *parlb* and homozygous

for *parla* mutation (*parlb* $^{+}$*; parla* ^{ot510}). At 11 dpf, *parlb* $^{+/ot512}$*; parla* ^{ot510} fish looked weak and less motile although double mutant fish appeared to be the weakest. From 12 dpf, double mutants and *parlb* $^{+/ot512}$*; parla* ^{ot510} fish started dying until 21 dpf where all the double mutants were dead. However, only 2 WT fish died by 21 dpf. The cause of the double mutant fish lethality is still unknown and could be the subject of additional investigations.

To summarize, we successfully generated a 1.4 kb exon 1 to exon 2 deletion (*parla* ^{ot510}), and a 15 kb exon 1 to exon 9 deletion (*parla* ^{ot511}) in the *parla* gene. Similarly, we generated a 16.6 kb exon 1 to exon 10 deletion (*parlb* ^{ot512}) in the *parlb* gene. A 5-nucleotide deletion in exon 1 of *parlb* gene (*parlb* ^{d9k}) was previously established in our laboratory. As the double mutants having a 1.4 kb deletion in the *parla* gene and a 16.6 kb deletion in the *parlb* gene (*parlb* ^{ot512}*; parla* ^{ot510}) were lethal, we were unable to use these fish in subsequent experiments. Therefore, we decided to proceed with our analysis using the double mutant fish carrying the 5-nucleotide deletion (*parlb* ^{d9k}) as these fish (*parlb* ^{d9k}*; parla* ^{ot510}) were found to be viable. Their viability might be explained by gene expression analysis (section 3.2) that we performed in which we found that *parlb* ^{d9k} homozygous fish have a partial *parlb* mRNA expression (~60%).

As for the *parla* ^{ot511} mutants having the 15 kb deletion in the *parla* gene, we decided not to use them in our experiments because they were generated later than the *parla* ^{ot510} mutants. Waiting for the establishment of *parla* ^{ot511} homozygous generation would have been time-consuming. Most of our results found for the loss of *parla* function using the *parla* ^{ot510} mutants were recently published (Merhi et al., 2021). Similarly, the *parlb* ^{ot512} mutants having the 16.6 kb deletion in the *parlb* gene were generated at a later timepoint during my Ph.D., after most of the experiments and analyses were performed for the *parlb* ^{d9k} fish. Future investigations could be done using the *parlb* ^{ot512} mutants to confirm our results found with the *parlb* ^{d9k} fish.

Thus, for the subsequent experiments, we used *parla* ^{ot510} mutant line and *parlb* ^{d9k} mutant line (Table 3.2). The double mutant fish used (*parlb* ^{d9k}*; parla* ^{ot510}) were both viable and fertile. Moreover, we did not notice any obvious gross morphological or behavioral defects in these mutants except for their smaller size (Figure 3.9).

Table 3.2. List of the *parla* and/or *parlb* mutants used in the subsequent analyses. Mutants with loss of *parla* function carry a 1.4 kb deletion in the *parla* gene. Mutants with loss of *parlb* function carry a 5-nucleotide deletion in the *parlb* gene.

Gene targeted	Homozygous	Heterozygous	WT
parla	*parla* ^{ot510}	*parla* $^{+/ot510}$	*parla* $^{+}$
parlb	*parlb* ^{d9k}	*parlb* $^{+/d9k}$	*parlb* $^{+}$
parla and parlb	*parlb* ^{d9k}*; parla* ^{ot510}	*parlb* $^{+/d9k}$*; parla* $^{+/ot510}$	*parlb* $^{+}$*; parla* $^{+}$

3.2 Cell death detection in *parla* ^{ot510} mutant larvae

To assess cell death throughout the entire body of *parla* ^{ot510} mutant larvae, we stained live embryos at 3 dpf (Figure 3.18). An autofluorescence was observed in the yolk and a non-specific signal was detected in the nasal pits. Interestingly, an increased density of stained cells were detected in the homozygous (*parla* ^{ot510}) and heterozygous (*parla* $^{+/ot510}$) mutants (Figure 3.18B,C) as compared to the WT larvae (Figure 3.18A). However, this increase was not quantified. Moreover, these cells, particularly in the homozygous fish, showed higher intensity and size when visualized under the fluorescent microscope. We also noticed that these cells were scattered throughout the entire body of the larvae, and most importantly, we observed an increased number of stained cells at the level of the head region as well as the tail fin in both the *parla* ^{ot510} larvae and *parla* $^{+/ot510}$ fish. Those cells were absent from WT larvae (*parla* $^{+}$).

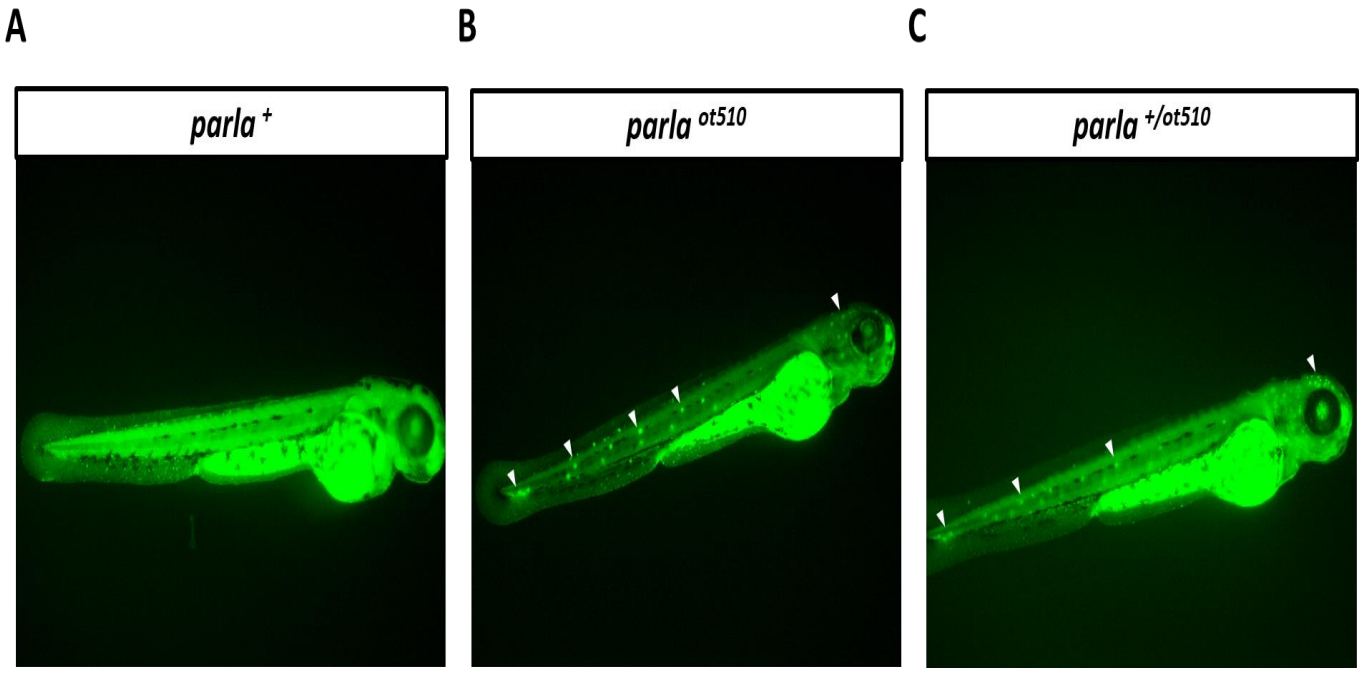

Figure 3.18. Acridine orange staining of 3 dpf larvae with loss of *parla* function. (A) Wild-type **(B)** homozygous mutant **(C)** heterozygous mutant. The white triangles show stained cells throughout the mid-part of the body, the tail, and the head region.

3.3 Gene expression analysis in *parla* ^{ot510} and *parlb* ^{d9k} mutants.

To assess the effect of *parla* and/or *parlb* loss-of-function on gene expression in the mutant larvae and in the adult zebrafish brain, we determined expression of genes such as PTEN-induced kinase 1 (gene: *pink1*; protein: PINK1) and optic dominant atrophy (gene: *opa1*; protein: OPA1), both of which encode for mitochondrial proteins thought to be PARL substrates (Whitworth et al. 2008 and McQuibban et al. 2003) (See also sections 1.3.1 and 1.3.3). Additionally, we investigated changes in expression of tyrosine hydroxylase 1 (gene: *th1*; protein: TH) and the dopamine transporter (gene: *dat*; protein: DAT) which might correlate to changes in DA cell number. Lastly, we checked whether expression of genes involved in mitochondrial function and dynamics is affected by analyzing expression of mitochondrial fission 1 (gene: *fis1*; protein: FIS1) and mitofusin 1 (gene: *mfn1*; protein: MFN1).

3.3.1 Gene expression in larvae with loss of *parla* function

Knowing that *parla* is expressed ubiquitously (Noble et al. 2012), we analyzed gene expression throughout the entire body of larvae with a loss of *parla* function. The most noticeable changes in expression were seen in *parla* ^{ot510} larvae for *th1*, *opa1*, *pink1*, and *fis1* genes.

There was a 41% decrease in *th1* expression in *parla* ^{ot510} larvae (Figure 3.19A). This decrease in expression is in line with the decrease in *th1* expression observed in the brain of *parla* ^{ot510} adults.

In addition, there were significant increases of 60% and 31% in *opa1* and *pink1* expression, respectively, in *parla* ^{ot510} larvae (Figure 3.19A).

The highest increase in expression was observed for *fis1* in *parla* ^{ot510} larvae, which reached 2.25 times the levels measured in WT (*parla* $^{+}$) controls (Figure 3.19A). This increase in *fis1* expression is in line with that seen in the brain of adult *parla* ^{ot510} fish.

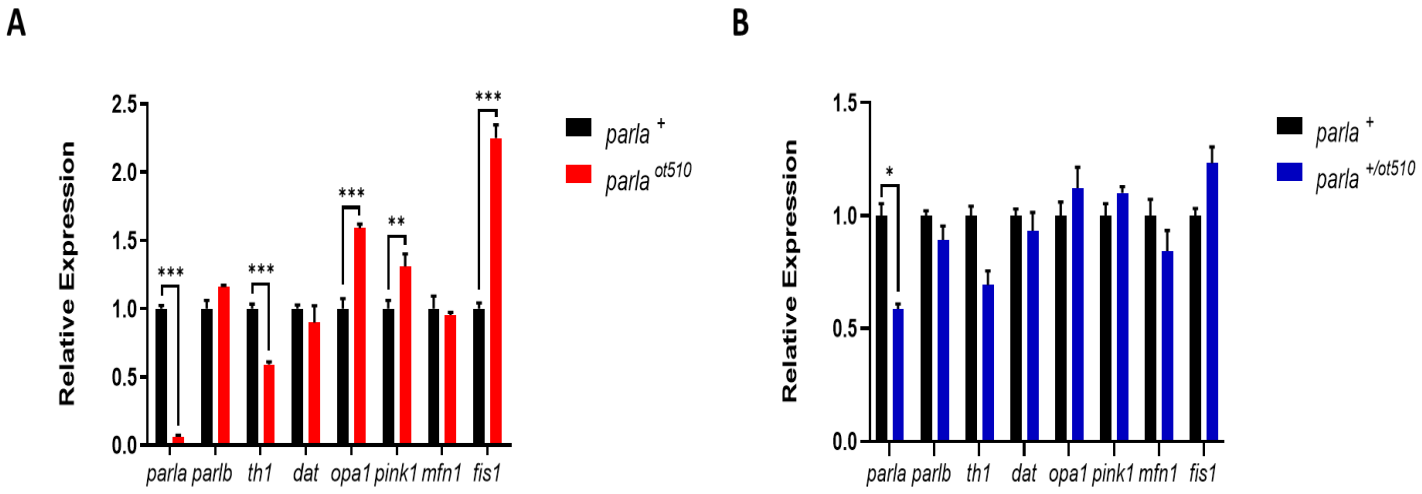

Figure 3.19. Effect of *parla* loss-of-function on the expression of genes associated with dopaminergic- and mitochondrial function in larvae. (**A,B**) Relative expression of *parla*, *parlb*, *th1*, *dat*, *opa1*, *pink1*, *mfn1*, and *fis1* of 5 dpf zebrafish larvae (n = 3. Each replicate corresponds to a different breeding and contains 7 homogenized whole larvae). WT fish are represented by *parla* $^{+}$, homozygous mutants by *parla* ^{ot510}, and heterozygous mutants by *parla* $^{+/ot510}$. Bars represent the Mean ± the SEM. * ($p < 0.05$), ** ($p < 0.01$), *** ($p < 0.001$).

3.3.2 Expression in Adult Brain

Following gene expression analyses performed in the mutant larvae, we investigated whether there are similar or differential gene expression levels between the mutant larvae and the adult mutant brain. Partial loss of *parlb* mRNA expression was confirmed by a 60% decrease in *parlb* expression levels observed in the homozygous mutants (*parlb* ^{d9k}) (Figure 3.20A). Fish that are heterozygous for the p*arlb* mutation (*parlb* $^{+/d9k}$) showed a 20% reduction in *parlb* transcript levels (Figure 3.20B). When *parla* expression was measured, it was increased by 57% in *parlb* ^{d9k} mutants. Similarly, there was a 15% increase in *parla* expression observed in *parlb* $^{+/d9k}$ mutants (Figure 3.20A,B).

Interestingly, *parlb* ^{d9k} and *parlb* $^{+/d9k}$ animals showed 35% and 17% decreases in the expression of *th1*, respectively (Figure 3.20A,B). Similarly, there was a slight 33% and 24% decrease in the expression of *dat* gene for *parlb* ^{d9k} and *parlb* $^{+/d9k}$ fish, respectively. The reductions seen for *th1* and *dat* genes might suggest lower DA cell numbers in the brain of adult *parlb* ^{d9k} and *parlb* $^{+/d9k}$ mutants.

Finally, the expression of *fis1* was increased by 49% and 19% in *parlb* ^{d9k} and *parlb* $^{+/d9k}$ animals, respectively (Figure 3.20A,B).

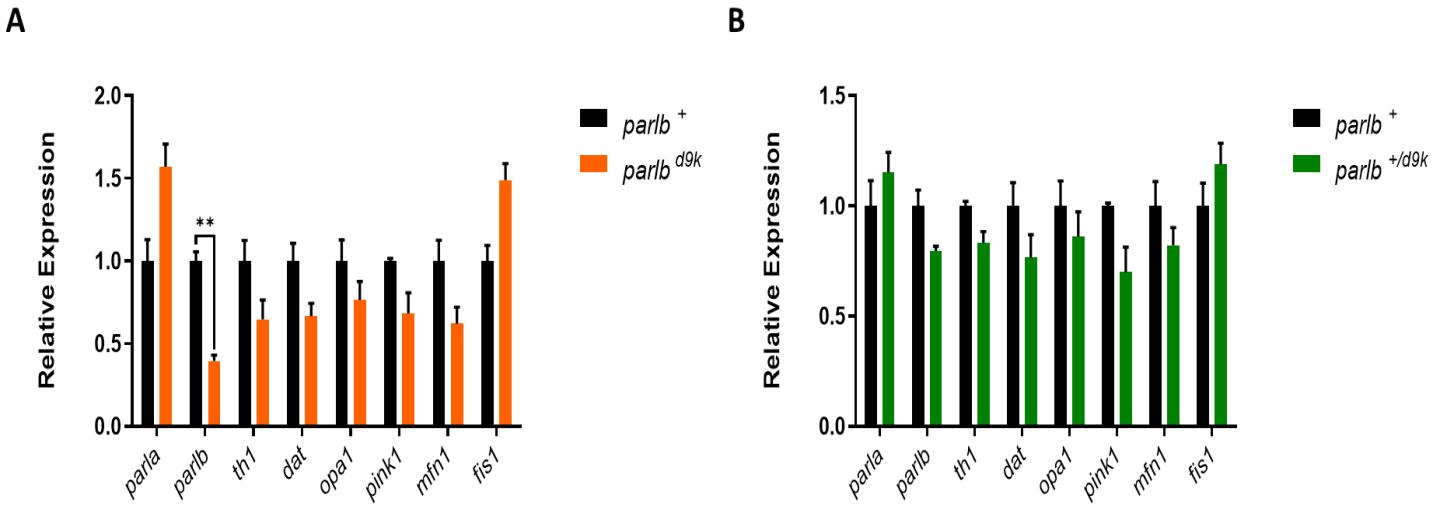

Figure 3.20. Effect of *parlb* loss-of-function on the expression of genes associated with dopaminergic- and mitochondrial function in the adult zebrafish brain. (**A,B**) Relative expression of *parla*, *parlb*, *th1*, *dat*, *opa1*, *pink1*, *mfn1*, and *fis1* of 4–10 mpf adult zebrafish brains (n = 3). WT fish are represented by *parlb* $^{+}$, homozygous mutants by *parlb* ^{d9k}, and heterozygous mutants by *parlb* $^{+/d9k}$. Bars represent the Mean ± the SEM. ** ($p < 0.01$).

As for the *parla* homozygous mutants (*parla* ^{ot510}), loss of the *parla* gene was confirmed by a 96% decrease in *parla* mRNA levels (Figure 3.21A). In addition, fish heterozygous for the mutation (*parla* $^{+/ot510}$) showed a 60% reduction in *parla* transcript levels (Figure 3.21B). Interestingly, we found that the paralogous *parlb* gene expression was increased by 42% in *parla*

ot510 mutants and by 12% in heterozygous fish (*parla* $^{+/ot510}$) similarly to the increase in *parla* expression previously observed in mutants with loss of *parlb* function (*parlb* ^{d9k}). This increase in expression observed for the paralogous gene might indicate the existence of a compensatory mechanism for the two paralogous genes *parla* and *parlb* (Figure 3.21A).

Intriguingly, *parla* ^{ot510} and *parla* $^{+/ot510}$ animals exhibited 70% and 30% decreases in the expression of *th1*, respectively (Figure 3.21A,B). These reductions in *th1* expression levels were larger (almost double) than the ones observed in *parlb* ^{d9k} (35%) and *parlb* $^{+/d9k}$ (17%) described previously, which might suggest proper DA development in zebrafish depends more on *parla* gene function. Interestingly, there was no change in the expression of the *dat* gene in both *parla* ^{ot510} and *parla* $^{+/ot510}$ mutants. This could be explained by a possible upregulation of *dat* in the DA neurons that survive.

Similarly, *opa1* showed no change in expression. As *opa1* encodes for a protein that plays a role in apoptosis, and as Noble and colleagues found increased cell death phenotype throughout the entire body in *parla* morphant larvae (Noble et al., 2012), we performed acridine orange staining (described above) and confirmed that there was an increased cell death in *parla* ^{ot510} mutant larvae (Figure 3.18B).

Expression levels of *pink1* showed a slight 27% and 7% upregulation in *parla* ^{ot510} and *parla* $^{+/ot510}$ individuals, respectively. A slight 24% and 14% decrease in the expression of *mfn1* were seen in both *parla* ^{ot510} and *parla* $^{+/ot510}$ zebrafish, respectively. Finally, *fis1* expression was increased by 86% and 25% in *parla* ^{ot510} and *parla* $^{+/ot510}$ mutants, respectively (Figure 3.21A,B). Similar to the increase in *fis1* expression described previously in fish with loss of *parlb* function (*parlb* ^{d9k} and parlb $^{+/d9k}$), this change in expression might suggest increased mitochondrial fission events in *parla* and in *parlb* mutant fish.

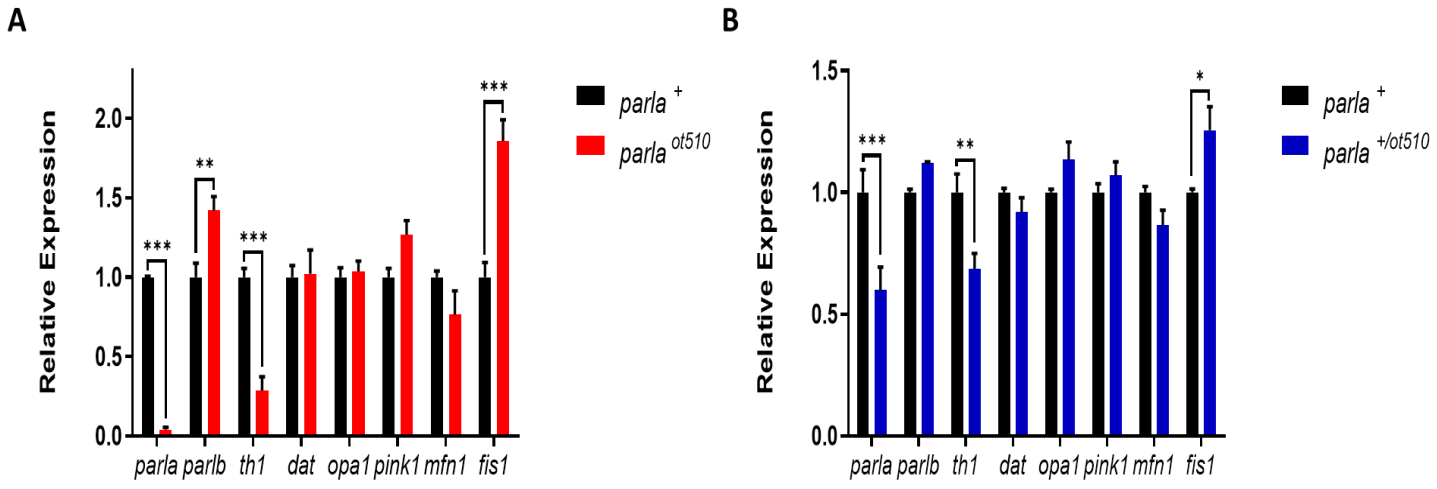

Figure 3.21. Effect of *parla* loss-of-function on the expression of genes associated with dopaminergic- and mitochondrial function in the adult zebrafish brain. (**A,B**) Relative expression of *parla*, *parlb*, *th1*, *dat*, *opa1*, *pink1*, *mfn1*, and *fis1* of 4–10 mpf adult zebrafish brains (n = 3). WT fish are represented by *parla* $^{+}$, homozygous mutants by *parla* ^{ot510}, and heterozygous mutants by *parla* $^{+ot510}$. Bars represent the Mean ± the SEM. * ($p < 0.05$), ** ($p < 0.01$), *** ($p < 0.001$).

Loss of *parla* function was confirmed by an 89% decrease in *parla* expression levels in the double homozygous fish (*parlb* ^{d9k}*; parla* ^{ot510}), and partial loss of the *parlb* mRNA expression was confirmed by a 55% decrease in *parlb* levels (Figure 3.22A). Double heterozygous fish (*parlb* $^{+/d9k}$*; parla* $^{+/ot510}$) showed a 50% and 33% reduction in *parla* and *parlb* transcript levels, respectively (Figure 3.22B).

Reductions in *th1* expression levels were observed in both *parlb* ^{d9k}*; parla* ^{ot510} and *parlb* $^{+/d9k}$*; parla* $^{+/ot510}$ animals and were found to be 87% and 40%, respectively (Figure 3.22A,B). We noticed that these reductions seen for loss of *parla* and *parlb* function, simultaneously, were greater than the reductions in *th1* expression levels observed for the single mutants described previously (*parla* ^{ot510} *or parlb* ^{d9k}).

Similarly, *dat* expression levels were decreased by 76% and 18% for the double homozygous and double heterozygous mutants (Figure 3.22A,B). As for *opa1* expression levels,

there was 46% and 33% reductions for *parlb* ^{d9k}*; parla* ^{ot510} and *parlb* $^{+/d9k}$*; parla* $^{+/ot510}$, respectively. In contrast, *pink1* expression levels increased by 50% and 13% in double homozygous and double heterozygous mutants, respectively. A 55% decrease in the expression of *mfn1* was seen for *parlb* ^{d9k}*; parla* ^{ot510} zebrafish which might indicate possible decreased mitochondrial fusion events in the double homozygous fish. Surprisingly, *parlb* $^{+/d9k}$*; parla* $^{+/ot510}$ showed a 56% increase in *mfn1* expression levels.

Finally, the expression of *fis1* was increased by 79% and 46% in *parlb* ^{d9k}*; parla* ^{ot510} and *parlb* $^{+/d9k}$*; parla* $^{+/ot510}$ animals, respectively (Figure 3.22A,B). These reductions of *mfn1* expression levels and the observed increases of *fis1* expression levels in the double homozygous mutants might indicate a reduction of mitochondrial fusion as opposed to an increase of mitochondrial fission events in *parlb* ^{d9k}*; parla* ^{ot510} fish.

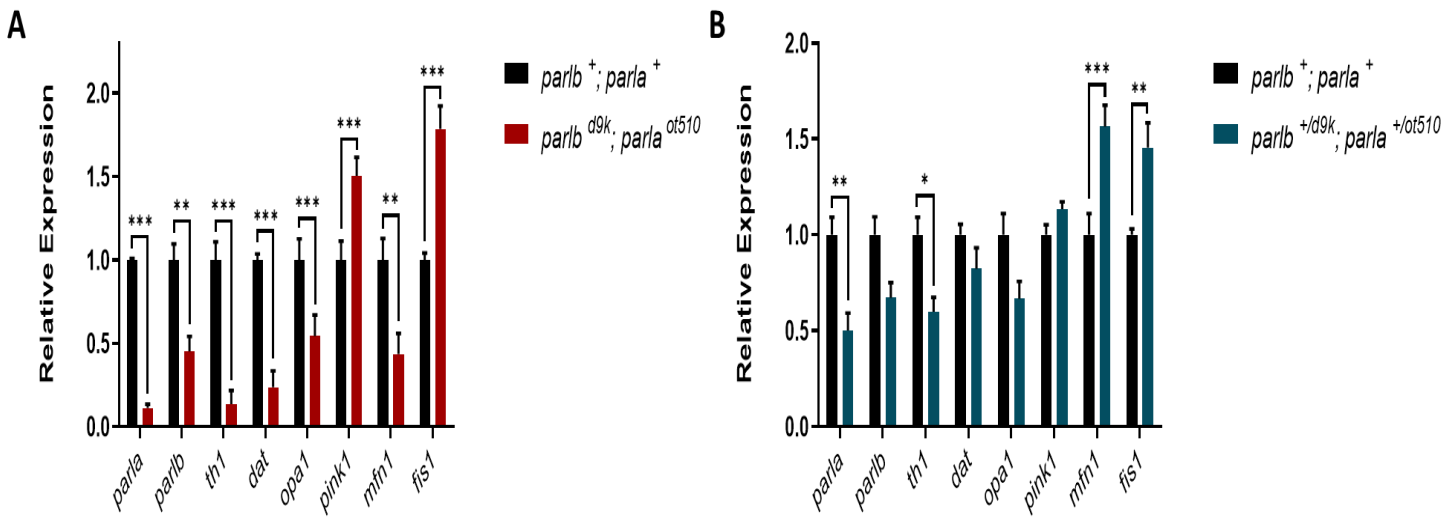

Figure 3.22. Effect of *parla* and *parlb* loss-of-function on the expression of genes associated with dopaminergic- and mitochondrial function in the adult zebrafish brain. (**A,B**) Relative expression of *parla*, *parlb*, *th1*, *dat*, *opa1*, *pink1*, *mfn1*, and *fis1* of 4–10 mpf adult zebrafish brains (n = 3). WT fish are represented by *parlb* $^{+}$*; parla* $^{+}$, double homozygous mutants by *parlb* ^{d9k}*; parla* ^{ot510}, and double heterozygous mutants by *parlb* $^{+/d9k}$*; parla* $^{+/ot510}$. Bars represent the Mean ± the SEM. * (p < 0.05), ** (p < 0.01), *** (p < 0.001).

3.4 DA neuronal loss in the telencephalon and olfactory bulb of *parla* ^{ot510} and *parlb* ^{d9k} mutants.

3.4.1 TH+ cell numbers in *parla* ^{ot510} adult fish brain

To determine the effect of *parla* loss-of-function on DA neuron number and patterning, we performed IHC assays in adults ranging from 7 to 12 mpf in both the telencephalon and olfactory bulb regions using TH1 antibody which is widely used for the detection of DA neurons (Vaz et al. 2018). A reduction in TH positive (TH+) cell number reflects loss of DA neurons. Numbers of TH+ cells for both *parla* ^{ot510} and *parla* $^{+/ot510}$ mutants were compared to WT (Figure 3.23A,D).

TH+ cell reductions of 60% and 20% were observed in the olfactory bulbs (OB) for both *parla* ^{ot510} and *parla* $^{+/ot510}$ animals, respectively (Figure 3.23B,C,G). Similarly, a mild reduction of 25% in TH+ cells was seen in the telencephalon for *parla* ^{ot510} mutants (Figure 3.23F,H). These reductions corroborate the previously observed decrease in *th1* mRNA expression level (Figure 3.23A,B). There was no observable decrease in TH+ cell number in the telencephalon of *parla* $^{+/ot510}$ heterozygous fish (Figure 3.23E).

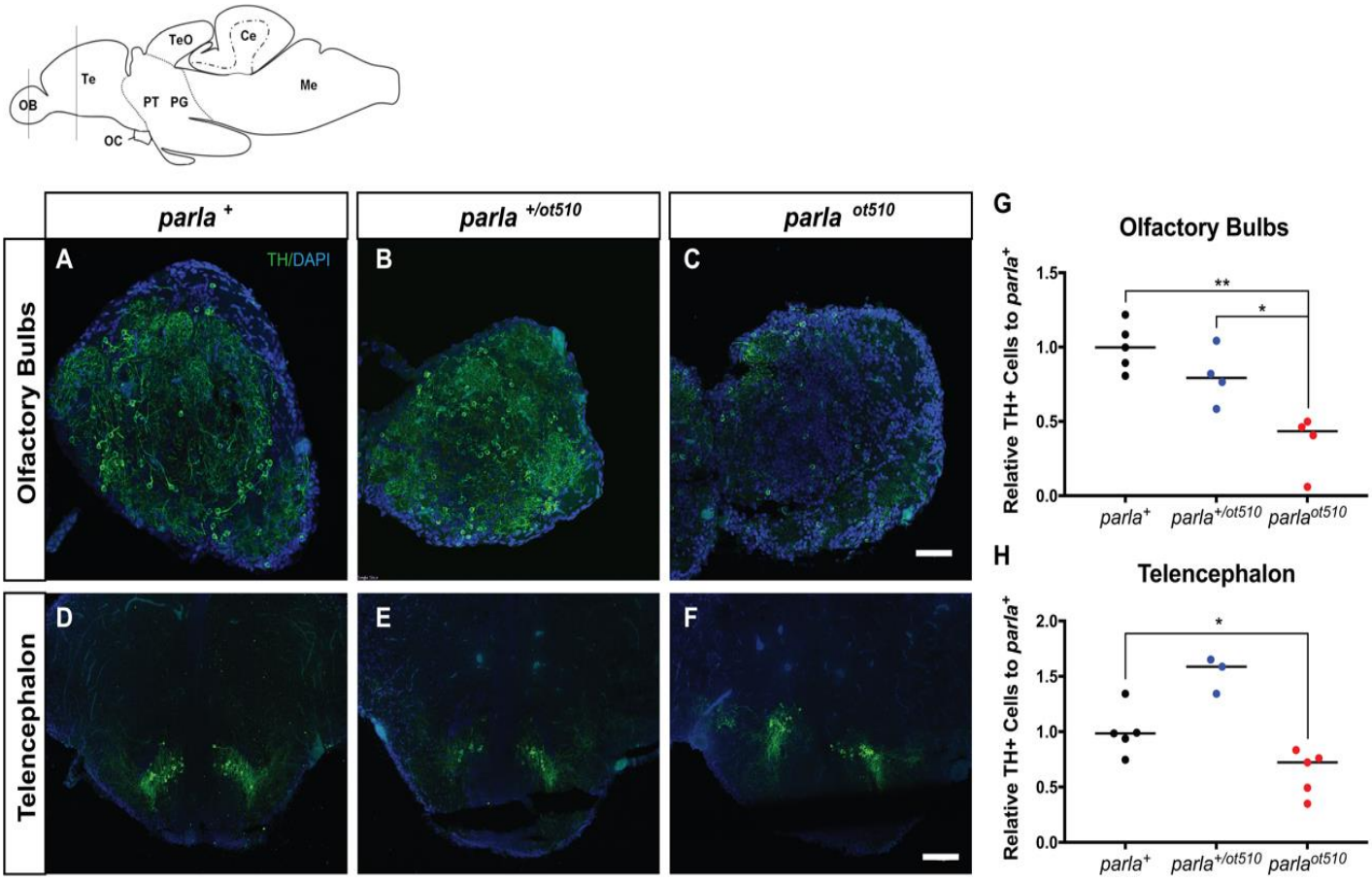

Figure 3.23. Impacts of *parla* loss-of-function on dopaminergic (DA) neuron cell number in the telencephalon and olfactory bulbs of adult zebrafish. Schematic representation of olfactory bulb (OB) and telencephalon sections depicted in the top left panel. (**A**–**F**) Transverse cryosections showing immunofluorescence of TH+ (Green) and DAPI stained (Blue) cells in dissected OB (**A**–**C**) and telencephalon (**D**–**F**) of 7-12 months adult zebrafish. Scale bar: 50 µm**.** (**G**,**H**) Quantification of the number of cells expressing TH. WT fish are represented by *parla* +, homozygous mutants by *parla* ^{ot510}, and heterozygous mutants by *parla* $^{+/ot510}$ (n = 5 for *parla* $^{+}$, n = 4–5 for *parla* ^{ot510} and n= 3–4 for *parla* $^{+/ot510}$ adult zebrafish). Bars represent the Median. * ($p < 0.05$), ** ($p < 0.01$).

3.4.2 TH+ cell numbers in *parlb* ^{d9k}; *parla* ^{ot510} adult fish brain

TH+ cell number was similarly assessed in the double mutant fish (*parlb* ^{d9k}*; parla* ^{ot510}) and compared to the WT (*parlb* $^{+}$*; parla* $^{+}$). A TH+ cell reduction of 55% was observed in the olfactory bulbs (OB) of *parlb* ^{d9k}*; parla* ^{ot510} animals (Figure 3.24A,B,E). Similarly, a reduction of 76% in TH+ cells was seen in the telencephalon for *parlb* ^{d9k}*; parla* ^{ot510} mutants (Figure 3.24C,D,F). These reductions corroborate the previously observed decrease in *th1* expression levels (Figure 3.22A,B).

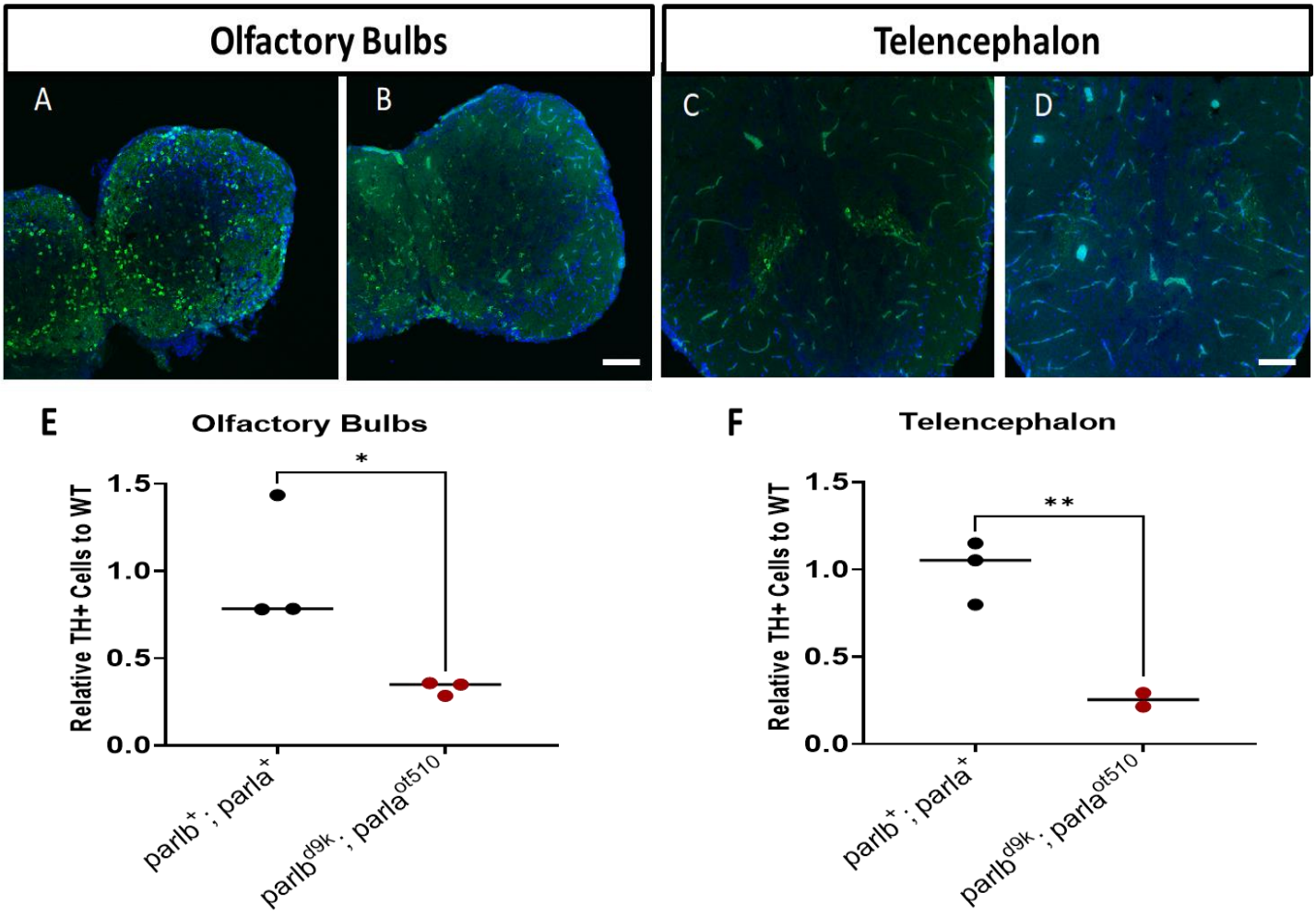

Figure 3.24. Impacts of *parla* and *parlb* loss-of-function on dopaminergic (DA) neuron cell number in the telencephalon and olfactory bulbs of adult zebrafish. (**A**–**D**) Transverse cryosections showing immunofluorescence of TH+ (Green) and DAPI stained (Blue) cells in dissected OB (**A**,**B**) and telencephalon (**C**,**D**) of 7-12 months adult zebrafish. Scale bar: 50 µm**.** (**E**,**F**) Quantification of the number of cells expressing TH. WT fish are represented by *parlb* $^{+}$*; parla* $^{+}$, double homozygous mutants by *parlb* ^{d9k}*; parla* ^{ot510}, and heterozygous mutants by *parlb* $^{+/d9k}$*; parla* $^{+/ot510}$ (n = 3 for *parlb* $^{+}$*; parla* $^{+}$ and n = 2–3 for *parlb* ^{d9k}*; parla* ^{ot510} adult zebrafish). Bars represent the Median. * ($p < 0.05$), ** ($p < 0.01$).

3.5 Behavioral studies of *parla* ^{ot510} and *parlb* ^{d9k} mutants.

3.5.1 Effects on Olfactory Function

To determine if the loss of DA neurons in the OB of adult mutants has implications on olfactory function, we performed a repulsive stimulus test on 7-12 months adult fish. The repulsive stimulus used in this experiment is cadaverine, which was administered to the arm of an apparatus (top right part in Figure 3.25B,C,D) in which the fish was acclimatized (Godoy et al. 2020). The time spent in each section of the tank was then recorded and the ratio of time spent in stimulus arm was calculated.

There was no significant change in the ratio of time spent in stimulus arm observed in *parlb* ^{d9k} and *parlb* $^{+/d9k}$ mutants as compared to the WT (*parlb* $^{+}$) zebrafish (Figure 3.25).

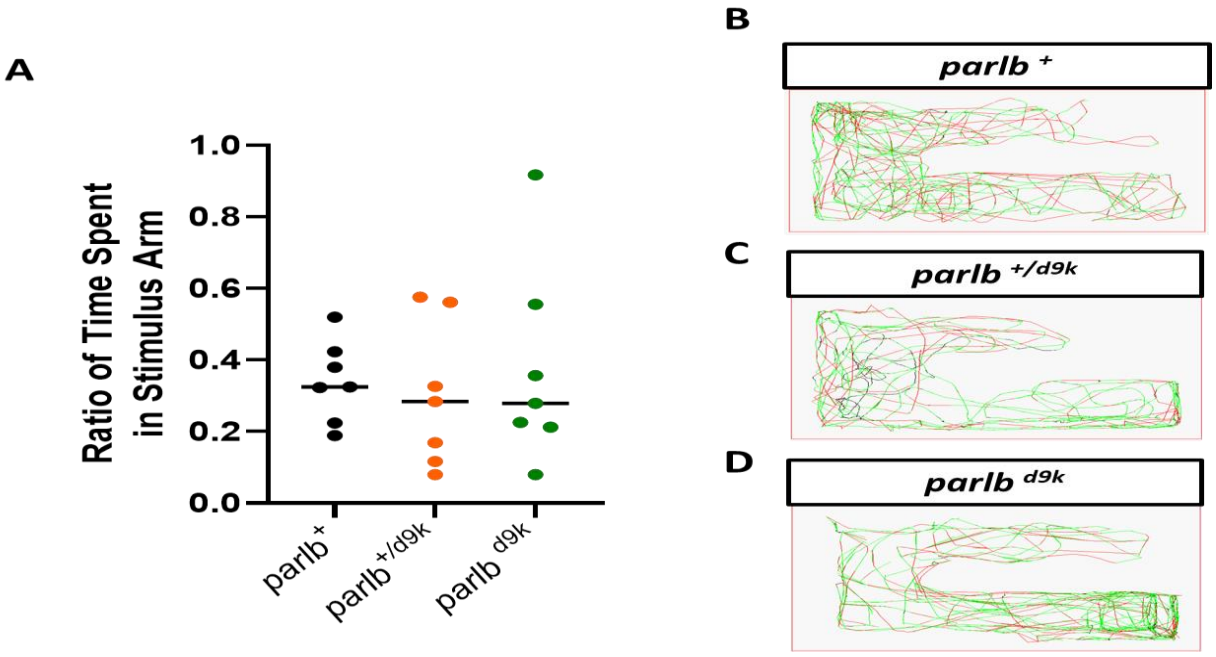

Figure 3.25. No change in olfactory function in adult zebrafish with loss of *parlb* function. (**A**) Ratio of time spent in stimulus arm (top) of 7–12 mpf adult zebrafish (n = 7). (**B**–**D**) Path images of a representative for WT fish (*parlb* $^{+}$), homozygous mutants (*parlb* ^{d9k}), and heterozygous mutants (*parlb* $^{+/d9k}$).

In contrast, *parla* ^{ot510} fish spent on average of more than 3.5 times of the recorded period in the stimulus arm where cadaverine was added compared to the WT (*parla* $^{+}$) zebrafish (Figure 3.26A,B,D). Similarly, there was a 2 times increase in the ratio of time spent in the stimulus arm observed in heterozygotes (*parla* $^{+/ot510}$) (Figure 3.26A,C).

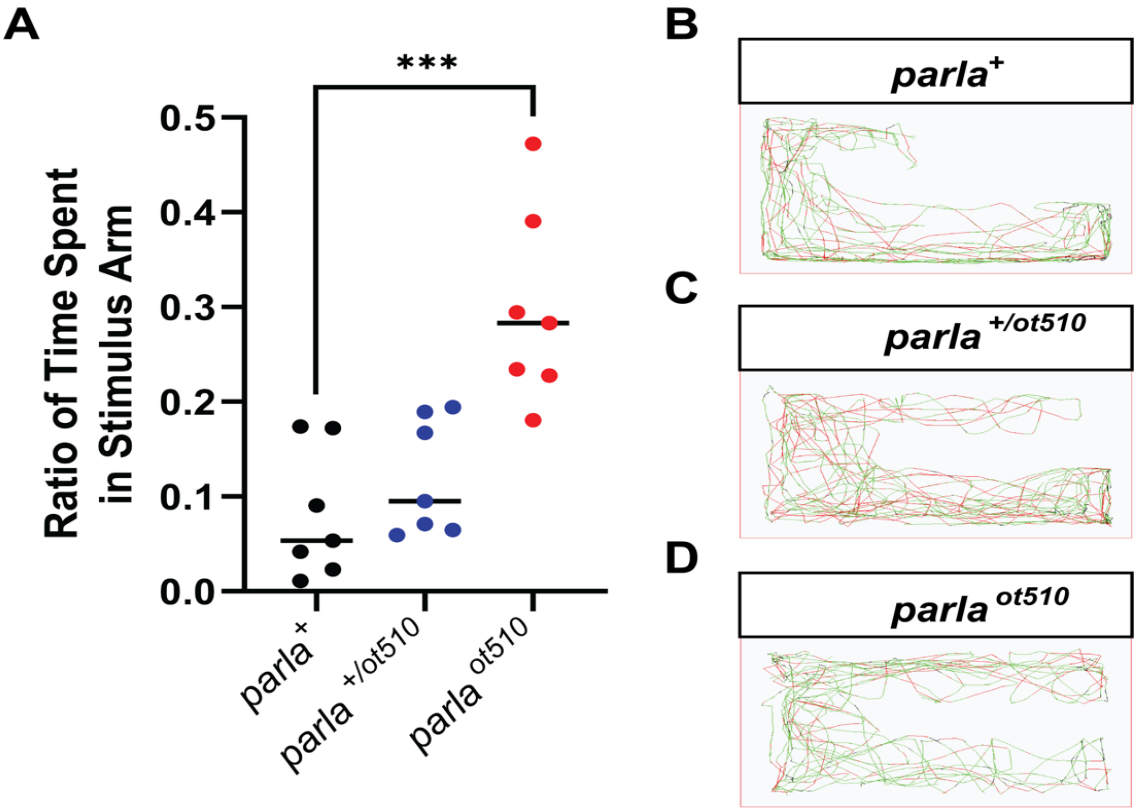

Figure 3.26. Decreased olfactory function in adult zebrafish with loss of *parla* function. (**A**) Ratio of time spent in stimulus arm (top) of 7–12 mpf adult zebrafish (n = 7). (**B**–**D**) Path images of a representative for WT fish (*parla* $^{+}$), homozygous mutants (*parla* ^{ot510}), and heterozygous mutants (*parla* $^{+/ot510}$). Bars represent the Median. *** ($p < 0.001$).

As for *parlb* ^{d9k}*; parla* ^{ot510} double homozygous mutants, they spent on average of 1.5 times of the ratio of time spent in stimulus arm compared to the WT (*parlb* $^{+}$*; parla* $^{+}$) fish (Figure

3.27A,B,D). However, there was no significant change in the ratio of time spent in stimulus arm observed for *parlb* $^{+/d9k}$*; parla* $^{+/ot510}$ double heterozygotes (Figure 3.27A,B,C).

These results were surprising as the double (*parlb* ^{d9k}*; parla* ^{ot510}) mutant fish spent less time in stimulus arm compared to the *parla* ^{ot510} single mutants. This might be explained by the fact that the WT fish used for the double mutants are different than the WT animals used for the single mutants, and thus, they have different ratios of time spent in cadaverine arm. In fact, we noticed that the ratio of time spent in stimulus arm was equal to 0.56 for the double homozygotes (*parlb* ^{d9k}*; parla* ^{ot510}), greater than that of the *parla* single mutants (*parla* ^{ot510}) which was equal to 0.28 (Figures 3.26A and 3.27A).

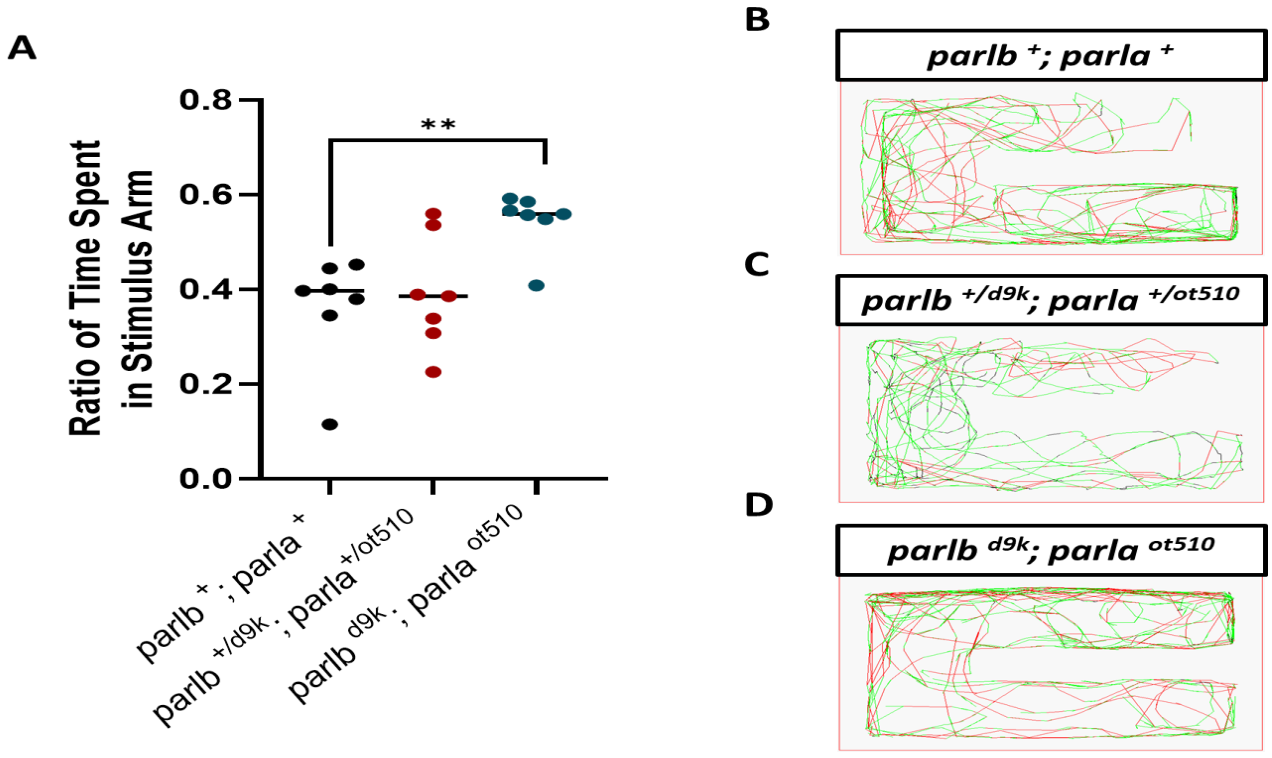

Figure 3.27. Decreased olfactory function in adult zebrafish with loss of *parla* and *parlb* function. (**A**) Ratio of time spent in stimulus arm of 7–12 mpf adult zebrafish (n = 7). (**B**–**D**) Path images of a representative for WT fish (*parlb* $^{+}$*; parla* $^{+}$), homozygous mutants (*parlb* ^{d9k}*; parla* ^{ot510}), and heterozygous mutants (*parlb* $^{+/d9k}$*; parla* $^{+/ot510}$). Bars represent the Median. ** ($p < 0.01$).

3.5.2 Effects on Locomotion

To further investigate whether the decreases seen in DA cell number in the brain of *parla* and *parlb* mutants translate into behavior impairing phenotypes, we also analyzed locomotor activity in 7-12 months adult zebrafish.

Intriguingly, we observed 39% and 20% decreases in distance travelled and average velocity for *parlb* ^{d9k} mutants and *parlb* $^{+/d9k}$ fish respectively (Figure 3.28A,B). Furthermore, there was an increase of 2.25 times on average in inactivity duration for *parlb* ^{d9k} mutants as compared to the WT animals (Figure 3.28C). However, no significant change in inactivity duration was observed for heterozygous (*parlb* $^{+/d9k}$) fish (Figure 3.28C).

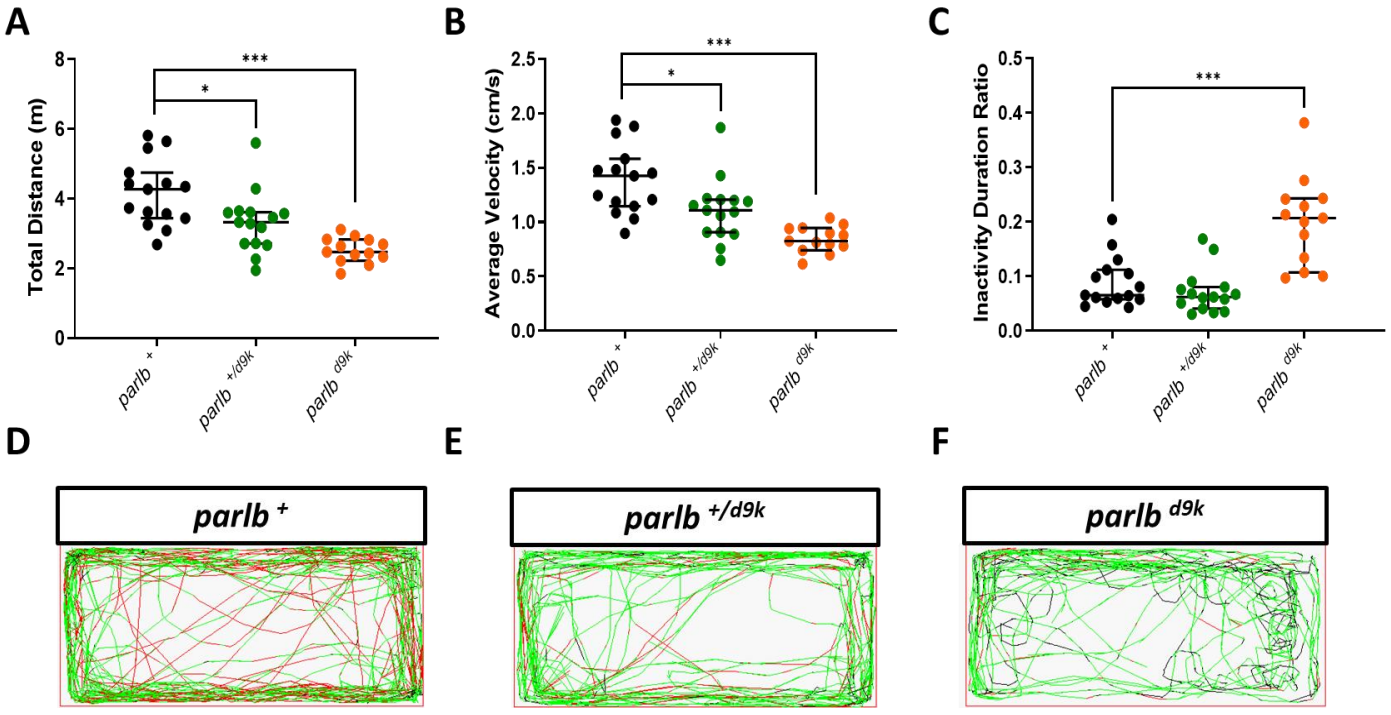

Figure 3.28. Swimming activity of adult mutants with loss of *parlb* function and WT zebrafish. (**A–C**) Impact of *parlb* loss-of-function on total swim distance, average swimming velocity and inactivity periods (n = 13-15 adult zebrafish). (**D–F**) Path images of a representative for WT fish (*parlb* $^{+}$), homozygous mutants (*parlb* ^{d9k}), and heterozygous mutants (*parlb* $^{+/d9k}$). Bars represent the Median with 95% CI. * ($p < 0.05$), *** ($p < 0.001$).

In *parla* ^{ot510} and *parla* $^{+/ot510}$ mutants, there was no significant change in the total distance travelled, average velocity and inactivity duration ratio (Figure 3.29A,B). Interestingly, *parla* ^{ot510} fish showed a 62% increase in inactivity duration as compared to WT (Figure 3.29C). In contrast, no significant impact on inactivity was observed for heterozygous (*parla* $^{+/ot510}$) animals.

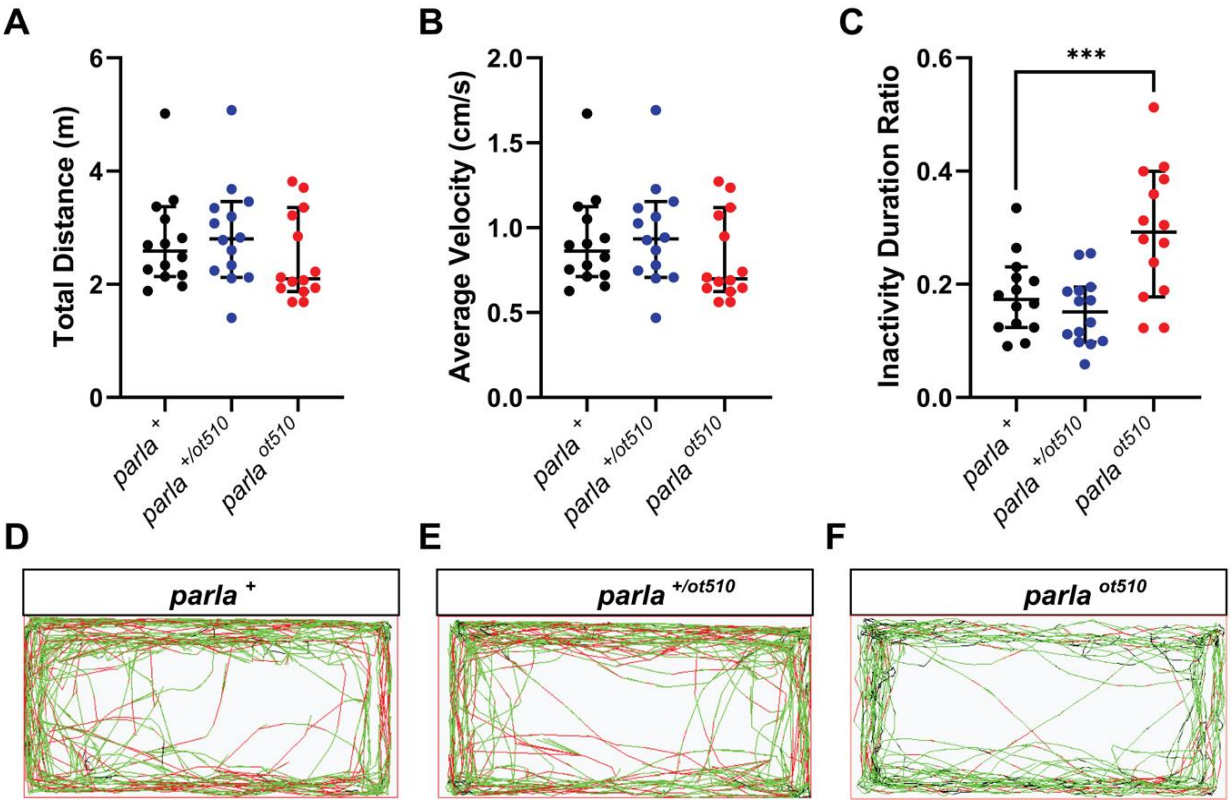

Figure 3.29. Swimming activity of adult mutants with loss of *parla* function and WT zebrafish. (**A–C**) Impact of *parla* loss-of-function on total swim distance, average swimming velocity and inactivity periods (n = 14 adult zebrafish). (**D–F**) Path images of a representative for WT fish (*parla* $^{+}$), homozygous mutants (*parla* ^{ot510}), and heterozygous mutants (*parla* $^{+/ot510}$). Bars represent the Median with 95% CI. *** ($p < 0.001$).

Furthermore, we found that distance travelled, average velocity, and inactivity duration were not affected for 5 dpf larvae and 10 dpf fish with loss of *parla* function (Appendix Figures A.5,A.6).

In contrast, we observed 54% and 26% decreases in distance travelled and average velocity for both *parlb* ^{d9k}*; parla* ^{ot510} double homozygous mutants and for *parlb* $^{+/d9k}$*; parla* $^{+/ot510}$ double heterozygous fish respectively (Figure 3.30A,B). Interestingly, there was an increase of 3 times on average in inactivity duration ratio for the double homozygous mutants (Figure 3.30C). Similarly, the double heterozygous fish showed on average 2.5 times increase in inactivity duration ratio compared to the WT animals (Figure 3.30C). These results show that locomotion is more disturbed in the double mutants than in the single mutants with loss of *parla* or *parlb* function.

No significant change in distance travelled, average velocity, and inactivity duration was detected for both *parlb* $^{+/d9k}$*; parla* ^{ot510} mutants and *parlb* ^{d9k}*; parla* $^{+/ot510}$ fish (Figure 3.30A,B,C). In this case, the presence of a *parla* or *parlb* WT allele seemed to rescue the behavioral phenotype observed for the double homozygous mutants.

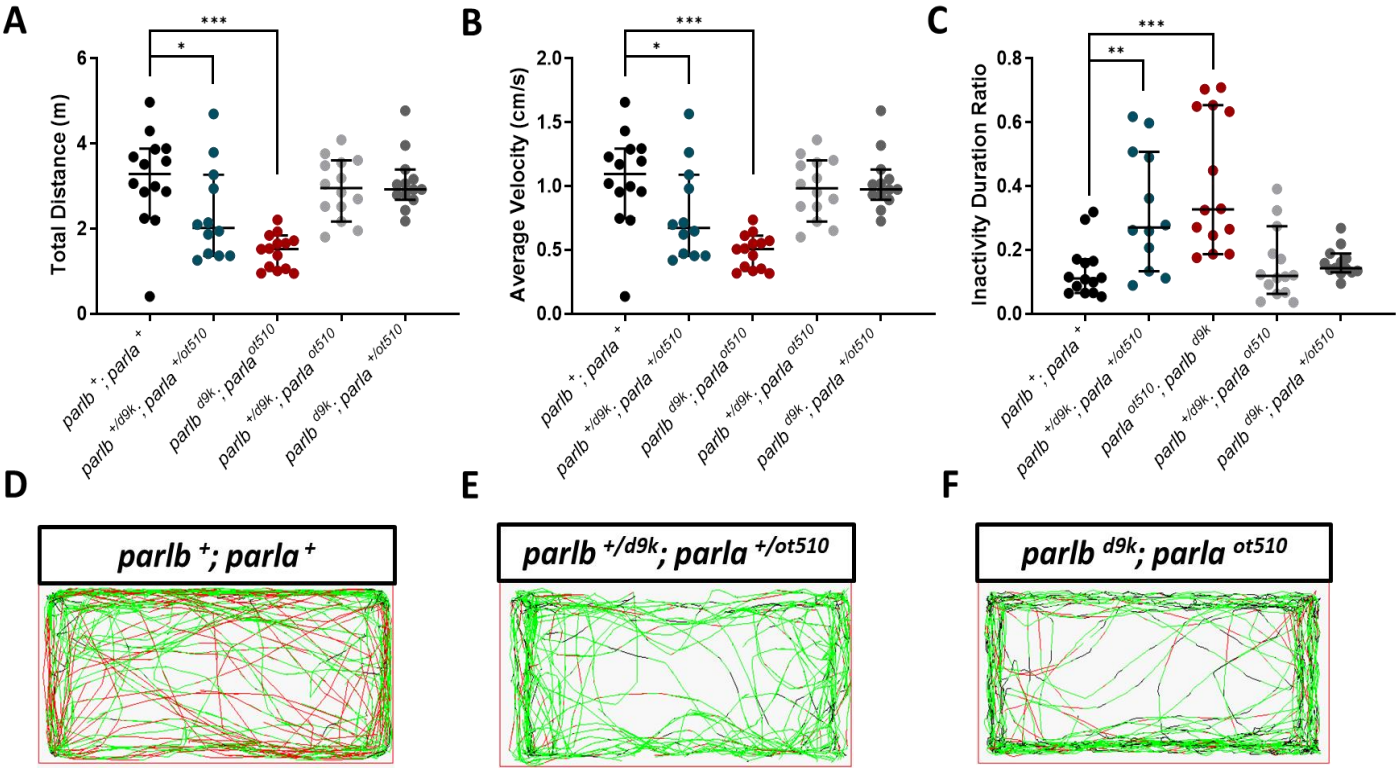

Figure 3.30. Swimming activity of adult mutants with loss of *parla* and *parlb* function and WT zebrafish. (**A–C**) Impact of *parla* and *parlb* loss-of-function on total swim distance, average swimming velocity and inactivity periods (*n* = 12-14 adult zebrafish). (**D–F**) Path images of a representative for WT fish (*parlb* $^{+}$*; parla* $^{+}$), double homozygous mutants (*parlb* ^{d9k}*; parla* ^{ot510}), and double heterozygous mutants (*parlb* $^{+/d9k}$*; parla* $^{+/ot510}$). Bars represent the Median with 95% CI. * ($p < 0.05$), ** ($p < 0.01$), *** ($p < 0.001$).

3.6 Treatments of *parla* ^{ot510} and *parlb* ^{d9k} mutant larvae with neurotoxin (MPTP).

Given the impact of loss of *parla* and *parlb* function on dopaminergic neurons, behavioral phenotypes, and gene expression levels, we tested whether fish with loss of *parla* and/or *parlb* function are more susceptible to neurotoxin exposure than the WT animals. All treatments were conducted using the neurotoxin, MPTP, on 3 dpf larva, as by this time, there are near complete DA neuron differentiation and blood brain barrier (BBB) development. This time point also avoids inhibition of neurogenesis (Du et al. 2016). Varying MPTP concentrations were used to determine the lethal dose for the mutant fish that would result in the least survival percentage by 5 days post-treatment (5 dpt). Developmental deformities such as a curved spine and edema were observed in the double homozygous fish (*parlb* ^{d9k}*; parla* ^{ot510}), double heterozygous mutants (*parlb* $^{+/d9k}$*; parla* $^{+/ot510}$), and WT fish (*parlb* $^{+}$*; parla* $^{+}$) (data not shown). These morphological deformities had previously been observed at higher MPTP doses (1 and 1.5 mM) (Kalyn et al, 2019).

3.6.1 Susceptibility of the mutants to MPTP exposure

Following exposure of *parlb* ^{d9k} and *parlb* $^{+/d9k}$ mutants to varying MPTP concentrations (0.1, 0.25, 0.5, 1 mM, and 2 mM), the lethal dose in mutants was found to be 0.5 mM, identical to that determined in WT larva (*parlb* $^{+}$) (Figure 3.31A,B,C). The highest concentrations of 1 and 2 mM resulted in complete mortality for all the mutants between 1 and 3 dpt. A 100% lethality was also observed for the concentration of 0.25 mM at 5 dpt for *parlb* ^{d9k} and *parlb* $^{+/d9k}$ mutants (Figure 3.31B,C), as opposed to 87.5% lethality identified for WT fish at 5 dpt (Figure 3.31A). The lowest concentration of 0.1 mM resulted in 40% and 55% mortality for WT larvae and *parlb* $^{+/d9k}$ mutants, respectively, but a complete lethality with the same concentration was observed for *parlb* ^{d9k} at 5 dpt (Figure 3.31A,B,C).

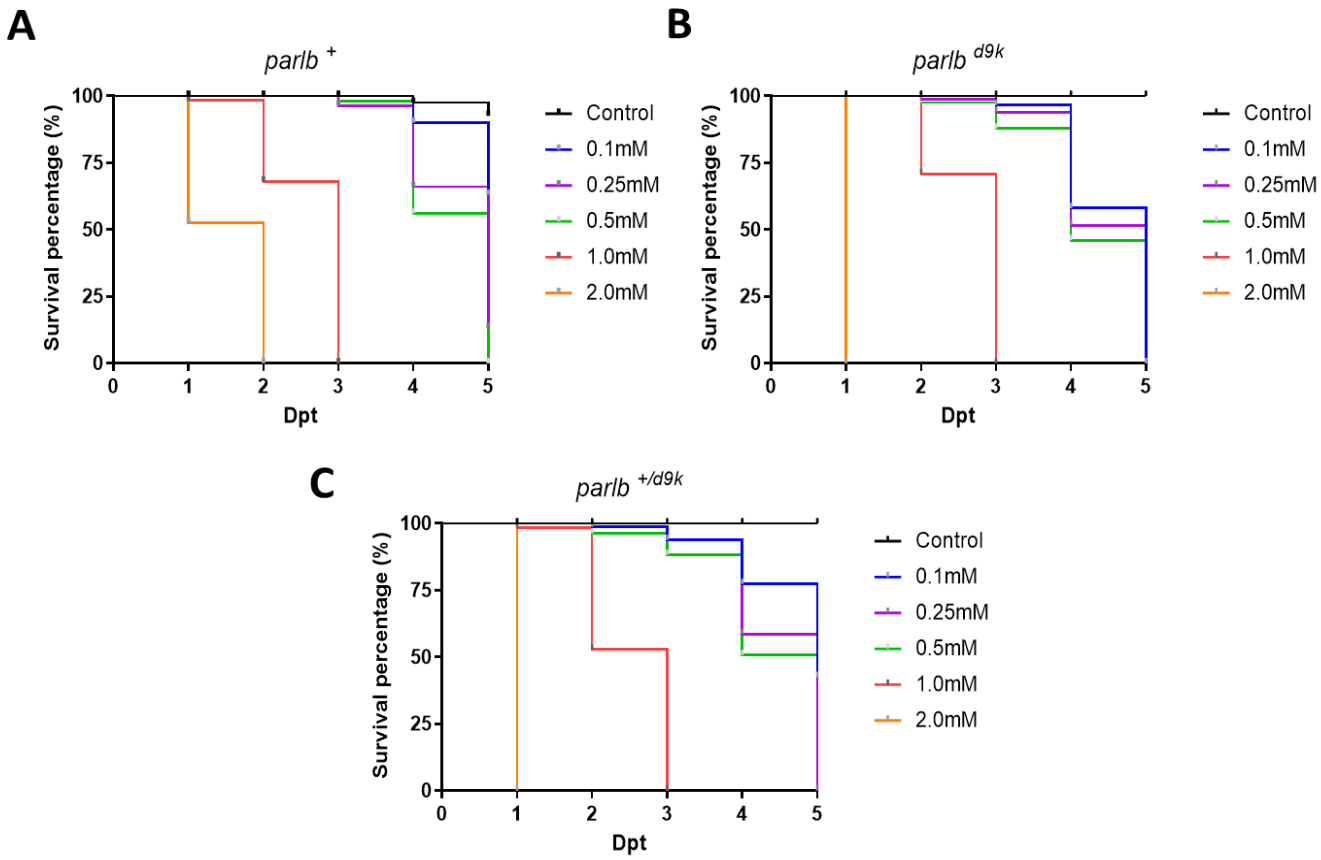

Figure 3.31. Survival curves of larvae with loss of *parlb* function and WT fish following MPTP exposure. 3 dpf embryos (n=20) were exposed to varying concentrations of MPTP to determine the lethal dose for (**A-C**) WT fish (*parlb* $^{+}$), homozygous mutants (*parlb* ^{d9k}), and heterozygous mutants (*parlb* $^{+/d9k}$). Lethality was quantified every day until the zebrafish reached 7 dpf.

As opposed to the *parlb* single mutants having a lethal dose of 0.5 mM (Figure 3.31), mutants with *parla* loss of function (*parla* ^{ot510} and *parla* $^{+/ot510}$) showed the least survivability with the lethal dose of 0.25 mM, identical to the lethal dose identified in WT larvae (*parla* $^{+}$) (Figure 3.32A,B,C). However, at a concentration of 0.5 mM, a complete lethality was observed at 4 dpt for *parla* ^{ot510} and *parla* $^{+/ot510}$ mutants (Figure 3.32B,C). In contrast, the lowest concentration of 0.1 mM resulted in few mortalities (35-50%) at 5 dpt for all fish.

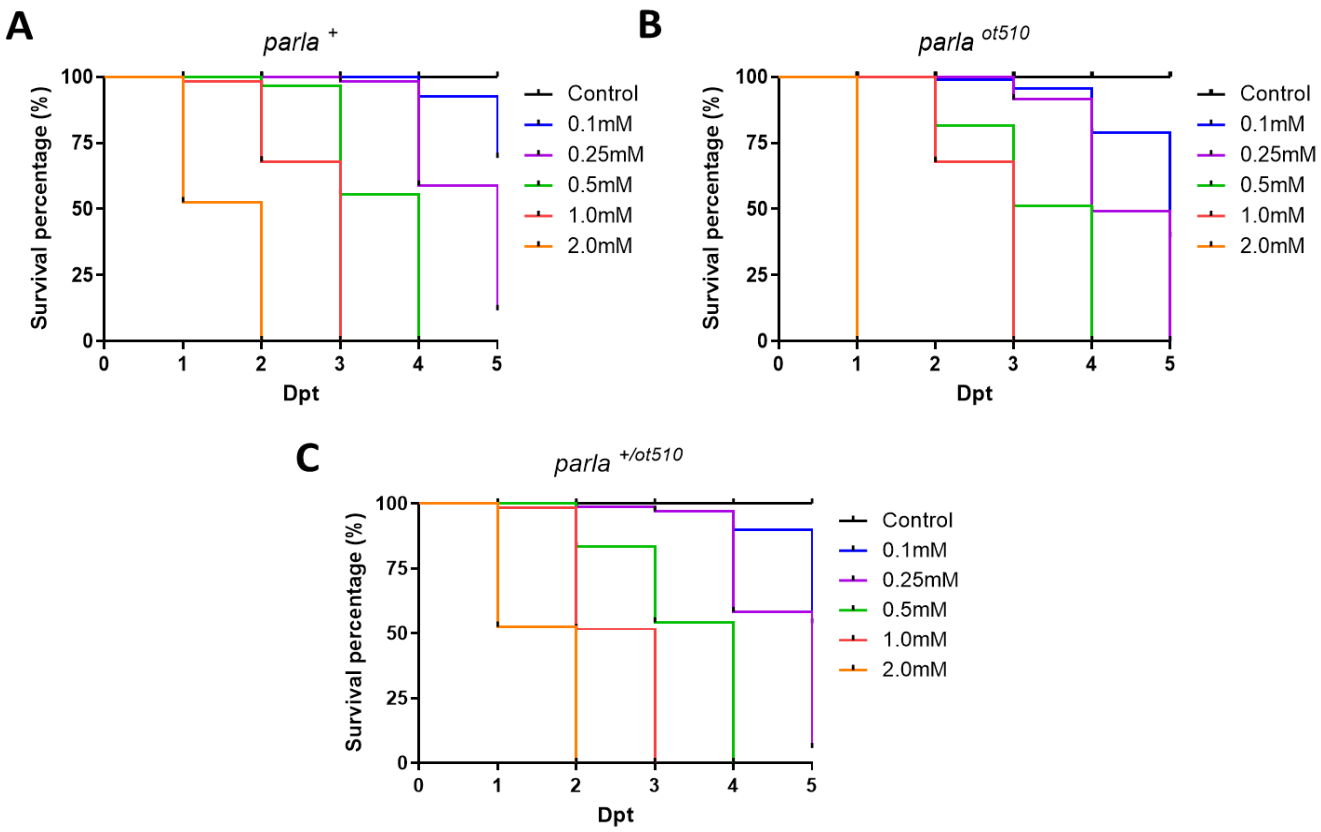

Figure 3.32. Survival curves of larvae with loss of *parla* function and WT fish following MPTP exposure. 3 dpf embryos (n=20) were exposed to varying concentrations of MPTP to determine the lethal dose for (**A-C**) WT fish (*parla* $^{+}$), homozygous mutants (*parla* ^{ot510}), and heterozygous mutants (*parla* $^{+/ot510}$). Lethality was quantified every day until the zebrafish reached 7 dpf.

As for the double homozygous mutants (*parlb* ^{d9k}*; parla* ^{ot510}), the lethal dose identified was lower than that of the single mutants (*parla* ^{ot510} or *parlb* ^{d9k}) and was found to be 0.1mM, the lowest concentration used in these treatments (Figure 3.33B). These results indicate a higher susceptibility of the double homozygotes as compared to the single mutants to MPTP exposure.

Interestingly, the lethal dose for the double heterozygous fish (*parlb* $^{+/d9k}$*; parla* $^{+/ot510}$) was 0.5 mM, identical to the lethal dose identified in WT larvae (*parlb* $^{+}$*; parla* $^{+}$) (Figure 3.33A,C).

However, double homozygous fish (*parlb* ^{d9k}*; parla* ^{ot510}) showed complete lethality at 4 dpt after exposure to 0.5 mM of MPTP. A 100% lethality was also observed for the concentration of 0.25 mM at 4 dpt for the double homozygous mutants (Figure 3.33B) as opposed to 88% and 40% lethality identified for *parlb* $^{+/d9k}$*; parla* $^{+/ot510}$ mutants and WT fish, respectively, at 5 dpt (Figure 3.33A,C).

It is to be noted that the lowest concentration of 0.1 mM that resulted in complete lethality at 5 dpt in the double homozygotes as mentioned previously, did not lead to complete mortality for WT larvae (45%) and double heterozygotes (40%) at 5 dpt (Figure 3.33A,C).

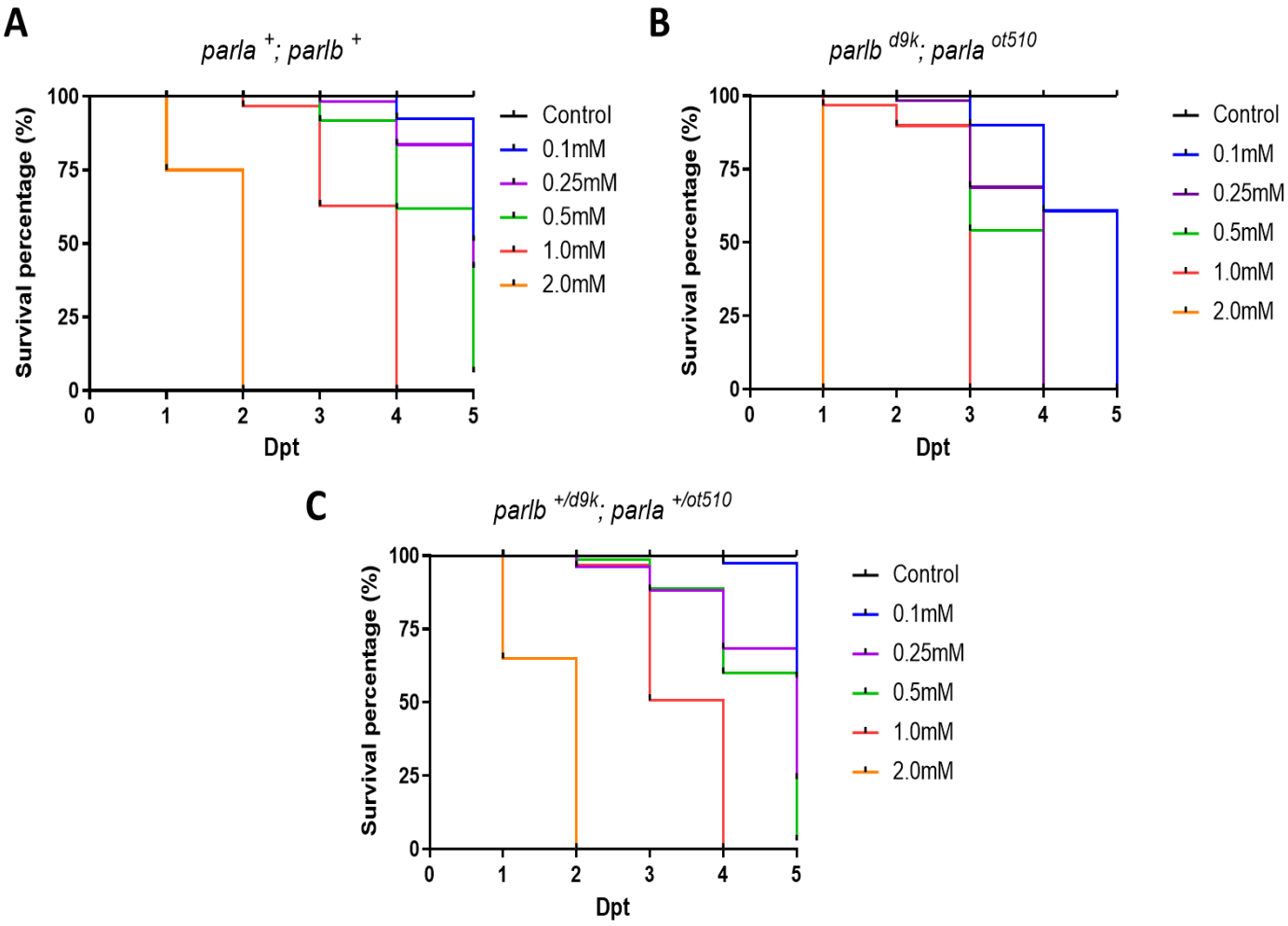

Figure 3.33. Survival curves of larvae with loss of *parla* and *parlb* function and WT fish following MPTP exposure. 3 dpf embryos (n=20) were exposed to varying concentrations of MPTP to determine the lethal dose for (**A-C**) WT fish (*parlb* $^{+}$*; parla* $^{+}$), double homozygous mutants (*parlb* ^{d9k}*; parla* ^{ot510}), and double heterozygous mutants (*parlb* $^{+/d9k}$*; parla* $^{+/ot510}$). Lethality was quantified every day until the zebrafish reached 7 dpf.

3.6.2 Gene expression analysis of double homozygous mutants treated with MPTP

Gene expression analysis was performed for the MPTP treated double homozygous fish (*parlb* ^{d9k}*; parla* ^{ot510}) as they showed increased susceptibility to MPTP exposure (lethal dose of 0.1 mM) observed with the survival curves as compared to WT fish and double heterozygous mutants (lethal dose of 0.5 mM) (section 3.5.1).

Double homozygous and WT larvae exposed to the lethal MPTP dose were collected at 5 dpt, for gene expression analysis. The expression of *th1*, *opa1*, and *fis1* was increased 3, 5 and 3.5-fold, respectively (Figure 3.34). The observed changes in the expression of *opa1* and *fis1* suggest increased apoptosis and mitochondrial fission events, respectively, in the double homozygous fish (*parlb* ^{d9k}*; parla* ^{ot510}) exposed to 0.1 mM of MPTP. However, the increase in *th1* expression level suggest an increase in dopamine biosynthesis occurring in the DA neurons that survive to compensate for the dopamine biosynthesis reduction in the degenerating DA neurons. Similarly, there was a slight 0.25-fold increase in *pink1* expression (Figure 3.34).

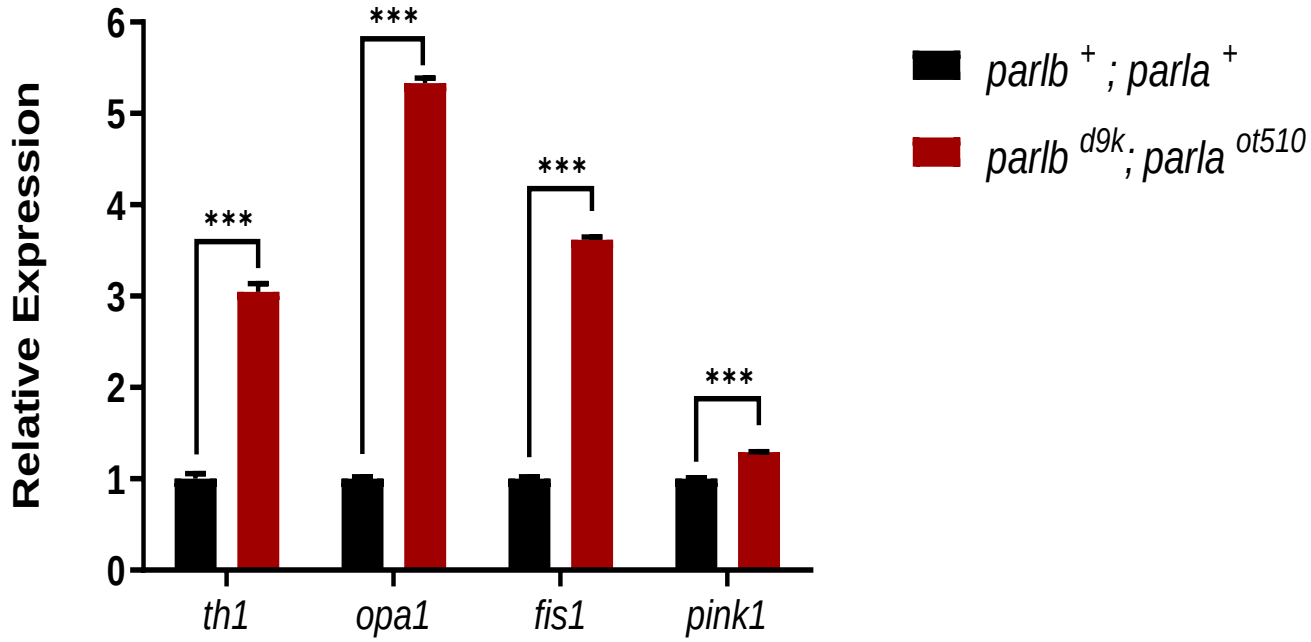

Figure 3.34. Effect of MPTP treatment on the expression of genes associated with dopaminergic- and mitochondrial function in larvae with loss of *parla* and *parlb* function. Relative expression of *th1*, *opa1*, *fis1*, and *pink1* of 7 dpf zebrafish larvae (n=3. Each replicate contains 7-9 homogenized whole larvae). WT fish are represented by *parlb* $^{+}$*; parla* $^{+}$ and double homozygous mutants by *parlb* ^{d9k}*; parla* ^{ot510}. Bars represent the Mean ± the SEM. *** ($p < 0.001$).

CHAPTER 4. Discussion & Conclusions

4.1 Multi-exon deletions were generated in both *parla* and *parlb* genes in zebrafish and we observed partial *parlb* gene expression in the previously established *parlb* ^{d9k} mutants

To date, the vast majority of studies addressing *PARL* function have been performed in yeast, *Drosophila*, and mammals (McQuibban et al., 2003; McQuibban et al., 2006; Spinazzi et al., 2019). The *PARL* paralogs have been previously identified in a zebrafish model (Noble et al., 2012). This evolutionary conservation of *PARL* is evidence of the critical role that this protease plays across the animal kingdom.

Morpholino-mediated knockdown of both *parla* and *parlb* genes resulted in embryonic lethality, increased cell death, and mild neurodegeneration of DA neurons (Noble et al., 2012). However, given the transient nature of gene-knockdown phenotypes, and the inability to carry further studies on adults using morpholino, additional loss-of-function studies in larvae and adult zebrafish needed to be performed.

In our study, we generated permanent multi-exon deletions in the *parla* and *parlb* genes via CRISPR/Cas9-mediated mutagenesis. These results are novel as the generation of multi-exon deletions in the *parl* genes was not previously performed in zebrafish. Consequently, mutants having a 1.4 kb deletion (exon 1 to exon 2) and a 15 kb deletion (exon 1 to exon 9) in *parla* gene were established using multiple sgRNAs. In fact, studies have shown that the use of multiple guide sequences increases mutation efficiency and success and leads to the deletion of the specific targeted set of nucleotides or exons (Cong et al., 2013). This was confirmed in our results in which the use of one sgRNA alone was not successful in inducing a mutation in the *parla* gene. Moreover, it was suggested by Sztal and colleagues that generating full-locus deletions in the gene of interest would avoid or minimize genetic compensation (Sztal and Stainier, 2020). It was argued that genetic compensation is likely to occur through transcriptional adaptation (TA) during which

mutations that result in mutant mRNA degradation activates the transcriptional modulation of adapting genes. Those genes could be paralogous that would increase their expression levels to compensate for the loss of the mutant gene's product (Sztal and Stainier, 2020).

A 5-nucleotide deletion in *parlb* gene was previously generated in our lab and resulted in a frameshift mutation in exon 1 of the *parlb* gene that would lead to a premature termination (Jung, 2017). The ideal way to confirm that the mutation resulted in the loss of a gene function is by performing genomic PCR amplification and sequencing followed by protein analyses such as Western Blots as a validation of whether a protein is being translated or not. In our study, we performed PCR amplification followed by sequencing that confirmed the deletion of the predicted nucleotide sequences and exons in the *parla* and *parlb* genes. Nevertheless, we did not perform an immunoblotting analysis to validate the absence of protein translation. Previous work in our lab tested anti-human PARL antibodies available commercially. However, there was a lack of recognition of the antibodies for Parla and Parlb in zebrafish or cell lysates. Moreover, results found previously using custom-generated antibodies against Parla and Parlb (Open Biosystems) were not promising as no specific bands were detected in zebrafish mitochondrial lysates and no signal was produced in immunoprecipitation experiments performed on cultured cells (Noble, 2014).

Thus, to confirm loss of *parla* and/or *parlb* function in our mutants, we performed gene expression studies. We found a 96% reduction in *parla* mRNA levels in the *parla* ^{ot510} mutants which confirmed loss of *parla* function. Intriguingly, we found a 60% decrease in *parlb* expression levels in the *parlb* ^{d9k} mutants which infers a partial loss of *parlb* function. In fact, previous studies done in our lab found that the genomic-based *parlb* mutation was transcribed into the mature mRNA (Jung, 2017). This was assessed by performing PAGE analysis of PCR amplified *parlb*

cDNA followed by sequencing which showed the presence of the mutation in the cDNA itself. It was then suggested that these mutant mRNAs might be possibly escaping the nonsense-mediated decay (Jung, 2017), a conserved surveillance mechanism to control the quality of mRNA produced in a cell by detecting and degrading mRNA containing premature stope codons (PTCs) (Behm-Ansmant et al., 2007).

4.2 The double mutants with complete loss-of-function in both *parla* and *parlb* gene (*parlb* ^{ot512}*; parla* ^{ot510}) are lethal

The functional and structural conservations of PARL are evidence that this protease plays a crucial role across the various species. In fact, PARL was found to play an indispensable role in cell homeostasis as illustrated by the severe phenotypes following its genetic ablation in the diverse investigated species (McQuibban et al., 2006; Noble et al., 2012).

In yeast, *rhomboid-1* (PARL ortholog)-deficient strains were unable to grow in glycerol medium and showed striking mitochondrial fragmentation and aggregation (McQuibban et al., 2003). In *Drosophila*, *rhomboid-7* deficient flies die before pupation. The few flies that make it to adulthood suffer from neurological defects and the males were found to be sterile, and do not survive longer than 3 days (McQuibban et al., 2006). In mammals, targeted *PARL* null mice show progressive muscle and immune organ atrophy with death occurring before the age of three months (Strooper et al., 2006). In zebrafish, morpholino-mediated knockdown of *parla* and *parlb* simultaneously was found to cause embryonic lethality of around 50% by 3 dpf (Noble et al., 2012). However, the knockdown of either of the two paralogs did not have a significant effect on

survival at 3 dpf. Thus, at least one functional copy of either *parla* or *parlb* gene is needed for early embryonic survival (Noble et al., 2012).

In our study, we found that the double mutants with a complete loss of *parla* and *parlb* function were lethal. These results corroborate with the lethality observed with loss of *PARL* function across the different species and with the morpholino knockdown study previously conducted in zebrafish. Moreover, we found that the double homozygous mutants were dying at an age ranging between 5 and 45 dpf. We then investigated the timepoint at which these double mutants died. Interestingly, all the double mutants and around 40% of fish that are heterozygous for *parlb* and homozygous for *parla* mutation died by 21 dpf. Moreover, the double mutant fish showed apparent spinal curvature and were swimming downwards with their heads directed towards the bottom of the tank. In fact, a previous study found that failure of swim bladder inflation at the larval stage had detrimental consequences for the survival of several teleost species, including zebrafish (Goolish and Okutake, 1999). Interestingly, at 21 dpf, the day that we observed 100% lethality in the double mutants, the anterior chamber of the swim bladder would normally get inflated during normal development in WT fish (Winata et al., 2009). The posterior chamber develops and gets inflated much earlier by 4.5 dpf. Thus, it might be that the posterior chamber of the swim bladder was defective in these fish leading to spinal curvature and swimming impairments. It is to be noted that as the double mutants with a complete loss-of-function of both *parla* and *parlb* genes (*parlb* ^{ot512}; *parla* ^{ot510}) were lethal, we have used in our studies the double homozygous fish that showed a partial *parlb* expression level as they were found to be viable (*parlb* ^{d9k}*; parla* ^{ot510}).

4.3 Gene expression of *fis1* was increased and the expression level of *th1* was reduced in the *parla* single mutants (*parla* ^{ot510}) and the double mutant fish (*parlb* ^{d9k}*; parla* ^{ot510})

Striking mitochondrial functional and morphological abnormalities such as fragmentation and aggregation have been observed in yeast, *Drosophila*, and mice with a loss-of-function mutation in the *PARL* gene (Cipolat et al., 2006; McQuibban et al., 2003; McQuibban et al., 2006; Spinazzi et al., 2019). Moreover, it has been suggested that mitochondrial damage, likely due to an increase in reactive oxygen species, results in depolarization of the inner mitochondrial membrane and loss of membrane potential which induces mitochondrial fragmentation (Ross et al., 2008).

In our study, we analyzed expression of the *fis1* gene involved in mitochondrial fission. We observed a significant increase in *fis1* mRNA expression in both *parla* single mutant (parla ot510) and double mutant (*parlb* ^{d9k}*; parla* ^{ot510}) adult brains and in *parla* mutant (*parla* ^{ot510}) larvae. We hypothesize that mitochondria of both adult fish brains and larvae with loss of *parla* function and mitochondria of adult brains with simultaneous loss of *parla* and *parlb* function undergo increased mitochondrial fission turnover due to mitochondrial dysfunction. A more concrete observation such as live mitochondrial imaging is still needed to confirm this hypothesis. Interestingly, *fis1* expression levels were found to be increased in mutants with loss of *parlb* function, however, this increase did not reach statistical significance. This might indicate a more prominent involvement of *parla* rather than *parlb* gene in regulating mitochondrial fission.

The mitochondrial morphology is influenced by the balance between opposing fission and fusion events, which are controlled by several large dynamin-related GTPase proteins such as MFN1 and OPA1 (Smirnova et al., 2001). During mitochondrial fusion, both the outer and the inner mitochondrial membranes undergo fusion. MFN1 and OPA1 are involved in the

mitochondrial outer membrane fusion and inner membrane fusion, respectively (Santel and Fuller, 2001). In our study, we analyzed the gene expression of *mfn1* and we found significant changes in the double homozygous (*parlb* ^{d9k}*; parla* ^{ot510}) fish where *mfn1* expression levels were significantly reduced. This was an expected result as the double mutants undergo increased mitochondrial fission turnover as mentioned previously which should be balanced by an opposing fusion event. In contrast, the double heterozygous mutants (*parlb* $^{+/d9k}$*; parla* $^{+/ot510}$) showed a significant increase in *mfn1* mRNA expression although these fish had increased fission evidenced by the high *fis1* expression level. Previous studies have proposed that PINK1, a mitochondrial kinase with a key role in regulation of mitophagy, mediates the degradation of several key dynamic regulators such as MFN1 (Wang et al., 2011). Our results show a significant increase in *pink1* gene expression level in the double homozygous mutants, that was not detected in the double heterozygotes. Thus, increased MFN1 degradation events might have occurred in the double homozygous fish and not in the double heterozygous mutants which might justify the increase of *mfn1* mRNA expression observed for the double heterozygotes. However, it is to be noted that mRNA expression levels do not always correlate to protein levels.

Robust evidence from previous studies indicates that PINK1 is a substrate of PARL in mammals and other organisms (Jin et al., 2010; Meissner et al., 2011; Noble et al., 2012; Whitworth et al., 2008). This kinase was also found to play a critical role in the regulation of complex I activity in mitochondria (Morais et al., 2014) and to be implicated in the pathogenesis of PD.

Interestingly, our gene expression analysis shows that *pink1* expression was not significantly affected in adult brain tissue following loss of either *parla* or *parlb* gene function, however, the simultaneous loss of *parla* and *parlb* function in brain tissue resulted in a significant

increase in *pink1* expression levels. Therefore, the two paralogs, *parla* and *parlb*, might have some compensatory functions and the loss of both genes might be affecting PINK1 processing. Noble and colleagues have shown that lack of both Parl proteins in larvae can be rescued by the expression of either zebrafish or human PINK1 and have suggested that compensatory mechanisms might be involved in Pink1 cleavage in zebrafish, despite the fact that Pink1 is a substrate of Parl (Noble et al., 2012). Moreover, using RNA interference, previous findings showed that three other mitochondrial proteases affected levels of PINK1 in HEK293T cells (Greene et al., 2012). Intriguingly, we observed an increase in *pink1* expression level in *parla* ^{ot510} larvae as opposed to the unchanged gene expression level observed in *parla* ^{ot510} adult brain. This might indicate the presence of a tissue-specific gene expression regulation.

Similar observations were noted for *opa1*, whose expression was significantly increased in *parla* ^{ot510} larvae, but not in *parla* or *parlb* single mutant adult brains. Interestingly, *opa1* expression level was significantly decreased in the double mutant adult brains. This decrease in *opa1* gene expression might be correlated to the decrease of *mfn1* mRNA transcripts observed in the double mutant adult brains knowing that OPA1 is involved in mitochondrial fusion, as mentioned earlier. In *Drosophila*, yeast, and mice, a genetic interaction between PARL and OPA1 seems to be established, although whether OPA1 is a substrate of PARL is still debatable. Given the differential *pink1* and *opa1* gene expression profiles seen in zebrafish mutant larvae versus adult mutant brains, we speculate that loss-of-function of *parla* in zebrafish might have different impacts on *pink1* and *opa1* gene expression in a tissue or developmental stage-dependent manner. The lack of significant effects on the expression of *pink1*, *opa1*, or other genes in *parla* ^{ot510} larvae or in *parla* ^{ot510} and *parlb* ^{d9k} single mutant adult brains might also be explained by possible compensatory mechanisms exerted by the paralogous *parlb* gene in zebrafish. In fact, *parlb*

expression was found to increase following the loss-of-function of *parla* in both adult brains and larvae. Similarly, *parla* gene expression increased following the loss of *parlb* function in adult brains. Moreover, we found that *parla* ^{ot510} or *parlb* ^{d9k} fish did not present significant larval mortalities and were viable into adulthood. In mice, loss of *Parl* function was found to be lethal (Cipolat et al., 2006). Thus, functional redundancy of the zebrafish *parl* paralogs confers some advantages to this organism (Postlethwait et al., 2004). For instance, paralogous genes such as *parla* and *parlb* can compensate against deleterious mutations and other stresses. This functional compensation can also be advantageous in critical regulatory processes and mechanisms, in particular, during development (Kafri et al., 2006). An unexpected discrepancy was previously observed between morphant and mutant phenotypes in zebrafish where morphants usually displayed an obvious phenotype whereas corresponding mutants appeared relatively normal due to gene compensation (Peng, 2019).

4.4 Loss of *parla* function alone (*parla* ^{ot510}), as well as the simultaneous loss of *parla* and *parlb* function (*parlb* ^{d9k}*; parla* ^{ot510}) result in loss of the DA neurons in the adult brain

Knowing that neuronal function and structure critically depend on mitochondrial function, alterations in mitochondrial dynamics greatly affect neuronal health. For instance, neurons were found to be vulnerable to the ablation of the mitochondrial dynamics' regulators such as MFN2 (Chen et al., 2007). Moreover, the deficiency of almost all mitochondrial fission and fusion regulators such as OPA1, MFN1, and FIS1 was found to impair mitochondrial proper localization and movement, resulting in mitochondrial depletion in neurites eventually leading to synaptic loss (Macaskill et al., 2009; Nguyen et al., 2014). Similarly, in a recent study, morphological abnormalities in mitochondria were detected in the brain, indicating that the accumulation of these

mitochondrial structural and functional defects was correlated to the significant neurodegeneration observed in *Parl* $^{-/-}$ mice (Spinazzi et al., 2019).

In our study, we found that, similarly to what was shown in the morpholino study in larvae (Noble et al., 2012), the simultaneous loss-of-function of the *parla* and *parlb* genes, as well as the loss of *parla* but not *parlb* function, leads to severe DA neuron loss and mis-patterning in the adult zebrafish brain. The neuronal loss was shown by the reduced number of TH+ cells in both the telencephalon and olfactory bulbs. We also observed disorganized axonal tracts of DA neurons in the olfactory bulbs.

Immunohistochemical analysis of Th1 was performed as it is widely expressed in all brain regions, whereas Th2 is localized to hypothalamic, posterior tubercular, and preoptic regions of the zebrafish brain (Barrios et al., 2020). In two of the sensory and behavioral epicenters of the brain, the telencephalon, and olfactory bulbs, we observed considerable reductions in Th1 at both the mRNA and protein level in *parla* ^{ot510} adult mutants and in *parlb* ^{d9k}*; parla* ^{ot510} double mutant adult zebrafish. Intriguingly, there was no change in the dopamine transporter (*dat)* transcript levels in both *parla* ^{ot510} single mutant adult brains and in *parla* ^{ot510} mutant larvae. This could be explained by a possible upregulation of *dat* in the DA neurons that survive. Loss of *parla* function might be affecting dopamine biosynthesis, although DA neurons that survive are still expressing *dat* for dopamine re-uptake. This was not seen in the double mutants. In fact, we observed significant reduction in *dat* expression level in the brains of the double mutants. This discrepancy in *dat* expression levels between *parla* single mutants and *parla* and *parlb* double mutants might be explained by the difference in the DA neurons that survive. Fish with a loss of *parla* function showed 60% and 25% TH1 reductions in the olfactory bulbs and telencephalon, respectively. In contrast, fish with a simultaneous loss of *parla* and *parlb* function showed greater total TH1

reductions of 55% and 76% in the olfactory bulbs and telencephalon, respectively. Thus, the surviving DA neurons that express *dat* for dopamine re-uptake are in total higher in *parla* single mutant adult brains as compared to the double mutants.

4.5 Olfactory impairment was observed in *parla* but not *parlb* single mutants and in the double mutant fish although locomotor dysfunction was detected in *parla* and/or *parlb* single and double mutants

In the adult zebrafish brain, DA neurons have been described in the telencephalon, diencephalon, olfactory bulb, pretectum, and preoptic area. It has been established that loss of DA neurons is associated with movement disorders, and it has been shown that DA neurons in the olfactory bulb (OB) carry sensory response to odor (Friedrich and Korsching, 1997; Metzger et al., 2019; Sebastian et al., 2012).

The severe DA neuron loss seen in the olfactory bulbs of both *parla* ^{ot510} fish and *parlb* ^{d9k}*; parla* ^{ot510} double mutants translates into an olfactory impairment observed in the repulsive stimulus test. However, the locomotor assessment showed that there were no remarkable effects on the *parla* ^{ot510} adult fish's ability to perform locomotor functions such as total distance travelled and velocity. This could possibly be explained by the considerable number of TH+ cells that remain (75%) within the telencephalon of the *parla* mutant fish. In contrast, we observed significant locomotor impairments in the double mutants possibly due to the severe TH+ cell loss seen in the telencephalon (76%) of these mutants.

The telencephalic region has been previously characterized with DA clusters and projections claimed to be analogous to the nigrostriatal pathway in humans involved in movement

modulation (Rink and Wullimann, 2002). It is highly unlikely that the inability of fish to swim away of the repulsive stimulus in the olfactory test could be due to locomotor impairments as fish with loss of *parla* function (*parla* ^{ot510}) did not present significant locomotor dysfunction. However, the inability of the mutants to swim away of the stimulus is rather due to the inability to detect or respond to the stimulus. Furthermore, it is possible that impaired olfaction precedes impaired locomotion in zebrafish as seen in human PD patients that manifest locomotor dysfunction after losing the ability to smell (Haehner et al., 2011; Ross et al., 2008). Intriguingly, mutant fish with loss of *parla* function showed high levels of inactivity periods. We hypothesize that the inactivity episodes noted are not due to muscle dysfunction, as distance travelled, and average velocity of these fish were not affected but are rather due to the mild DA neuron reduction observed in the telencephalic region. Interestingly, unlike the *parla* mutant fish the double mutants, fish with loss of *parlb* function (*parlb* ^{d9k}) did not show disrupted olfactory function in the repulsive stimulus test, however, significant locomotor dysfunction was observed. We hypothesize that loss of *parlb* function might not have a significant impact on DA neuron number in the olfactory bulbs but might lead to a more significant loss of DA neurons in the telencephalic region of the adult brain. Interestingly, we observed similar loss of DA neurons in the olfactory bulbs of the *parla* single mutants and the double mutants (60% and 55%, respectively). However, the simultaneous loss of *parla* and *parlb* function resulted in a greater DA neuron loss in the telencephalon of the *parla* mutants and the double mutants (25% and 76%, respectively). These observations might indicate a greater tissue specific involvement of *parlb* gene in the maintenance of DA neuron number in the telencephalon rather than the olfactory bulbs.

4.6 The double mutant fish (*parlb* ^{d9k}*; parla* ^{ot510}) but not the single mutants (*parlb* ^{d9k} or *parla* ^{ot510}) are susceptible to MPTP exposure

The vast majority of PD pathologies are sporadic with less than 10% being genetic. Thus, it is important to study the role of environmental toxins and how they might lead to PD. Previous studies investigated the sensitivity of zebrafish neurons to diverse environmental toxins, such as MPTP, paraquat, and rotenone in zebrafish larvae and adults (Bretaud et al., 2004; Kalyn et al., 2019). Results have shown that of these neurotoxins, only MPTP specifically affected DA neurons in zebrafish larvae (Lam et al., 2005).

In our study, we treated the *parla* and/or *parlb* mutant larvae at 3 dpf with MPTP and then assessed the lethal dose that resulted in the lowest survival rate by the end of the treatment (5 dpt). Our results show that the double mutant fish (*parlb* ^{d9k}*; parla* ^{ot510}) but not the single mutants (*parlb* ^{d9k} or *parla* ^{ot510}) had a significantly lower lethal dose as compared to the WT (0.1 mM versus 0.5 mM, respectively). This might indicate that the simultaneous loss of *parla* and *parlb* function is needed for increased susceptibility to the neurotoxin. Interestingly, the double heterozygous mutants had a lethal dose similar to that of the WT larvae (0.5 mM). Thus, the presence of one allele of each of the *parla* and *parlb* genes might be sufficient to rescue increased vulnerability to neurotoxin exposure. Moreover, we did not observe increased susceptibility to MPTP treatment for the single mutants (*parlb* ^{d9k} or *parla* ^{ot510}). This might be explained by the existence of a compensatory function between the two paralogous genes, *parla* and *parlb*.

Interestingly, we noticed that all of the mutant larvae treated with MPTP showed significant immobility and the absence of touch-evoked response as compared to WT treated fish. In fact, a recent paper showed that the most important reductions in both total distance travelled and average velocity of rotenone, paraquat, MPTP and MPP+ treated larvae were obtained for

MPTP-treated larvae (Kalyn et al., 2019). However, further quantitative locomotion and behavioral tests are needed to confirm our observations. Furthermore, we noticed the development of cardiac edemas and upwards tail curvatures in all of our MPTP-treated larvae, particularly in the double mutants. These observations corroborate to previous findings in which heart and tail malformations were observed with the MPTP-treated larvae (Kalyn et al., 2019).

Finally, as the double mutants showed increased susceptibility to neurotoxin exposure seen with a lower MPTP lethal dose and with the locomotor and developmental impairments, we can suggest that these double mutants following treatment with MPTP might be a good model for the advanced stages of PD pathology. Additional immunohistochemical analyses using TH marker could be performed to investigate whether the MPTP treated double mutants would show severe dopaminergic neuron degeneration as compared to the non-treated double mutants, and whether it could potentially reflect the DA neuron loss observed during the advanced stages of PD.

4.7. Loss of *parla* function in larvae (*parla* ^{ot510}) results in increased cell death throughout the entire body

Severe apoptosis accompanied with mitochondrial morphological changes at the level of the cristae occurred in the fibroblasts and liver of *PARL* KO mice suggesting that *PARL* plays an anti-apoptotic role by regulating cristae morphology (Cipolat et al., 2006). Moreover, faster cytochrome c release was detected in cell cultures following treatment with several pro-apoptotic stimuli. An increase in apoptotic markers was also observed in the striatum of mice treated with siRNA against Parl (Yoshioka et al., 2013). Previous studies have found potential mechanisms and substrates that link PARL to apoptosis (Chao et al., 2008; Cipolat et al., 2006). The soluble form

of OPA1 is one candidate, although whether OPA1 is a direct substrate of PARL is still debatable. While data obviously indicate a crucial role for PARL in protecting cells from cell death *in vivo* and *in vitro*, the exact cause of the decreased life span of the *Parl* $^{-/-}$ mice remains to be further investigated (Cipolat et al., 2006). A previous study showed that *parla* and *parlb* morphants exhibited extensive cell death throughout the entire body in zebrafish larvae (Noble et al., 2012). In this study, morphants were stained at 1, 2, and 3 dpf with acridine orange to check whether loss of Parl function would induce apoptosis. Results showed that *parla* morphants exhibited staining that was detected throughout the entire body at 1, 2, and 3 dpf. In contrast, *parlb* morphants showed staining at 1 dpf but decreased afterwards in the surviving larvae.

Following these previous findings, we performed acridine orange staining on 3 dpf larvae with loss of *parla* function (*parla* ^{ot510}) and compared the number and intensity of the stained cells to WT (*parla* $^{+}$). We noticed that there were significantly more stained cells throughout the entire body of the mutant larvae as compared to WT larvae that exhibited few stained cells probably resulting from normal cell death events. Interestingly, stained cells showed higher intensity and were greater in size in the *parla* mutant larvae than in the WT. Moreover, we observed staining on the head region that was not detected in WT larvae. The staining observed throughout the whole body of *parla* mutant larvae corroborate with the morpholino findings described above (Noble et al., 2012). However, it is to be noted that acridine orange staining does not only stain apoptotic cells, but it generally acts on cells that undergo cell death. In fact, a recent study claimed that the neurodegeneration detected in *Parl* $^{-/-}$ mice was characterized by neuronal necrosis without overtly altered apoptosis (Spinazzi et al., 2019).

Taking these results together, further investigations need to be performed to confirm whether the cell death observed in *parla* mutants throughout the entire body, and/or the head region

in particular, is caused by apoptosis. For that purpose, TUNEL assay or caspase-3 staining could be used to detect apoptosis.

4.8. General conclusions

The overall goal of this research was to explore the role of the two paralogs, *parla* and *parlb*, in the zebrafish adults and larvae, as little is known about *PARL* function and its role in dopaminergic neuron development in vertebrates. For that, we used the zebrafish as a model system, as it also presents high genetic similarities, as well as neuronal organizational and functional homology with the human brain. Given the prevalence of mitochondrial dysfunction in PD pathologies and the role of *PARL* in mitochondrial homeostasis, the generation of *PARL* zebrafish mutant lines is beneficial in the understanding of the specific function played by *PARL* on the onset of PD.

We have shown through targeted CRISPR/Cas9-mediated loss-of-function of the *parla* and/or *parlb* gene, the importance of the two paralogs for DA neuron number and patterning in the telencephalon and olfactory bulb of the adult zebrafish brain. We also suggested that loss of DA neurons is correlated with the behavioral and olfactory impairments observed in the adult fish. Moreover, we investigated the susceptibility of the mutants following exposure to the environmental neurotoxin, MPTP. Finally, we showed that the two paralogs, *parla* and *parlb* genes, possess redundant as well as divergent functions.

Given the important roles already identified for the *PARL* gene in mammals and other species, we believe the research presented here is a valuable contribution for understanding the function of the *parl* paralogs in the vertebrate central nervous system.

References

Adrain, C., Strisovsky, K., Zettl, M., Hu, L., Lemberg, M. K., & Freeman, M. (2011). Mammalian EGF receptor activation by the rhomboid protease RHBDL2. *Embo Reports, 12*(5), 421-427. doi:10.1038/embor.2011.50

Alexander, G. E. (2004). Biology of Parkinson's disease: pathogenesis and pathophysiology of a multisystem neurodegenerative disorder. *Dialogues in clinical neuroscience, 6*(3), 259-280.

Altmann, K., Frank, M., Neumann, D., Jakobs, S., & Westermann, B. (2008). The class V myosin motor protein, Myo2, plays a major role in mitochondrial motility in Saccharomyces cerevisiae. *Journal of Cell Biology, 181*(1), 119-130. doi:10.1083/jcb.200709099

Anand, R., Wai, T., Baker, M. J., Kladt, N., Schauss, A. C., Rugarli, E., & Langer, T. (2014). The i-AAA protease YME1L and OMA1 cleave OPA1 to balance mitochondrial fusion and fission. *Journal of Cell Biology, 204*(6), 919-929. doi:10.1083/jcb.201308006

Barrios, J. P., Wang, W.-C., England, R., Reifenberg, E., & Douglass, A. D. (2020). Hypothalamic Dopamine Neurons Control Sensorimotor Behavior by Modulating Brainstem Premotor Nuclei in Zebrafish. *Current Biology, 30*(23), 4606-+. doi:10.1016/j.cub.2020.09.002

Bravo, S., Rangel-Barajas, C., & Floran, B. (2014). Pathophysiology of L-Dopa Induced Dyskinesia — Changes in D1/D3 Receptors and Their Signaling Pathway

Broughton, R. E., Milam, J. E., & Roe, B. A. (2001). The complete sequence of the zebrafish (Danio rerio) mitochondrial genome and evolutionary patterns in vertebrate mitochondrial DNA. *Genome Research, 11*(11), 1958-1967. doi:10.1101/gr.156801

Candy, J., & Collet, C. (2005). Two tyrosine hydroxylase genes in teleosts. *Biochimica Et Biophysica Acta-Gene Structure and Expression, 1727*(1), 35-44. doi:10.1016/j.bbaexp.2004.11.005

Chao, J.-R., Parganas, E., Boyd, K., Hong, C. Y., Opferman, J. T., & Ihle, J. N. (2008). Hax1-mediated processing of HtrA2 by Parl allows survival of lymphocytes and neurons. *Nature, 452*(7183), 98-U10. doi:10.1038/nature06604

Charpentier, E., & Doudna, J. A. (2013). BIOTECHNOLOGY Rewriting a genome. *Nature, 495*(7439), 50-51. doi:10.1038/495050a

Chia, S. J., Tan, E. K., & Chao, Y. X. (2020). Historical Perspective: Models of Parkinson's Disease. *International Journal of Molecular Sciences, 21*(7). doi:10.3390/ijms21072464

Cipolat, S., Rudka, T., Hartmann, D., Costa, V., Serneels, L., Craessaerts, K., . . . De Strooper, B. (2006a). Mitochondrial rhomboid PARL regulates cytochrome c release during apoptosis via OPA1-dependent cristae remodeling. *Cell, 126*(1), 163-175. doi:10.1016/j.cell.2006.06.021

Cookson, M. R. (2005). The biochemistry of Parkinson's disease. *Annual Review of Biochemistry, 74*, 29-52. doi:10.1146/annurev.biochem.74.082803.133400

Daubner, S. C., Le, T., & Wang, S. Z. (2011). Tyrosine hydroxylase and regulation of dopamine synthesis. *Archives of Biochemistry and Biophysics, 508*(1), 1-12. doi:10.1016/j.abb.2010.12.017

den Dunnen, J. T., & Antonarakis, E. (2001). Nomenclature for the description of human sequence variations. *Human Genetics, 109*(1), 121-124. doi:10.1007/s004390100505

Dusterhoft, S., Kunzel, U., & Freeman, M. (2017). Rhomboid proteases in human disease: Mechanisms and future prospects. *Biochimica Et Biophysica Acta-Molecular Cell Research, 1864*(11), 2200-2209. doi:10.1016/j.bbamcr.2017.04.016

Farrer, M. J. (2006a). Genetics of Parkinson disease: paradigm shifts and future prospects. *Nature Reviews Genetics, 7*(4), 306-318. doi:10.1038/nrg1831

Frederick, R. L., & Shaw, J. M. (2007). Moving mitochondria: Establishing distribution of an essential organelle. *Traffic, 8*(12), 1668-1675. doi:10.1111/j.1600-0854.2007.00644.x

Freeman, M. (2014). The Rhomboid-Like Superfamily: Molecular Mechanisms and Biological Roles. *Annual Review of Cell and Developmental Biology, Vol 30, 30*, 235-254. doi:10.1146/annurev-cellbio-100913-012944

Gagnon, J. A., Valen, E., Thyme, S. B., Huang, P., & Ahkmetova, L. (2014). Efficient Mutagenesis by Cas9 Protein-Mediated Oligonucleotide Insertion and Large-Scale Assessment of Single-Guide RNAs (vol 9, e98186, 2014). *Plos One, 9*(8). doi:10.1371/journal.pone.0106396

Gao, J., Wang, L., Liu, J., Xie, F., Su, B., & Wang, X. (2017). Abnormalities of Mitochondrial Dynamics in Neurodegenerative Diseases. *Antioxidants, 6*(2). doi:10.3390/antiox6020025

Glater, E. E., Megeath, L. J., Stowers, R. S., & Schwarz, T. L. (2006). Axonal transport of mitochondria requires milton to recruit kinesin heavy chain and is light chain independent. *Journal of Cell Biology, 173*(4), 545-557. doi:10.1083/jcb.200601067

Godoy, R., Hua, K., Kalyn, M., Cusson, V. M., Anisman, H., & Ekker, M. (2020). Dopaminergic neurons regenerate following chemogenetic ablation in the olfactory bulb of adult Zebrafish (Danio rerio). *Scientific reports*, 10(1), 12825. https://doi-org.proxy.bib.uottawa.ca/10.1038/s41598-020-69734-0

Greene, A. W., Grenier, K., Aguileta, M. A., Muise, S., Farazifard, R., Haque, M. E., . . . Fon, E. A. (2012a). Mitochondrial processing peptidase regulates PINK1 processing, import and Parkin recruitment. *Embo Reports, 13*(4), 378-385. doi:10.1038/embor.2012.14

Guo, X. F., Macleod, G. T., Wellington, A., Hu, F., Panchumarthi, S., Schoenfield, M., . . . Zinsmaier, K. E. (2005). The GTPase dMiro is required for axonal transport of mitochondria to Drosophila synapses. *Neuron, 47*(3), 379-393. doi:10.1016/j.neuron.2005.06.027

Haehner, A., Hummel, T., & Reichmann, H. (2011). Olfactory Loss in Parkinson's Disease. *Parkinsons Disease, 2011*. doi:10.4061/2011/450939

Han, J., Bai, J., Yang, Y., Yin, H., Gao, W., Lu, A., . . . Zhong, L. (2015). Lentivirus-mediated knockdown of rhomboid domain containing 1 inhibits colorectal cancer cell growth. *Molecular Medicine Reports, 12*(1), 377-381. doi:10.3892/mmr.2015.3365

Heinitz, S., Klein, C., & Djarmati, A. (2011). The p.S77N presenilin-associated rhomboid-like protein mutation is not a frequent cause of early-onset Parkinson's disease. *Movement Disorders, 26*(13), 2441-2442. doi:10.1002/mds.23889

Hruscha, A., & Schmid, B. (2015). Generation of zebrafish models by CRISPR /Cas9 genome editing. *Methods in molecular biology (Clifton, N.J.), 1254*, 341-350. doi:10.1007/978-1-4939-2152-2_24

Hwang, W. Y., Fu, Y., Reyon, D., Maeder, M. L., Tsai, S. Q., Sander, J. D., . . . Joung, J. K. (2013). Efficient genome editing in zebrafish using a CRISPR-Cas system. *Nature Biotechnology, 31*(3), 227-229. doi:10.1038/nbt.2501

Ishihara, N., Eura, Y., & Mihara, K. (2004). Mitofusin 1 and 2 play distinct roles in mitochondrial fusion reactions via GTPase activity. *Journal of Cell Science, 117*(26), 6535-6546. doi:10.1242/jcs.01565

Ishihara, N., Fujita, Y., Oka, T., & Mihara, K. (2006). Regulation of mitochondrial morphology through proteolytic cleavage of OPA1. *Embo Journal, 25*(13), 2966-2977. doi:10.1038/sj.emboj.7601184

Jeyaraju, D. V., McBride, H. M., Hill, R. B., & Pellegrini, L. (2011). Structural and mechanistic basis of Parl activity and regulation. *Cell Death and Differentiation, 18*(9), 1531-1539. doi:10.1038/cdd.2011.22

Jeyaraju, D. V., Xu, L., Letellier, M.-C., Bandaru, S., Zunino, R., Berg, E. A., . . . Pellegrini, L. (2006). Phosphorylation and cleavage of presenilin-associated rhomboid-like protein (PARL) promotes changes in mitochondrial morphology. *Proceedings of the National Academy of Sciences of the United States of America, 103*(49), 18562-18567. doi:10.1073/pnas.0604983103

Jin, S. M., Lazarou, M., Wang, C., Kane, L. A., Narendra, D. P., & Youle, R. J. (2010a). Mitochondrial membrane potential regulates PINK1 import and proteolytic destabilization by PARL. *Journal of Cell Biology, 191*(5), 933-942. doi:10.1083/jcb.201008084

Jinek, M., Chylinski, K., Fonfara, I., Hauer, M., Doudna, J. A., & Charpentier, E. (2012). A Programmable Dual-RNA-Guided DNA Endonuclease in Adaptive Bacterial Immunity. *Science, 337*(6096), 816-821. doi:10.1126/science.1225829

Jung, M. (2017). Functional Analysis of Zebrafish Paralogs, parla and parlb, by CRISPR-Cas9 Mediated Mutagenesis. *Master's Thesis*. University of Ottawa.

Jurgens, G., Wieschaus, E., Nussleinvolhard, C., & Kluding, H. (1984). MUTATIONS AFFECTING THE PATTERN OF THE LARVAL CUTICLE IN DROSOPHILA-MELANOGASTER .2. ZYGOTIC LOCI ON THE 3RD CHROMOSOME. *Wilhelm Rouxs Archives of Developmental Biology, 193*(5), 283-295. doi:10.1007/bf00848157

Kalyn, M., Hua, K., Noor, S. M., Wong, C. E. D., & Ekker, M. (2020). Comprehensive Analysis of Neurotoxin-Induced Ablation of Dopaminergic Neurons in Zebrafish Larvae. *Biomedicines, 8*(1). doi:10.3390/biomedicines8010001

Kann, O., & Kovacs, R. (2007). Mitochondria and neuronal activity. *American Journal of Physiology-Cell Physiology, 292*(2), C641-C657. doi:10.1152/ajpcell.00222.2006

Kimmel, C. B., Ballard, W. W., Kimmel, S. R., Ullmann, B., & Schilling, T. F. (1995). STAGES OF EMBRYONIC-DEVELOPMENT OF THE ZEBRAFISH. *Developmental Dynamics, 203*(3), 253-310. doi:10.1002/aja.1002030302

Klein, C., & Schlossmacher, M. G. (2006). The genetics of Parkinson disease: implications for neurological care. *Nature Clinical Practice Neurology, 2*(3), 136-146. doi:10.1038/ncpneuro0126

Klein, C., & Westenberger, A. (2012). Genetics of Parkinson's Disease. *Cold Spring Harbor Perspectives in Medicine, 2*(1). doi:10.1101/cshperspect.a008888

Kubli, D. A., & Gustafsson, A. B. (2012). Mitochondria and Mitophagy The Yin and Yang of Cell Death Control. *Circulation Research, 111*(9), 1208-1221. doi:10.1161/circresaha.112.265819

Lang, A. E. (2011). A Critical Appraisal of the Premotor Symptoms of Parkinson's Disease: Potential Usefulness in Early Diagnosis and Design of Neuroprotective Trials. *Movement Disorders, 26*(5), 775-783. doi:10.1002/mds.23609

Langosch, D., Scharnagl, C., Steiner, H., & Lemberg, M. K. (2015). Understanding intramembrane proteolysis: from protein dynamics to reaction kinetics. *Trends in Biochemical Sciences, 40*(6), 318-327. doi:10.1016/j.tibs.2015.04.001

Lastun, V. L., Grieve, A. G., & Freeman, M. (2016). Substrates and physiological functions of secretase rhomboid proteases. *Seminars in Cell & Developmental Biology, 60*, 10-18. doi:10.1016/j.semcdb.2016.07.033

Lee, J. E., Westrate, L. M., Wu, H. X., Page, C., & Voeltz, G. K. (2016). Multiple dynamin family members collaborate to drive mitochondrial division. *Nature, 540*(7631), 139-+. doi:10.1038/nature20555

Lee, J. R., Urban, S., Garvey, C. F., & Freeman, M. (2001). Regulated intracellular ligand transport and proteolysis control EGF signal activation in Drosophila. *Cell, 107*(2), 161-171. doi:10.1016/s0092-8674(01)00526-8

Lemberg, M. K., & Freeman, M. (2007). Functional and evolutionary implications of enhanced genomic analysis of rhomboid intramembrane proteases. *Genome Research, 17*(11), 1634-1646. doi:10.1101/gr.6425307

Lin, M. T., & Beal, M. F. (2006). Mitochondrial dysfunction and oxidative stress in neurodegenerative diseases. *Nature, 443*(7113), 787-795. doi:10.1038/nature05292

Liu, X.-N., Tang, Z.-H., Zhang, Y., Pan, Q.-C., Chen, X.-H., Yu, Y.-S., & Zang, G.-Q. (2013). Lentivirus-mediated Silencing of Rhomboid Domain Containing 1 Suppresses Tumor Growth and Induces Apoptosis in Hepatoma HepG2 Cells. *Asian Pacific Journal of Cancer Prevention, 14*(1), 5-9. doi:10.7314/apjcp.2013.14.1.5

Loson, O. C., Song, Z., Chen, H., & Chan, D. C. (2013). Fis1, Mff, MiD49, and MiD51 mediate Drp1 recruitment in mitochondrial fission. *Molecular Biology of the Cell, 24*(5), 659-667. doi:10.1091/mbc.E12-10-0721

Lu, W., Karuppagounder, S. S., Springer, D. A., Allen, M. D., Zheng, L., Chao, B., . . . Lenardo, M. (2014). Genetic deficiency of the mitochondrial protein PGAM5 causes a Parkinson's-like movement disorder. *Nature Communications, 5*. doi:10.1038/ncomms5930

McQuibban, G. A., Lee, J. R., Zheng, L., Juusola, M., & Freeman, M. (2006). Normal mitochondrial dynamics requires rhomboid-7 and affects Drosophila lifespan and neuronal function. *Current Biology, 16*(10), 982-989. doi:10.1016/j.cub.2006.03.062

McQuibban, G. A., Saurya, S., & Freeman, M. (2003a). Mitochondrial membrane remodelling regulated by a conserved rhomboid protease. *Nature, 423*(6939), 537-541. doi:10.1038/nature01633

Meissner, C., Lorenz, H., Weihofen, A., Selkoe, D. J., & Lemberg, M. K. (2011a). The mitochondrial intramembrane protease PARL cleaves human Pink1 to regulate Pink1 trafficking. *Journal of Neurochemistry, 117*(5), 856-867. doi:10.1111/j.1471-4159.2011.07253.x

Metzger, J. M., & Emborg, M. E. (2019a). Autonomic dysfunction in Parkinson disease and animal models. *Clinical Autonomic Research, 29*(4), 397-414. doi:10.1007/s10286-018-00584-7

Mishra, P., & Chan, D. C. (2016). Metabolic regulation of mitochondrial dynamics. *Journal of Cell Biology, 212*(4), 379-387. doi:10.1083/jcb.201511036

Montague, T. G., Cruz, J. M., Gagnon, J. A., Church, G. M., & Valen, E. (2014). CHOPCHOP: a CRISPR/Cas9 and TALEN web tool for genome editing. *Nucleic Acids Research, 42*(W1), W401-W407. doi:10.1093/nar/gku410

Morais, V. A., Haddad, D., Craessaerts, K., De Bock, P.-J., Swerts, J., Vilain, S., . . . De Strooper, B. (2014). PINK1 Loss-of-Function Mutations Affect Mitochondrial Complex I Activity via NdufA10 Ubiquinone Uncoupling. *Science, 344*(6180), 203-207. doi:10.1126/science.1249161

Narendra, D. P., Jin, S. M., Tanaka, A., Suen, D.-F., Gautier, C. A., Shen, J., . . . Youle, R. J. (2010). PINK1 Is Selectively Stabilized on Impaired Mitochondria to Activate Parkin. *Plos Biology, 8*(1). doi:10.1371/journal.pbio.1000298

Noble, S. (2014). Functional Characterization of the PARL Mitochondrial Proteins in Zebrafish (Danio Rerio). *Ph.D. Thesis*. University of Ottawa.

Noble, S., Ismail, A., Godoy, R., Xi, Y., & Ekker, M. (2012). Zebrafish Parla- and Parlb-deficiency affects dopaminergic neuron patterning and embryonic survival. *Journal of Neurochemistry, 122*(1), 196-207. doi:10.1111/j.1471-4159.2012.07758.x

Parkinson J. (1817). An Essay on the Shaking Palsy. London: *Whittingham and Rowland for Sherwood, Neely, and Jones*.

Pellegrini, L., Passer, B. J., Canelles, M., Lefterov, I., Ganjei, J. K., Fowlkes, B. J., . . . D'Adamio, L. (2001). PAMP and PARL, two novel putative metalloproteases interacting with the COOH-terminus of Presenilin-1 and-2. *Journal of Alzheimers Disease, 3*(2), 181-190.

Pickrell, A. M., & Youle, R. J. (2015). The Roles of PINK1, Parkin, and Mitochondrial Fidelity in Parkinson's Disease. *Neuron, 85*(2), 257-273. doi:10.1016/j.neuron.2014.12.007

Rathke-Hartlieb, S., Schlomann, U., Heimann, P., Meisler, M. H., Jockusch, H., & Bartsch, J. W. (2002). Progressive loss of striatal neurons causes motor dysfunction in MND2 mutant mice and is not prevented by Bcl-2. *Experimental Neurology, 175*(1), 87-97. doi:10.1006/exnr.2002.7868

Rink, E., & Wullimann, M. F. (2002a). Development of the catecholaminergic system in the early zebrafish brain: an immunohistochemical study. *Developmental Brain Research, 137*(1), 89-100. doi:10.1016/s0165-3806(02)00354-1

Ross, G. W., Petrovitch, H., Abbott, R. D., Tanner, C. M., Popper, J., Masaki, K., . . . White, L. R. (2008). Association of olfactory dysfunction with risk for future Parkinson's disease. *Annals of Neurology, 63*(2), 167-173. doi:10.1002/ana.21291

Santel, A., & Fuller, M. T. (2001). Control of mitochondrial morphology by a human mitofusin. *Journal of Cell Science, 114*(5), 867-874.

Sekine, S., Kanamaru, Y., Koike, M., Nishihara, A., Okada, M., Kinoshita, H., . . . Ichijo, H. (2012). Rhomboid Protease PARL Mediates the Mitochondrial Membrane Potential Loss-induced Cleavage of PGAM5. *Journal of Biological Chemistry, 287*(41), 34635-34645. doi:10.1074/jbc.M112.357509

Shi, G., Lee, J. R., Grimes, D. A., Racacho, L., Ye, D., Yang, H., . . . Bulman, D. E. (2011a). Functional alteration of PARL contributes to mitochondrial dysregulation in Parkinson's disease. *Human Molecular Genetics, 20*(10), 1966-1974. doi:10.1093/hmg/ddr077

Shiba-Fukushima, K., Imai, Y., Yoshida, S., Ishihama, Y., Kanao, T., Sato, S., & Hattori, N. (2012). PINK1-mediated phosphorylation of the Parkin ubiquitin-like domain primes mitochondrial translocation of Parkin and regulates mitophagy. *Scientific Reports, 2*. doi:10.1038/srep01002

Sik, A., Passer, B. J., Koonin, E. V., & Pellegrini, L. (2004). Self-regulated cleavage of the mitochondrial intramembrane-cleaving protease PARL yields P beta, a nuclear-targeted peptide. *Journal of Biological Chemistry, 279*(15), 15323-15329. doi:10.1074/jbc.M313756200

Smirnova, E., Griparic, L., Shurland, D. L., & van der Bliek, A. M. (2001). Dynamin-related protein Drp1 is required for mitochondrial division in mammalian cells. *Molecular Biology of the Cell, 12*(8), 2245-2256. doi:10.1091/mbc.12.8.2245

Song, W., Liu, W., Zhao, H., Li, S., Guan, X., Ying, J., . . . Wang, L. (2015). Rhomboid domain containing 1 promotes colorectal cancer growth through activation of the EGFR signalling pathway. *Nature Communications, 6*. doi:10.1038/ncomms9022

Spinazzi, M., & De Strooper, B. (2016). PARL: The mitochondrial rhomboid protease. *Seminars in Cell & Developmental Biology, 60*, 19-28. doi:10.1016/j.semcdb.2016.07.034

Spinazzi, M., Radaelli, E., Horre, K., Arranz, A. M., Gounko, N. V., Agostinis, P., . . . De Strooper, B. (2019). PARL deficiency in mouse causes Complex III defects, coenzyme Q depletion, and Leigh-like syndrome. *Proceedings of the National Academy of Sciences of the United States of America, 116*(1), 277-286. doi:10.1073/pnas.1811938116

Steele, S. L., Prykhozhij, S. V., & Berman, J. N. (2014). Zebrafish as a model system for mitochondrial biology and diseases. *Translational Research, 163*(2), 79-98. doi:10.1016/j.trsl.2013.08.008

Suen, D. F., Norris, K. L., & Youle, R. J. (2008). Mitochondrial dynamics and apoptosis. *Genes & Development, 22*(12), 1577-1590. doi:10.1101/gad.1658508

Sztal, T. E., & Stainier, D. Y. R. (2020). Transcriptional adaptation: a mechanism underlying genetic robustness. *Development, 147*(15). doi:10.1242/dev.186452

Takeda, K., Komuro, Y., Hayakawa, T., Oguchi, H., Ishida, Y., Murakami, S., . . . Ichijo, H. (2009). Mitochondrial phosphoglycerate mutase 5 uses alternate catalytic activity as a protein serine/threonine phosphatase to activate ASK1. *Proceedings of the National Academy of Sciences of the United States of America, 106*(30), 12301-12305. doi:10.1073/pnas.0901823106

Tang, R., Dodd, A., Lai, D., McNabb, W. C., & Love, D. R. (2007). Validation of zebrafish (Danio rerio) reference genes for quantitative real-time RT-PCR normalization. *Acta Biochimica Et Biophysica Sinica, 39*(5), 384-390. doi:10.1111/j.1745-7270.2007.00283.x

Tay, T. L., Ronneberger, O., Ryu, S., Nitschke, R., & Driever, W. (2011a). Comprehensive catecholaminergic projectome analysis reveals single-neuron integration of zebrafish ascending and descending dopaminergic systems. *Nature Communications, 2*. doi:10.1038/ncomms1171

Twig, G., Elorza, A., Molina, A. J. A., Mohamed, H., Wikstrom, J. D., Walzer, G., . . . Shirihai, O. S. (2008a). Fission and selective fusion govern mitochondrial segregation and elimination by autophagy. *Embo Journal, 27*(2), 433-446. doi:10.1038/sj.emboj.7601963

Urban, S., & Dickey, S. W. (2011). The rhomboid protease family: a decade of progress on function and mechanism. *Genome Biology, 12*(10). doi:10.1186/gb-2011-12-10-231

Urban, S., Lee, J. R., & Freeman, M. (2001). Drosophila Rhomboid-1 defines a family of putative intramembrane serine proteases. *Cell, 107*(2), 173-182. doi:10.1016/s0092-8674(01)00525-6

Urban, S., & Wolfe, M. S. (2005). Reconstitution of intramembrane proteolysis in vitro reveals that pure rhomboid is sufficient for catalysis and specificity. *Proceedings of the National Academy of Sciences of the United States of America, 102*(6), 1883-1888. doi:10.1073/pnas.0408306102

Vaz, R. L., Outeiro, T. F., & Ferreira, J. J. (2018). Zebrafish as an Animal Model for Drug Discovery in Parkinson's Disease and Other Movement Disorders: A Systematic Review. *Frontiers in Neurology, 9*. doi:10.3389/fneur.2018.00347

Vives-Bauza, C., Zhou, C., Huang, Y., Cui, M., de Vries, R. L. A., Kim, J., . . . Przedborski, S. (2010). PINK1-dependent recruitment of Parkin to mitochondria in mitophagy. *Proceedings of the National Academy of Sciences of the United States of America, 107*(1), 378-383. doi:10.1073/pnas.0911187107

Wang, Z., Jiang, H., Chen, S., Du, F., & Wang, X. (2012). The Mitochondrial Phosphatase PGAM5 Functions at the Convergence Point of Multiple Necrotic Death Pathways. *Cell, 148*(1-2), 228-243. doi:10.1016/j.cell.2011.11.030

Wei, X., Lv, T., Chen, D., & Guan, J. (2014). Lentiviral Vector Mediated Delivery of RHBDD1 shRNA Down Regulated the Proliferation of Human Glioblastoma Cells. *Technology in Cancer Research & Treatment, 13*(1), 87-93. doi:10.7785/tcrt.2012.500362

Westermann, B. (2012). Bioenergetic role of mitochondrial fusion and fission. *Biochimica Et Biophysica Acta-Bioenergetics, 1817*(10), 1833-1838. doi:10.1016/j.bbabio.2012.02.033

Whitworth, A. J., Lee, J. R., Ho, V. M. W., Flick, R., Chowdhury, R., & McQuibban, G. A. (2008a). Rhomboid-7 and HtrA2/Omi act in a common pathway with the Parkinson's disease factors Pink1 and Parkin. *Disease Models & Mechanisms, 1*(2-3), 168-174. doi:10.1242/dmm.000109

Wuest, R., Maurer, B., Hauser, K., Woitalla, D., Sharma, M., & Krueger, R. (2016). Mutation analyses and association studies to assess the role of the presenilin-associated rhomboid-like gene in Parkinson's disease. *Neurobiology of Aging, 39*. doi:10.1016/j.neurobiolaging.2015.11.025

Yang, Q. H., Church-Hajduk, R., Ren, J. Y., Newton, M. L., & Du, C. Y. (2003). Omi/HtrA2 catalytic cleavage of inhibitor of apoptosis (IAP) irreversibly inactivates IAPs and facilitates caspase activity in apoptosis. *Genes & Development, 17*(12), 1487-1496. doi:10.1101/gad.1097903

Yoshioka, H., Katsu, M., Sakata, H., Okami, N., Wakai, T., Kinouchi, H., & Chan, P. H. (2013). The role of PARL and HtrA2 in striatal neuronal injury after transient global cerebral ischemia. *Journal of Cerebral Blood Flow and Metabolism, 33*(11), 1658-1665. doi:10.1038/jcbfm.2013.139

Zhang, F., Wen, Y., & Guo, X. (2014). CRISPR/Cas9 for genome editing: progress, implications and challenges. *Human Molecular Genetics, 23*, R40-R46. doi:10.1093/hmg/ddu125

APPENDIX 1 – Supplementary Figures

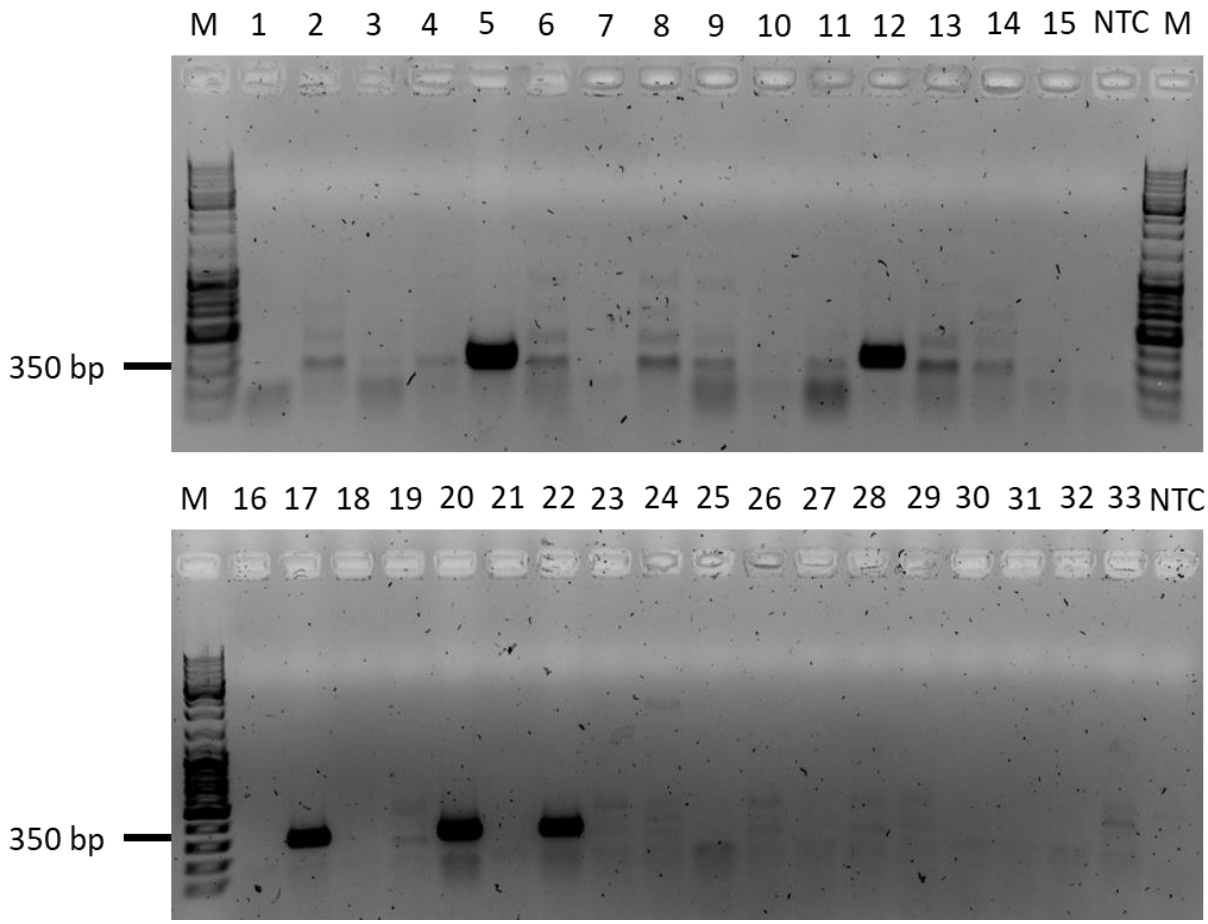

Figure A.1. Detection of *parla* mutation on agarose gel in 24 hours post-fertilization F1 generation embryos from founder 1 parental fish. A total number of 33 individual embryos was used. Size of the mutant band is 350 bp observed in embryo 5, 12, 17, 20 and 22. The marker (M) used is a 10 kb DNA ladder mix (GeneRuler^{TM}). No template control is referred to as NTC.

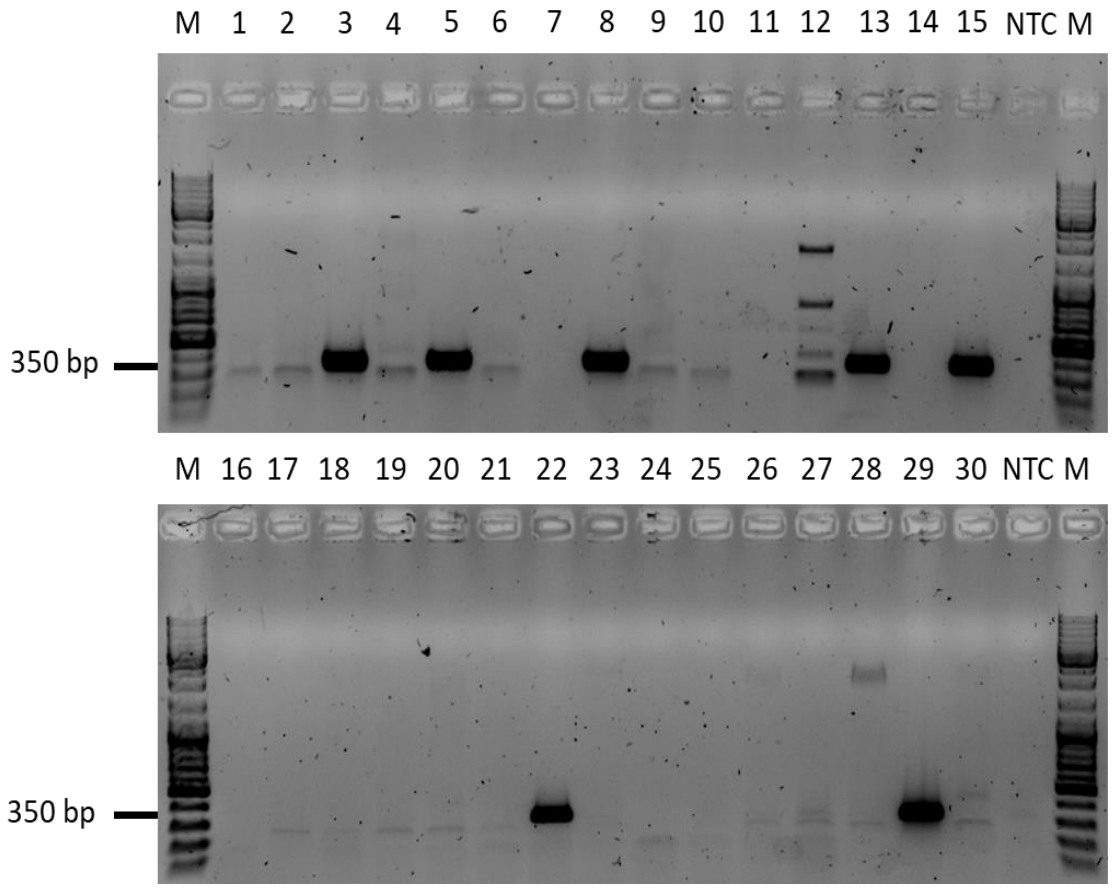

Figure A.2. Detection of *parla* mutation on agarose gel in 24 hours post-fertilization F1 generation embryos from founder 2 parental fish. A total number of 30 individual embryos was used. Size of the mutant band is 350 bp observed in embryo 3, 5, 8, 13, 15, 22, and 29. The marker (M) used is a 10 kb DNA ladder mix (GeneRuler^{TM}). No template control is referred to as NTC.

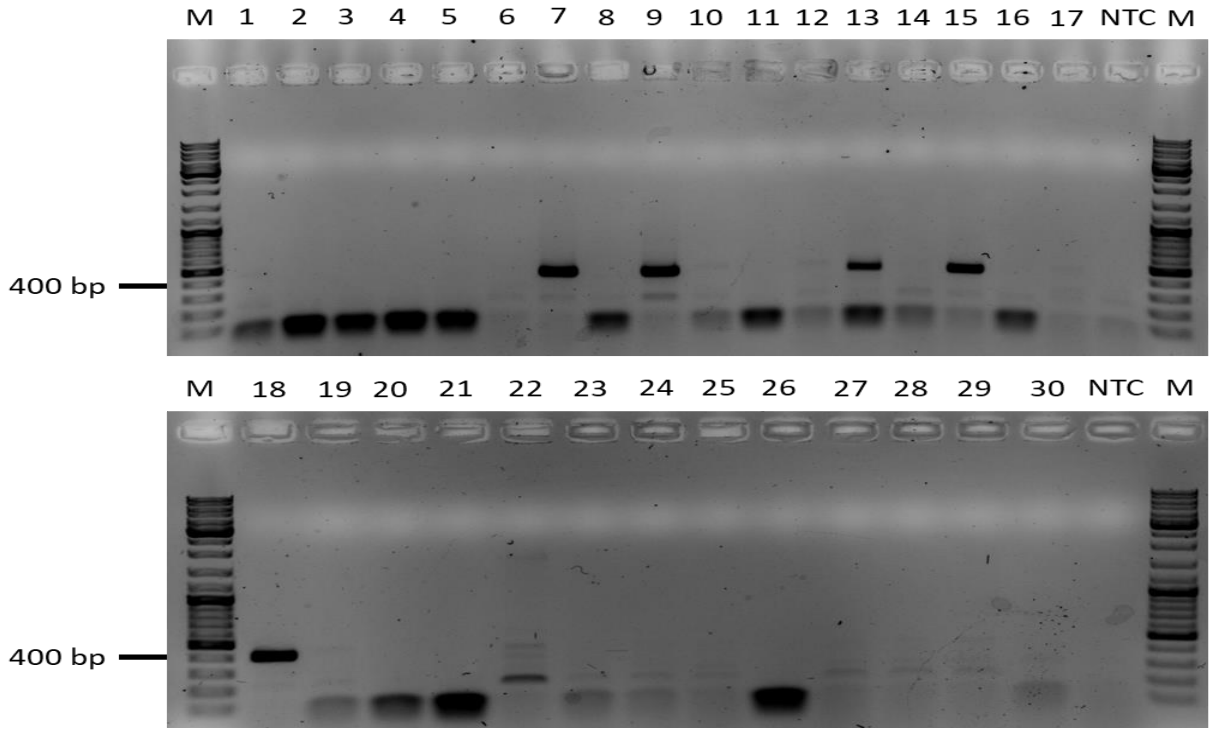

Figure A.3. Detection of *parla* mutation on agarose gel in 24 hours post-fertilization F1 generation embryos from founder 3 parental fish. A total number of 30 individual embryos was used. Size of the mutant band is 400 bp observed in embryo 7, 9, 13, 15, 15, and 18. The marker (M) used is a 10 kb DNA ladder mix (GeneRuler^{TM}). No template control is referred to as NTC.

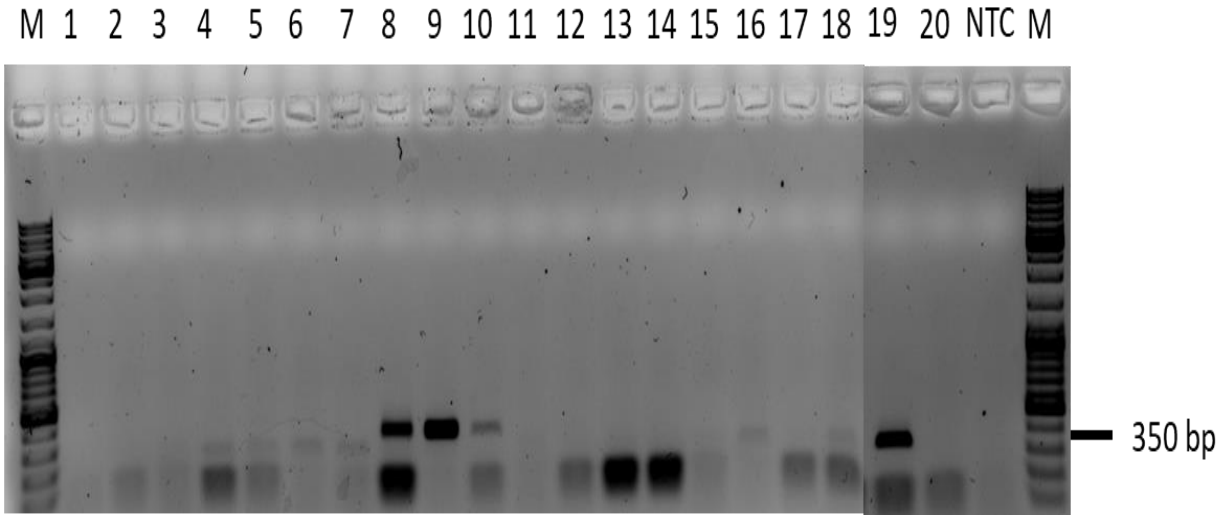

Figure A.4. Detection of *parla* mutation on agarose gel in 24 hours post-fertilization F1 generation embryos from founder 1 parental fish bred with *parlb* ^{d9k} homozygous mutant. A total number of 20 individual embryos was used. Size of the mutant band is 350 bp observed in embryo 8, 9, and 19. The marker (M) used is a 10 kb DNA ladder mix (GeneRuler^{TM}). No template control is referred to as NTC.

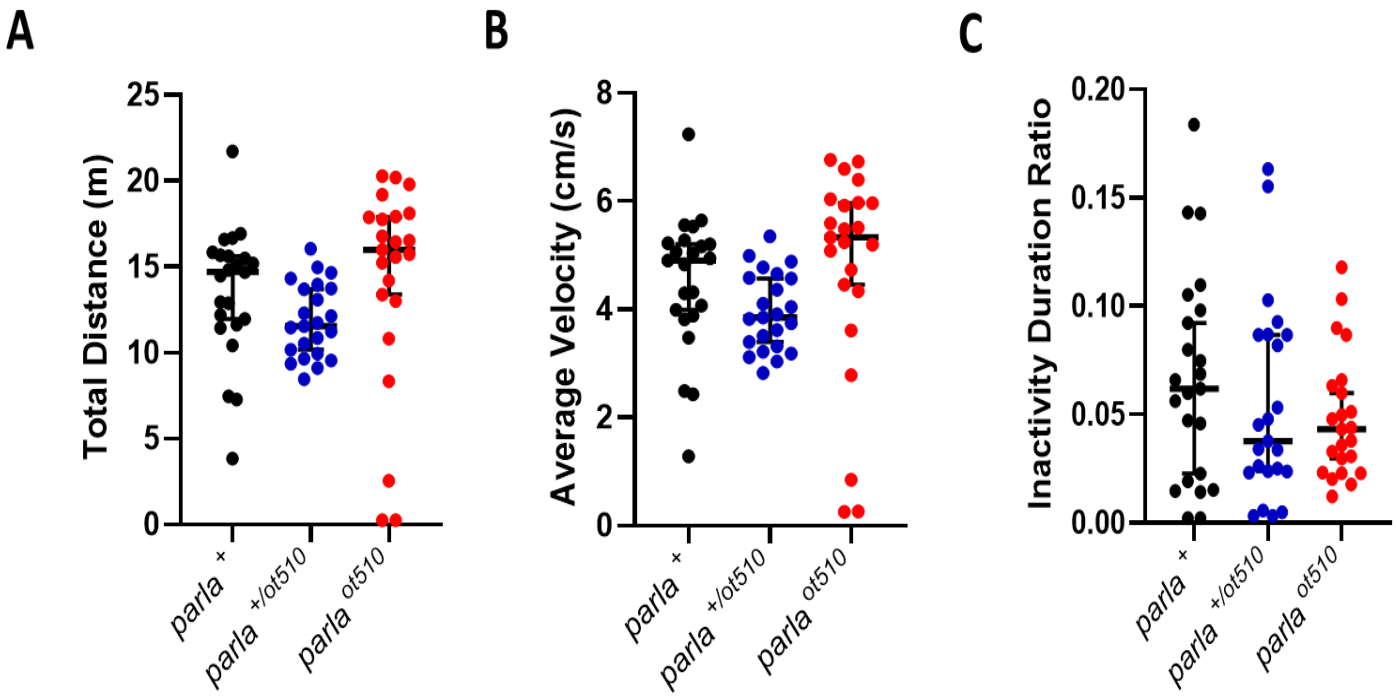

Figure A.5. Swimming activity of 5 dpf mutant larvae and WT zebrafish. (**A–C**) Impact of *parla* loss-of-function on total swim distance, average swimming velocity and inactivity periods (*n* = 23 mutant larvae). WT fish are represented by *parla* $^{+}$, homozygous mutants by *parla* ^{ot510}, and heterozygous mutants by *parla* $^{+/ot510}$. Bars represent the Median with 95% CI.

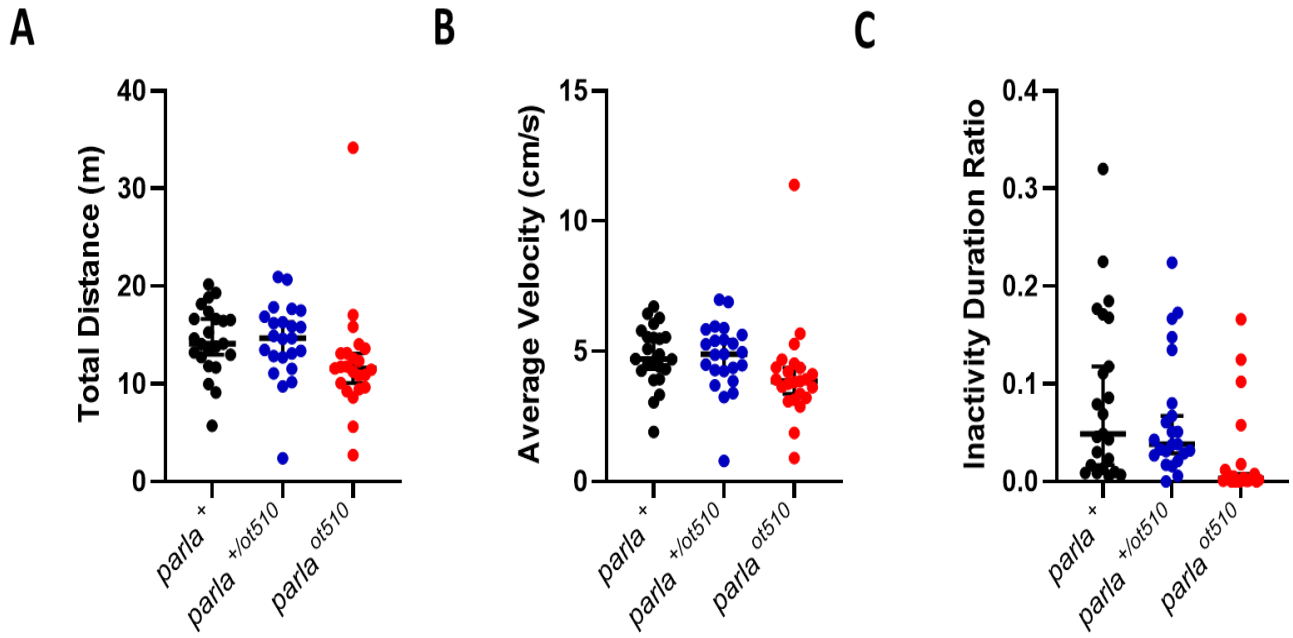

Figure A.6. Swimming activity of 10 dpf mutant larvae and WT zebrafish. (**A–C**) Impact of *parla* loss-of-function on total swim distance, average swimming velocity and inactivity periods (n = 23 mutant larvae). WT fish are represented by *parla* $^{+}$, homozygous mutants by *parla* ^{ot510}, and heterozygous mutants by *parla* $^{+/ot510}$. Bars represent the Median with 95% CI.

APPENDIX 2 – Contributions to Manuscripts

During my Ph.D., some of the data obtained on single mutants with loss of *parla* function described in this thesis led to one publication in the Journal Biomedicines- Special Issue Dopamine in Health and Disease.

- Merhi, R., Kalyn, M., Zhu-Pawlowsky, A., & Ekker, M. (2021). Loss of *parla* Function Results in Inactivity, Olfactory Impairment, and Dopamine Neuron Loss in Zebrafish. *Biomedicines*, *9*(2), 205. doi:10.3390/biomedicines9020205

As the first author, I performed all the experiments included in the paper, in addition to the writing of the manuscript draft, proof-reading, and making the corresponding edits prior to publication. My supervisor, Dr. Marc Ekker contributed to the supervision, data analysis, proof-reading, and editing the manuscript draft. Michael Kalyn, a current Ph.D. candidate in our laboratory, contributed to the confocal imaging performed in the experiments and to proof-reading the manuscript draft. Amanda Zhu-Pawlowsky, an undergraduate student in our laboratory, contributed to the behavioral data presented in the manuscript.